

SDO

Solar Dynamics Observatory

2020 Senior Review Proposal

W. Dean Pesnell, Project Scientist
NASA, Goddard Space Flight Center
Greenbelt, Maryland 20771

This document was prepared by the SDO science team

Submitted in response to the Request for Proposals for the
Senior Review of Heliophysics Operating Missions, April 2020

SDO: Our Eye on the Sun

Mission Fact Sheet

Name:	Solar Dynamics Observatory http://sdo.gsfc.nasa.gov
Launched:	February 11, 2010
Orbit:	Geosynchronous, 28° inclination
Data Downlink Rate	150 Mbps, continuous to dedicated ground station
Prime Mission	May 1, 2010 – September 30, 2015
First & Second Extended Missions	October 1, 2015 – September 30, 2020
Proposed Third Extended Mission	October 1, 2020 – September 30, 2023
Project Scientist	W. Dean Pesnell (NASA GSFC)
Science Investigation Team Principal Investigators	
AIA	Mark Cheung Coronal images at many wavelengths and temperatures that capture the dynamics at scales up to the full disk http://aia.lmsal.com
EVE	Thomas Woods High-cadence extreme ultraviolet spectral irradiances for studying flares and planetary atmospheres http://lasp.colorado.edu/home/eve/
HMI	Philip Scherrer A continuous series of high-cadence, full-disk Dopplergrams and vector magnetograms http://hmi.stanford.edu

The Solar Dynamics Observatory

William D. Pesnell, Philip H. Scherrer, Mark Cheung, Thomas N. Woods

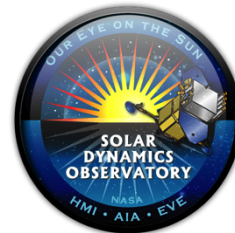
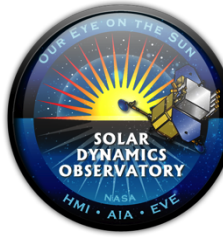


Table of Contents

1	Science Plan and Implementation	1
1.1	Introduction	1
1.2	Contribution of SDO to Heliophysics Science	2
1.3	State of the Mission during the Second Extended Mission of SDO.....	2
1.4	Community Engagement in the Second Extended Mission	3
1.4.1	SDO 2018 Workshop “Catalyzing Solar Connections”.....	3
1.4.2	Data Science and Machine Learning for SDO.....	4
1.4.3	EUV Irradiance Working Group	4
1.4.4	Public Involvement in SDO	4
1.5	Satisfaction of PSGs from Second Extended Mission.....	5
1.5.1	PSG 1. Tracking Subsurface Flows and Structures as Activity Fades	5
1.5.2	PSG 2. Magnetic Variability and the Solar Cycle	6
1.5.3	PSG 3. The Magnetic Connection Between the Sun and the Heliosphere	7
1.5.4	PSG 4. Revealing the Fundamental Physics of Solar Eruptive Events (SEEs)	8
1.5.5	PSG 5. Understanding the Solar Drivers for Geospace and Planetary Atmospheres	8
1.5.6	PSG 6. SDO Cooperative Research with Astrophysics	9
1.5.7	PSG 7. Special Observing Opportunities and Rare Events.....	11
1.6	Science Plans and Implementation for SDO’s Third Extended Mission.....	11
1.6.1	SO #1: Track Subsurface Flows and Structures as Activity Rises	12
1.6.2	SO #2: Unmask Magnetic Variability of the Solar Cycle.....	13
1.6.3	SO #3: Explore Magnetic Connections from the Sun Throughout the Heliosphere.....	13
1.6.4	SO #4: Reveal the Fundamental Physics of Solar Atmospheric Dynamics and Eruptive Events	14
1.6.5	SO #5: Understand Space Weather and Space Climate for Earth and Other Planets	15
1.7	Recommendations from the 2017 Senior Review Panel	16
2	Observatory Status and Performance	18
2.1	SDO Spacecraft Status.....	18
2.2	SDO End of Mission Plan	19
2.3	Mission Operations Status	19
2.4	SDO Ground System (SDOGS) Status.....	19
2.4.1	Data Distribution System.....	19
2.4.2	SDO MOC	20
2.5	Instruments and Science Operations Status and Performance.....	20
2.6	AIA Instrument Status and Performance	20
2.7	EVE Instrument Status and Performance	21
2.8	HMI Instrument Status and Performance	22
2.9	Instrument Operations and Data Center Status.....	23
2.9.1	JSOC-IOC Operations	23
2.9.2	EVE Operations	24
2.9.3	JSOC-SDP Operations	24
2.9.4	JSOC-AVC Operations	25
3	Budget	25
3.1	Plan for Requested Over-guide Scenario.....	25
3.2	In-guide Scenario and Impact Assessment	26
3.2.1	Mission Operations Over-guide Impact	26
3.2.2	AIA Over-guide Impact	27
3.2.3	EVE Over-guide Impact	27
3.2.4	HMI Over-guide Impact	27
3.3	GSFC Science Over-guide Impact	28
3.4	Budget Detail Explanation.....	28
4	Data and Code Management Plans.....	29
4.1	Data Management Plan.....	29
4.2	Calibration and Measurement Algorithm Document (CMAD).....	29
4.3	Code Management Plan	29
5	References	29

The Solar Dynamics Observatory

William D. Pesnell, Philip H. Scherrer, Mark Cheung, Thomas N. Woods



Summary: Solar Cycle 25 has begun and the Solar Dynamics Observatory (SDO) is ready! As the large-scale features of solar minimum fade, the Sun begins to present a more familiar face of active regions and filaments. SDO will complete its three-year Second Extended Mission on September 30, 2020. We watched as coronal holes grew in size and importance and gave the polar regions a fresh look with our high-contrast EUV images and full-disk vector magnetograms. The seeds of Solar Cycle 25's magnetic activity were sown and we will now watch to see whether the polar fields acted as an accurate precursor of the strength of Solar Cycle 25. **It's a perfect time for SDO!** We will use the suite of full-disk, high-resolution, high-sensitivity instruments to study the solar interior flows, the surface magnetic field, and the outer-atmosphere dynamics that drive the Sun-Earth system. SDO captured the rise from an unusually extended solar minimum to the peak and decline of Solar Cycle 24 and is now ready to study the rising phase of Cycle 25. During its 10 years on-orbit, SDO has collected 25 times more data than all other space-based solar missions combined. During the proposed Third Extended Mission, SDO will carry out high-priority research using current and future data and modeling assets to address emerging science topics most relevant to the Heliophysics research focus areas. The spacecraft, instruments, ground systems, and science team will continue to meet the challenges associated with supporting the large number of external science investigations that use SDO data products throughout its extended mission.

This proposal lays out our vision of an over-guide proposal to study the Sun during the rise to maximum of Solar Cycle 25.

1 Science Plan and Implementation

1.1 Introduction

SDO has been an extremely productive mission, supporting over 4500¹ research papers since its launch February 11, 2010 (Figure 1.1), including 1700 from 2017-2019. The SDO team may be small in number but our efforts are multiplied many-fold throughout the international heliophysics community. Our team is dedicated to operating the mission, performing high-impact research projects, and serving the data to a large community. SDO has also been very successful in reaching the public and media (Section 1.4.4). The media, from the web to television to print, use SDO images to illustrate news stories.

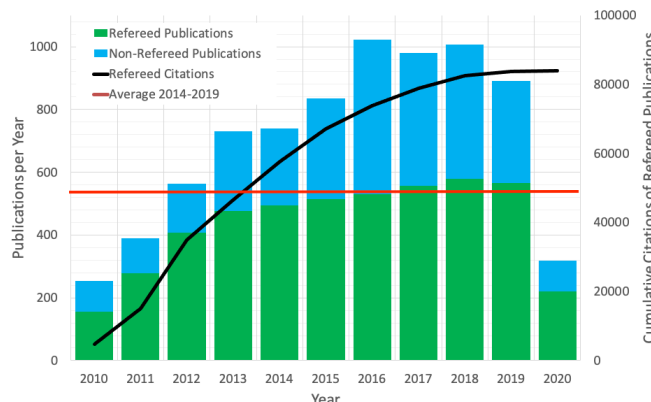


Figure 1.1: A graph of the yearly number of papers using SDO data in the NASA ADS database, along with the cumulative number of refereed citations. The horizontal line shows the 2014-2019 average.

ments over the wide range of length- and time-scales researchers need. By constantly observing the entire

SDO is uniquely suited to observe features of the rising phase of Solar Cycle 25 (SC 25). SDO provided a number of surprises during the rise and maximum of Solar Cycle 24. We expect new discoveries in the coming cycle. The opportunity to make consistent observations of two successive rises to maximum with SDO instruments means new understanding of the interior and atmosphere. SDO observations are enhanced by collaborative observations from new observatories. This is an especially exciting time to observe our star.

SDO produces continuous full-Sun observations with high cadence, low latency, and excellent signal-to-noise, providing measurements over the wide range of length- and time-scales researchers need. By constantly observing the entire

¹ <https://sdo.gsfc.nasa.gov/mission/publications.php>

Sun, no events are missed. Rapid data access allows scientists to monitor solar conditions for space weather purposes and supports planning of other missions and launch decisions of sounding rockets. High cadence allows changes previously missed due to the strobing effect of lower cadences to be more completely observed, enabling new discoveries as well as forcing models to more precise agreement with the solar conditions. The high signal-to-noise allows creation of more advanced data products, such as vector magnetograms and coronal temperature maps; it also enhances the sensitivity to weak wave signals that had been rarely detected before but are regularly produced by SDO. While many research topics can be addressed using SDO data alone, SDO's full potential is realized when observations are combined with measurements from other Heliophysics System Observatory (HSO) assets.

1.2 Contribution of SDO to Heliophysics Science

In addition to its value for heliophysics science, SDO data are used routinely for applied operations and for cross-disciplinary studies. No other mission produces the high-cadence, low-latency solar data that space weather centers around the world rely on to forecast solar conditions and that other observatories with limited fields of view use to plan and guide daily operations.

Beyond the intrinsic scientific value of SDO data, the potential synergies between SDO and other facilities make a compelling case for a Third Extended Mission (EM-3). SDO will continue to support the science of the current fleet of satellites in the HSO. For example, the Sun will not only continue to produce eruptions that impact geospace (seen in the Lyman- α irradiance in Figure 1.2), it will also create increasing

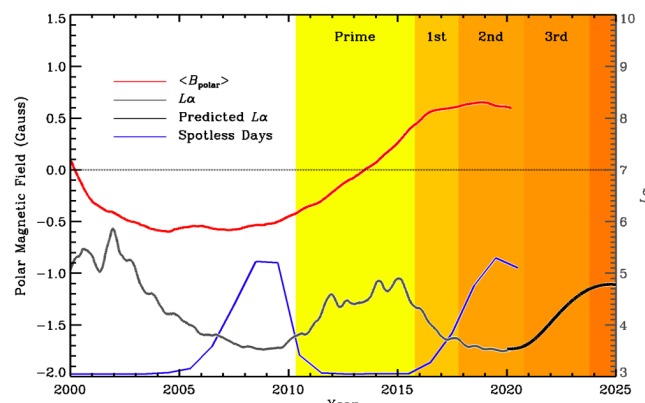


Figure 1.2: The rise of Solar Cycle 25 shown as a prediction of the Lyman- α irradiance derived from Pesnell and Schatten (2018) is the dominant feature of the next three years. The polar magnetic field and spotless day count show that we are past solar minimum and ready for the rise.

SDO has provided vital context observations for the Parker Solar Probe (PSP, launched 18 Aug 2018) by marking PSP perihelion passes as no-maneuver times. Similar no-maneuver marking will ensure uninterrupted observations during science passes of Solar Orbiter (Solo, launched 10 Feb 2020). New ground-based facilities are also available to assist in SDO research. The Atacama Large Millimeter Array (ALMA) has already been using SDO data to understand their instrument and help their science. The most recent addition to solar observatories, the 4 m-class Daniel K. Inouye Solar Telescope (DKIST), released its first light images 29 Jan 2020 and begins science operations soon. The rise to the maximum of Solar Cycle 25 will be well observed!

1.3 State of the Mission during the Second Extended Mission of SDO

SDO continues to provide an indispensable set of solar observations required by the community. *The spacecraft and instruments are healthy and continue to operate in their nominal mode with only a few new anomalies identified during EM-2. The SDO-dedicated ground station in New Mexico captures the*

numbers of filaments and active regions that cause hazardous space weather throughout the solar system. SDO also provides crucial mission planning support for IRIS, Hinode, and other missions. The MinXSS CubeSat mission planners used SDO data, along with GOES X-ray time series, to select for downlink only the most important 10-second high-cadence data intervals for their collaborative flare energetics studies. The Second Extended Mission (EM-2) also supported the prime mission science of the Ionospheric CONnections (ICON, launched 10 Oct 2019) and Global-scale Observations of the Limb and Disk (GOLD, data released starting 6 Oct 2018) missions by measuring the critical energy input of solar EUV irradiance and solar eruptive events (SEEs) that are key drivers in the ionosphere, thermosphere, and mesosphere.

continuous stream of science data and uplinks commands to the spacecraft. As a whole, SDO is operating exceptionally well and is expected to continue for many more years.

All three SDO instruments continuously observe the full solar disk at high cadence from Geosynchronous Earth Orbit (GEO). The Helioseismic and Magnetic Imager (HMI) has two cameras that capture full-disk, polarized 4096x4096-pixel filtergrams used to make maps of photospheric intensity and line-of-sight velocity and magnetic field every 45 seconds with the resolution and noise level, data recovery rate (98.4%) and data completeness (>99% for each Dopplergram) required for helioseismology. HMI also collects the data needed to produce full-disk vector magnetograms as rapidly as every 90 seconds. HMI measurements continue to satisfy the requirements of the Prime Mission.

The Atmospheric Imaging Assembly (AIA) captures eight 4096x4096-pixel images every 12 seconds: 7 EUV bands at full cadence and two chromospheric bands alternating between 12-s cycles. A visible-light band is included at a very low cadence to monitor co-alignment with HMI. The AIA images continue to meet Prime Mission requirements.

The EUV Variability Experiment (EVE) measures the solar EUV spectral irradiance from 33.2-105 nm with a spectral resolution of 0.1 nm in its MEGS-B channel and in ~4 nm bands in the 0.1-37 nm range with its ESP channel. The high-cadence EVE measurements include ESP bands at 0.25 s, while MEGS-B spectra have a 60-s cadence. The MEGS-B 33.2-105 nm spectra and Ly α 121.6 nm irradiances are typically obtained for a few hours per day to study solar forcing in Earth's ionosphere-thermosphere and during flare campaigns for studying solar eruptive events (SEEs). Even with the failure of the MEGS-A CCD on 26 May 2014, ESP and MEGS-B are sufficient to continue addressing its primary objectives. The EVE flight software was changed in 2015 to provide autonomous flare campaigns for MEGS-B observations whenever the ESP soft X-ray (SXR) signal goes above a M1 flare magnitude. As shown in Figure 2.3, the flare campaign has captured almost all flares and generated zero false positives.

All of SDO's measurement objectives are being met by the ongoing observation sequences on the three instruments. SDO science data have been collected almost continuously since the beginning of the Prime Mission with no significant interruptions. Definitive data products are routinely generated along with some near real time (NRT) products that are useful for space weather applications. AIA and HMI NRT images are regularly used for space weather operations and provide solar feature context for planning other solar missions. EVE NRT data are provided to NOAA and the Air Force as a backup X-ray monitor for their space weather operations. The team enabled easy access to the data by developing tools for browsing, searching, and exporting subsets of data from the SDO Data Centers. This access is so ingrained into the SDO mission that we consider the Data Centers to be a "fourth instrument."

SDO operates with a high degree of automation, relying on a small core science team whose prime functions are satellite and instrument operations, data validation, and forefront science, giving priority to supporting the larger research community. The large data stream of 1.3 TB/day requires continuous attention from scientists and engineers all along the path – from the dedicated ground system, data processing and distribution, and production of crucial metadata to the data search capabilities and scientific validation. The SDO team has supported this highly productive program even as the budget has fallen to a basic operational level. In EM-3 we will keep science data flowing, continue a few selected high-priority studies of solar dynamic phenomena, and report events such as filament eruptions and flares, while maintaining broad professional and public use of the definitive and NRT products.

1.4 Community Engagement in the Second Extended Mission

1.4.1 SDO 2018 Workshop "Catalyzing Solar Connections"

The SDO team convened the SDO 2018 Workshop: Catalyzing Solar Connections, from 29 October - 2 November 2018, in Ghent, Belgium. 130 scientists representing a wide range of solar research topics attended. The meeting was organized around the PSGs of EM-2. Eight plenary speakers described recent developments, and 56 oral and 100 poster presentations provided detailed discussions of progress in each PSG. Progress on the SDO 2017 PSGs is reported in the broader discussion of the PSGs presented in Section 1.5. We are grateful that the AAS SPD Metcalf Travel Fund supported participation of several early career

scientists at the workshop. In addition to the PSG-focused sessions, a series of mini-workshops were held on the last day of the meeting. The mini-workshops covered topics related to instrument calibration, use of Python to analyze SDO data, a summary of efforts to understand and remove the 12- and 24-hour periods in HMI data, a meeting of the Vector Magnetogram Working Group, and a tutorial/workshop on how to use machine learning algorithms to analyze SDO data. These sessions allow community members to interact in person with the SDO Science Team, providing a direct link to how the instruments are working and how to improve the data products.

1.4.2 Data Science and Machine Learning for SDO

SDO team members have been leaders in developing machine learning tools and data sets for those tools. SDO data has been processed to form three major “AI-ready” data sets that are available to the global community and optimized for ingestion by machine learning tools and platforms, such as Amazon Cloud. The translation of science data to AI-ready requires several deliberate steps, with the intention of making it usable by non-experts. The Heliophysics Event Knowledgebase (HEK), with its ten years of feature and event data, complements the AI-ready sets and forms the basis of numerous AI labelled data projects. A 2018 Frontier Development Lab (FDL) team produced a curated SDO data set for use in machine learning studies (Galvez et al. 2019², see PSG 2 in Sec. 1.5.2). Examples include generating proxy EVE EUV spectral irradiances from AIA images (Szenicer et al. 2019²), translating EUV observations into magnetograms (Park et al. 2020; Chen et al. 2020²), and creating super-resolution magnetograms (Gitiaux et al. 2019²; Jungbluth et al. 2019²). We anticipate this curated data set will facilitate machine learning research in heliophysics and other physical sciences, increasing the scientific return of SDO. SDO team members actively worked with the SunPy community (SunPy 2020) to develop open-source Python modules for SDO data access and analysis (including drms and aiapy modules). Bobra & Mason (2019²) published a freely available electronic textbook on machine learning for heliophysics.

As well as the machine learning tutorial at SDO 2018, SDO data played a major role in the Machine Learning in Heliophysics Workshop (ML in Helio, <https://ml-helio.github.io>), held 16-20 Sep 2019 in Amsterdam, The Netherlands. Numerous applications of machine learning to SDO data were presented at the meeting. Some of these research projects may be usable in the SDO data pipelines for feature identification and tracking; others for short-term predictions. A great deal of science can be enabled by the combination of curated SDO data archives and machine learning algorithms.

1.4.3 EUV Irradiance Working Group

The aim of this ongoing SDO-led, 36-member working group is to produce an absolutely calibrated measure of the solar EUV irradiance, and to provide a long-term record of the solar EUV irradiance and its variability. This is accomplished by validating the EUV irradiance products from more than a dozen instruments (SDO-AIA & EVE, SOHO-EIT & SEM, STEREO-EUVI, GOES-SUVI & EUVS, Proba2-SWAP & LYRA, Hinode-EIS, SORCE XPS, TIMED-SEE, and MinXSS-2) and understanding their calibration and degradation. The group has met seven times since 2011. A mini-workshop was held as part of the SDO 2018 meeting in Ghent, Brussels, and a weeklong workshop took place in October 2019 at the Royal Observatory of Belgium. The next working group meeting will occur at the next SDO science workshop in Vancouver. SDO-EVE and EVE sounding rocket data are key contributions to this effort.

1.4.4 Public Involvement in SDO

SDO’s images and outreach activities continue to be extremely popular. Since launch, SDO images have been featured regularly in news stories, television shows, and documentaries about the Sun, space, and space weather. The “Little SDO” Facebook page had over 1,300,000 followers and was one of the most popular NASA-related pages ever. SDO’s social media presence has been handled by NASA Heliophysics since 25 Jan 2017. SDO Dashboard movies were developed as an easier way for museums and public venues to show current solar data with a minimum of effort. The Heliovieviewer website (<http://heliovieviewer.org>),

² The ☀ symbol indicates the publication was supported with SDO funding.

developed with partial support from SDO, continues to provide a window into solar data for citizen scientists to make and post movies of solar activity. Tools at the Helioviewer website provide access to HMI and AIA data through an archive of 36-second cadence jpeg2000 images generated at the JSOC. These tools provide web and local Java tools to examine and combine solar data in a convenient form. They also have interfaces to query the HEK and display the solar events captured there. Public users have created over 2 million SDO movies using Helioviewer interfaces, including over 300,000 in 2019, with 1 million unique users between June and December 2019. These users are “SDO ambassadors” who share and publish their efforts. Other activities are ongoing and we plan to continue their support through EM-3.

The SDO team has organized five SDO Data Events, in which NRT data for rare events is made available to the public through specially prepared websites and activities. All five involved special modes of spacecraft operation. Each SDO Data Event required significant effort to handle the large data flows generated by the enormous public interest in the SDO images. The Venus Transit Data Event in June 2012 served 8 TB of data while the Comet ISON Perihelion Data Event in November 2012 delivered 15 TB of data to over a million users. The latest SDO Data Event served 100 TB during the Mercury transit in November 2019. We plan to continue outreach activities during EM-3. New Data Events could arise if an unexpected event happens such as a Sun-grazing comet entering SDO’s field of view.

1.5 Satisfaction of PSGs from Second Extended Mission

The SDO investigations have enabled significant advances towards the NASA Science Objective “Understand the Sun and its interactions with Earth and the solar system, including space weather,” specifically the 2014 NASA Science Plan’s overarching science goals to “Explore the physical processes in the space environment from the Sun to the Earth and throughout the solar system” and to “Advance our understanding of the connections that link the Sun, the Earth, planetary space environments, and the outer reaches of our solar system.”

We have made significant progress on the science questions of the mission, and the SDO science investigation teams have achieved all of the original observing objectives of the mission. Studies related to SDO have led to the publication of over 4500 refereed papers (a pace of over one publication per day, see Figure 1.1). There are 62 Ph.D. dissertations (not including some Chinese-language dissertations) and at least 2900 conference papers describing SDO science. A complete list is on the SDO website <https://sdo.gsfc.nasa.gov>.

Research that supported the Prioritized Science Goals (PSGs) of EM-2 listed in the 2017 SDO Senior Review proposal is described below.

1.5.1 PSG 1. Tracking Subsurface Flows and Structures as Activity Fades

Determine the meridional-circulation profile with depth and how it evolves with solar cycle. Chen (2019 ☀) and [Lin & Chou \(2018\)](#) reported single circulation cells in each hemisphere during solar maximum and multiple cells with depth near solar minimum. [Liang et al. \(2018\)](#) reported a persistent single cell in the southern hemisphere and anomalous results in the north. [Böning et al. \(2017\)](#) showed that the detected number of cells depends on inversion regularization. Disagreements between studies can be attributed to systematic errors that are as large or larger than the signal, such as the center-to-limb (Ctl) effect. Longer observations will help reveal the evolution of meridional circulation within one cycle and between cycles.

Understand the center-to-limb effect. [Chen & Zhao \(2018\)](#) ☀ found that to understand the Ctl effect one must account for its dependence on acoustic frequency. The Ctl effect exhibits opposite signs below and above the cut-off frequency, suggesting a possible mechanism to understand and remove the effect from helioseismic measurements.

The evolution of long-lived subsurface structures. By tracking motions of surface supergranular patterns, [Löptien et al. \(2018\)](#) reported detecting Rossby waves in the shallow interior of the Sun having a dispersion relation characteristic of sectoral Rossby waves. [Liang et al. \(2019\)](#) confirmed the report using travel times measured by time-distance helioseismology.

Improve the quality of far-side active regions for space weather forecasting. [Zhao et al. \(2019\)](#) ☀ substantially improved the quality of far-side active-region imaging using local helioseismology. By com-

paring helioseismic far-side images with STEREO-observed EUV images, Chen et al. (2020, under preparation) used machine learning methods to calibrate the helioseismic far-side images and produce magnetic flux maps (Figure 1.3).

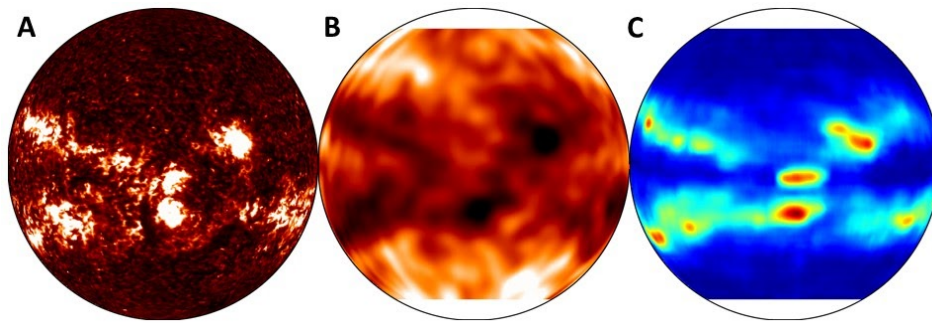


Figure 1.3: (A) STEREO-observed EUV image of the far-side Sun on 13 Mar 2014. (B) Helioseismic imaging of the far-side on the same date. (C) Magnetic flux map inferred from helioseismic imaging using machine learning.

Study connections between the solar interior and the chromosphere and corona.

Zhao & Chen (2018) reported the first observation of waves in the magnetic field associated with the sunquake event of 6 Sep 2017. Quinn et al. (2019)

reported a chromo-

spheric response to the same sunquake, suggesting that crests in the waves are caused by upflows. Chen (2019) found that only 24 of 60 strong flares in Cycle 24 produced sunquakes, and that the phase of the background solar oscillations at the footpoints of the flare at the time of the impulse strongly influenced the occurrence of a sunquake. Coupling observations of photospheric oscillations, magnetic fields, and chromospheric oscillations, Rajaguru et al. (2019) argued that low-frequency waves also play an important role in chromospheric heating.

Determine whether long, deep solar minima differ from regular minima in the interior. Howe et al. (2018) and Basu & Antia (2019) found that the torsional oscillations (zonal flows) in Cycle 24 were weaker and less well-defined than those in Cycle 23, and that the global rotation rate slowed down in latitudes above 30°. Signs of Cycle 25 are already apparent in zonal flows. Lekshmi et al. (2018) found that a north-south asymmetry observed in the near-surface torsional oscillations preceded the magnetic field asymmetry in flux and sunspot number. Kosovichev & Pipin (2019) linked subsurface zonal-flow acceleration to dynamo waves, which suggests that the dynamo is located around 60° latitude in the tachocline.

1.5.2 PSG 2. Magnetic Variability and the Solar Cycle

Develop an accessible catalog of quantitative AR characteristics using HMI observations. Li (2018) used HMI and MDI to measure magnetic tilt angles, spot areas, flux, and polarity separations for 4385 sunspot groups during their disk passages in Cycles 23 and 24. McIntosh et al. (2019) & Leamon et al. (2020) used SDO and STEREO data to determine that the rapid onset of solar activity is both constrained in longitude and nearly simultaneous around the star, suggesting that information travels very rapidly within the Sun. The uniform data sets from SDO have enabled the application of machine learning to solar data (see §1.3.2; Neuberg et al. 2019; Salvetelli et al. 2019).

Continue to improve HMI vector magnetic field and other HMI data products. New data products were made available during the EM-2 and others were improved. The photospheric electric field can now be computed from photospheric vector magnetic and velocity fields (Kazachenko et al. 2014) and is available at the JSOC as the *cgem.pdfi_output* data series. Magnetic squashing-factor Q-maps showing the detailed magnetic structure of the inner corona are now routinely produced (Hoeksema et al. 2017) and are available in series *hmi.q_synop*, *hmi.q_synframe*, and *mdi.q_synop*.

We improved HMI data products by implementing stray light removal from the full-disk solar images using a point-spread function (PSF) developed by pre-launch testing and post-launch image analysis (Covidat et al. 2016). Deconvolved data are particularly advantageous for irradiance modeling, tracking, co-alignment, plage magnetic field measurement, and helioseismology around sunspots (e.g., Houston et al. 2018; Attie et al. 2018). Daily images have been created and extended higher-time-cadence runs are

produced upon request in velocity, line-of-sight and vector magnetic field, line width and depth, continuum intensity, and Stokes parameters (IQUV). The empirical method to correct for the small but systematic 24-hour oscillation in magnetic field (Hoeksema et al. 2014 ☀) has been refined by increasing the sample from 20 simple, stable sunspots to 55 and by determining separate corrections for weak and strong fields.

High-cadence vector magnetograms continue to be produced on demand to support research on various topics, including exploring eruption mechanisms (e.g., Bi et al. 2018, Kleint 2018). Lumme et al. (2019) evaluated the impact of data cadence (12 min vs 135s/90s) on magnetic energy and helicity flux estimates for AR 11158 using DAVE4VM and PDFI (Faraday-law constrained), and found the higher cadence to be more robust.

Determine how structures in the solar atmosphere form, evolve, store energy, and destabilize. A sample of 31 emerging active regions with simple bipolar magnetic configuration was analyzed to understand the origin of twist and the relation of eruption of magnetic field to the development of twist (Liu 2019 ☀). The magnetic twist in the flux tubes is fairly small, less than the instability threshold. Simulations indicated how the presence of non-neutralized currents affected the eruptive nature of active regions (Liu et al. 2017 ☀). Thalmann et al. (2019) explored the relationship between evolution of magnetic helicity in active regions and solar eruptions. The component of helicity due to electric-current-carrying magnetic field has been found to relate to solar eruption. This component of helicity is mostly associated with magnetic twist. Norton et al. (2017 ☀) reported that magnetic flux-emergence rate scales with total emerging flux. As flux emergence simulations often produce faster flux emergence rates than do the observations, this work could justify adjusting the simulations to produce more realistic flux emergence rates.

Perform higher-resolution and shorter time-scale studies to determine the effects of energy transport by MHD waves. Houston et al. (2018) used HMI data, including PSF-corrected data, to coalign ROSA, IBIS, and FIRS data from Sac Peak using slit imaging to investigate shock physics in sunspot umbrae. Magnetic field enhancements produced by umbral flashes are directed along the motion path of the developing shock, hence producing relatively small changes, up to a maximum of $\sim 8^\circ$, in the inclination and/or azimuthal directions of the magnetic field. Importantly, this work highlights that umbral flashes are able to modify the full vector magnetic field. SDO observations of MHD waves featured extensively at the [ISSI Workshop on Oscillatory Processes in Solar and Stellar Coronae](#). ☀

1.5.3 PSG 3. The Magnetic Connection Between the Sun and the Heliosphere

Develop data-constrained and data-driven magnetic models of the solar corona and heliosphere. A number of research groups have developed these data-driven models ([Guo et al. 2019](#), [Price et al. 2019](#), [Chintzoglou et al. 2019](#) ☀; [Toriumi et al. 2020](#) ☀). Many use HMI magnetograms for the bottom boundary condition and AIA EUV images for validation of coronal structure. For instance, [James et al. \(2018\)](#) ☀ used AIA differential emission measure (DEM) inversions to infer a hot structure overlying an AR's polarity inversion line, which coincides with a magnetic flux rope in a nonlinear force-free field extrapolation.

Validation of models with *in situ* measurements (including Parker Solar Probe and Solar Orbiter). [Riley et al. \(2019\)](#) used HMI magnetograms as the photospheric boundary condition for a solar MHD model to support PSP measurements. Many similar analyses with SDO and PSP data are anticipated.

Testing models against remote sensing data from SDO, RHESSI, IRIS, Hinode, ALMA, DKIST, and NST. [Kowalski et al. \(2017\)](#) used HMI filtergrams to constrain their 1D RADYN model of flare loops, which were also used to compare with RHESSI and IRIS observations. [Su et al. \(2018\)](#) ☀ tuned the AIA team's DEM inversion code to agree with RHESSI X-ray observations of flares, and concluded AIA EUV channels contain information about plasma up to 30 MK. [Effenberger et al. \(2017\)](#) ☀ studied 116 partially occulted flares using RHESSI, SDO and STEREO data, and concluded that coronal X-ray sources, in general, have a thermal and non-thermal component. [Cheung et al. \(2019\)](#) ☀ (see also PSG 4) provide a possible alternate explanation in terms of multi-thermal sources. [Kazachenko et al. \(2017\)](#) ☀ released a database of 3137 flare ribbons identified in SDO data. They reported a scaling relation of peak X-ray flux $I \propto \Phi^{1.5}$, where Φ is the flux swept by flare-ribbons (reconnected flux), consistent with hydrodynamic loop models.

Continued monitoring of the Sun to enable continuous improvement of models with different magnetic field topologies at different phases of the solar cycle. [DeRosa & Barnes \(2018\)](#) ☀ performed a statistical study of the possible association between access to open field regions (from PFSS models) and the eruptivity of X-flares. They suggest that “X-class flares with access to open fields are eruptive at a higher rate... [though] this result should be moderated due to the small number of non-eruptive X-class flares.”

1.5.4 PSG 4. Revealing the Fundamental Physics of Solar Eruptive Events (SEEs)

Take a systems view of SEEs, determine physical links between different SEE-related phenomena (e.g. flares, CMEs, coronal waves, dimmings). [Liu et al. \(2018\)](#) ☀ studied the SOL2017-09-10 event, which produced an X8.2 flare accompanied by a CME, global EUV wave, coronal dimming, solar energetic particle events, and a ground-level event detected by the Radiation Assessment Detector on the Curiosity rover ([Guo et al. 2018](#)).

Provide physical links between different layers of the atmosphere. [Cheung et al. \(2019\)](#) ☀, inspired by SDO and IRIS observations of NOAA AR 12017, created a 3D radiative MHD model of a flare that couples the near-surface convection zone through the photosphere, chromosphere, transition region and corona (see also [Bjørgen et al. 2019](#) ☀). Studies using AIA and IRIS observations, and 1D hydrodynamic loop models support the need for electron beams (in addition to thermal conduction) in coronal heating models ([Polito et al. 2018](#); [Reep et al. 2018](#); [Reale et al. 2019](#); [Graham et al. 2019](#) – using AIA and Hi-C).

Provide observational constraints to test physical theories describing magnetized plasmas. [Wang & Ofman \(2019\)](#) used AIA observations of flare loops and 1D hydrodynamic loop modeling to show saturation of thermal conductivity. [Jin et al. \(2018\)](#) ☀ performed data-driven MHD modeling of a behind-the-limb eruption, and found that the eruption-induced shock created conditions amenable for diffusive shock acceleration, which may explain the presence of front-side gamma-rays observed by detectors on Fermi.

Clarify whether different physical mechanisms are responsible for the formation and destabilization of flux ropes from ARs vs. from quiescent filaments. [Panesar et al. \(2018\)](#) ☀ analyzed 13 randomly selected coronal jets in AIA data and found they result from mini-filament eruptions following photospheric flux cancellation. Flux emergence immediately prior to cancellation was not required. At the other end of the size spectrum, [Chintzoglou et al. \(2019\)](#) ☀ analyzed X-flare-productive ARs and found collisional polarity inversion lines between emerging dipoles to be sites of large flare activity.

Determine the scaling relation between flare emission measure and temperature. [Aschwanden \(2019\)](#) ☀ examined whether the largest flares are a “Dragon-King” phenomenon – extreme events in a distribution that may be due to a different mechanism than lower energy events – and concluded they likely belong to the same distribution as smaller flares. [Toriumi et al. \(2017\)](#) studied 51 large (M5.0+) solar flares to examine scaling relations of flare parameters and found them to be consistent with stellar flare scaling relations. A study of stealth CMEs by [O’Kane et al. \(2019\)](#) concluded such events can be considered lower-energy eruption events, and not a magnetically distinct phenomenon from CMEs with flares (see also [Nitta & Mulligan 2017](#) ☀).

1.5.5 PSG 5. Understanding the Solar Drivers for Geospace and Planetary Atmospheres

SDO EVE solar irradiance data continue to be an important input for data analysis and modeling of terrestrial and other planetary atmospheres. Furthermore, models of the solar EUV irradiance are being improved with SDO EVE data. The following highlights progress on this PSG.

Measure the upcoming solar minimum and compare with the 2008-10 minimum to explore secular trends, and extend the comparison to earlier minima. SDO EVE has contributed solar EUV reference spectra for the international Whole Heliosphere and Planetary Interactions (WHPI) campaigns: <https://whpi.hao.ucar.edu>. There was a WHPI session at the AGU 2019 Fall meeting to discuss the recent solar minimum, and papers are anticipated to be submitted in 2020 on those comparisons between different cycle minima.

Determine how much of the long-term changes in the IT are driven by changes in long-term solar variations vs. increases in anthropogenic CO₂ that cool the thermosphere. Venkat Ratnam et al. (2019) show that long-term cooling of -1.7K/decade in Earth's atmosphere at 30-80 km is mostly related to greenhouse gas (e.g., CO₂) increases. On the other hand, solar cycle variability is the primary driver for changes at altitudes above 100 km ([Solomon et al. 2019](#)). It is too soon to know the consequences in Earth's ionosphere / thermosphere for the new minimum in 2019-2020. Lin & Chu (2017) have developed an improved ionosphere model for Earth using SDO EVE inputs; their modeling results agree well with the ionosphere's solar cycle variability.

Improve solar irradiance models. Using SDO EVE data, solar EUV spectral irradiance models were extended to Mars ([Thiemann et al. 2017](#) ☀) and a solar model for Sun-Climate studies was extended into the EUV range ([Fontenla et al. 2017](#) ☀). Based on EVE data, Schonfeld et al. (2019) proposed a solar EUV proxy that is better than F10.7, a popular proxy used as input for planetary atmospheric models. One operational data product is an EUV spectral irradiance proxy model based on SDO EVE and driven by EUV and X-Ray Irradiance Sensors (EXIS) measurements on the GOES-R satellites ([Thiemann et al. 2019](#) ☀).

Improve terrestrial and planetary atmosphere data analysis and modeling with SDO data input. With

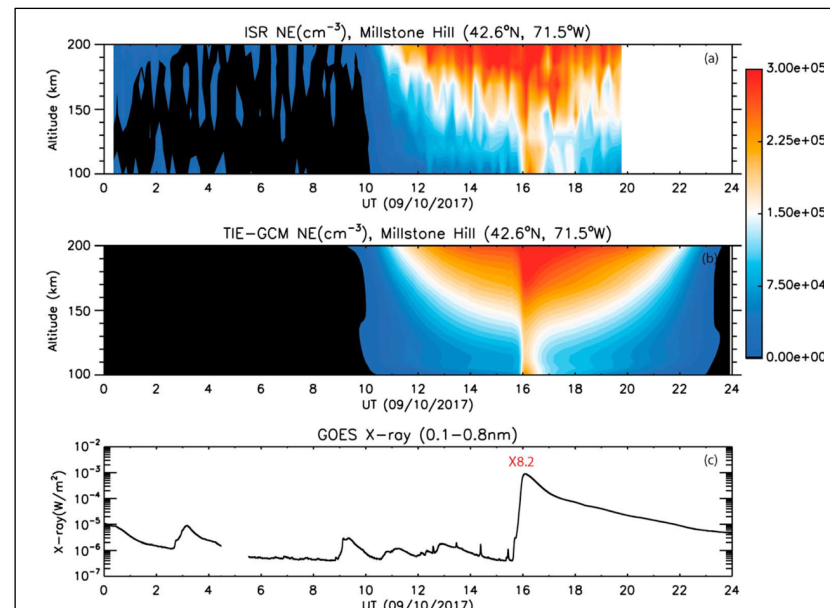


Figure 1.4: Solar flares rapidly enhance Earth's ionosphere (electron density, NE) during the Sep 2017 storms as shown by ISR measurements and TIE-GCM modeling using FISM-2, an EVE-based solar EUV irradiance model, as input. This figure is from Qian et al. (2019), who find that both solar flares and geomagnetic storms need to be present to drive large-scale traveling atmosphere disturbances (TADs).

tions ([Grava et al. 2018](#)).

Make the EUV spectral irradiance observations needed for the ICON and GOLD missions. SDO provides solar EUV irradiance data that are important for studies of Earth's ionosphere and thermosphere involving NASA AIM, TIMED, GOLD, and ICON missions. The irradiance models mentioned above also aid science with these missions.

1.5.6 PSG 6. SDO Cooperative Research with Astrophysics

SDO continues to provide key data products to support collaborative studies with other HSO missions to achieve their science goals. SDO provides real-time images that are used for planning HSO missions such as Hinode and IRIS, suborbital flights such as CLASP2, and ground-based observatories such as ALMA and (soon) DKIST. SDO full-disk images with high cadence are also useful for solar observatories with

EVE data, [Sato et al. \(2019\)](#) reveal how much the solar EUV impacts the radio noise in Global Navigation Satellite Systems (GNSS) signals during the large storms on 6 Sep 2017. The high cadence of SDO EVE data enabled [Schmolter et al. \(2018\)](#) to determine an average delay of 17 hours for Earth's ionosphere response to solar EUV variations. Using the EVE-based Flare Irradiance Spectral Model 2 (FISM-2), [Qian et al. \(2019\)](#) ☀ isolated the solar flare irradiance influence in Earth's atmosphere from other storm effects (SEPs and CMEs) during the large solar storm period in Sep 2017 (see Figure 1.4). SDO EVE data are also used to study the response of Martian ionospheric flares (e.g., [Thiemann et al. 2018](#) ☀) and Interstellar Medium (ISM) varia-

small FOV for their definitive science analysis (e.g., [Loukitcheva et al. 2019](#)). The solar variability results from SDO are increasingly important for planetary and stellar applications as exoplanet research and interests continue to rapidly expand. The following are some highlights related to this PSG.

Understand the relationships of active region magnetic complexity to occurrence of EUV late-phase flares and how these results apply for stellar magnetic behaviors. [Woods et al. \(2011\)](#) revealed a new class of flares from SDO observations called the EUV late-phase, which is characterized by having a second EUV peak many minutes after the X-ray flare peak. [Dai & Ding \(2018\)](#) modeled the two likely processes for EUV late-phase flares, long-lasting cooling or secondary heating for flare-associated coronal loops of two distinct lengths. Their study indicates that secondary heating is more favorable for explaining the observed late-phase time profiles. The secondary heating mechanism is further supported by [Zhou et al. \(2019\)](#) who show that post-flare magnetic reconnection within a quadrupolar magnetic configuration caused the enhancements during the EUV late-phase flare on 25 Apr 2014 (Figure 1.5).

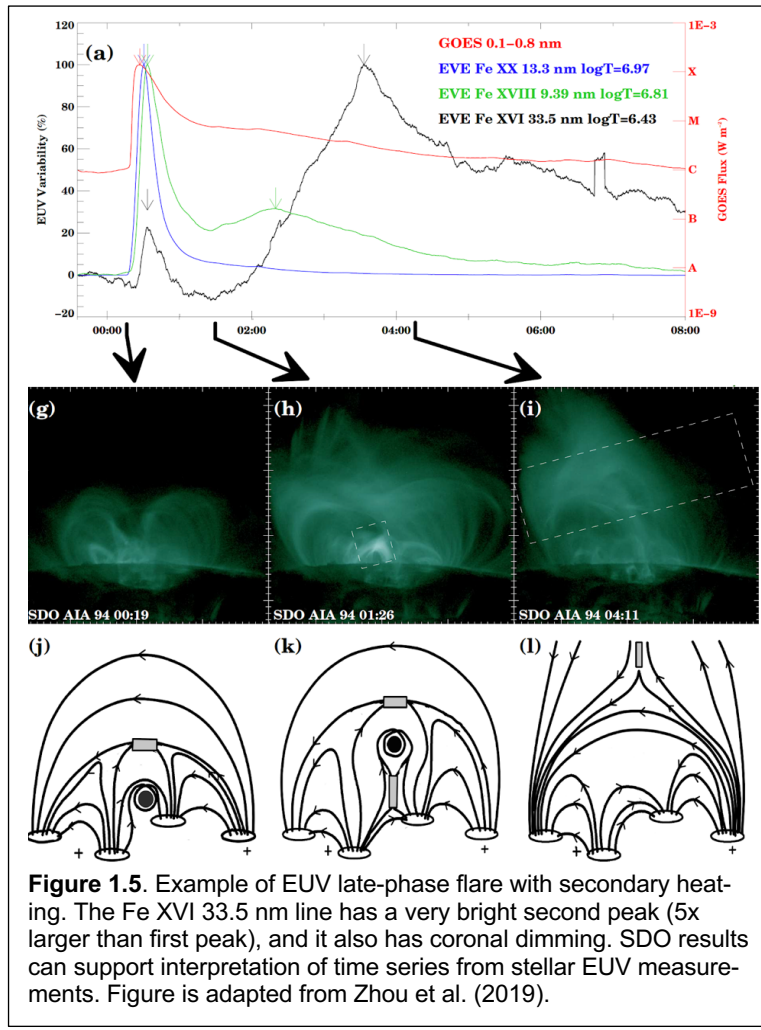


Figure 1.5. Example of EUV late-phase flare with secondary heating. The Fe XVI 33.5 nm line has a very bright second peak (5x larger than first peak), and it also has coronal dimming. SDO results can support interpretation of time series from stellar EUV measurements. Figure is adapted from Zhou et al. (2019).

Study how the relationships regarding eruptive phenomena established during solar cycle maximum change during minimum and how those results apply for stellar systems and exoplanet habitability. [Namekata et al. \(2017a\)](#) used MHD simulations of magnetic reconnection to establish scaling laws of magnetic field strength and coronal loop lengths based on flare peak temperature and emission measure, which was validated with SDO HMI and AIA data and are applicable for stellar flares. This study, also related to PSG-4, suggests that flare physics is similar over the solar cycle. In another Sun-star application, [Namekata et al. \(2017b\)](#) used 50 white-light flares from SDO HMI to make predictions of the rate for stellar superflares. Additionally, Keenan et al. (2017) used SDO EVE flare observations to determine which pairs of Fe line ratios to improve for the analysis of stellar flares from the astrophysics EUVE mission.

Using SDO results relating coronal dimming and CME properties, how large and energetic are the CMEs from sun-like stars, and how do CMEs impact exoplanets atmos-

pheres and habitability? There has been much progress in better understanding coronal dimming with EVE (e.g., [Mason et al. 2019](#)) and AIA (e.g., [Dissauer et al. 2018; 2019](#)). Harra et al. (2016) determined that coronal dimming is the only sun-as-a-star observation consistently associated with CMEs, and thus can be plausibly employed to detect and quantify CMEs events on other stars. The astrophysics SMEX mission ESCAPE, selected for Phase A study (France, 2019), will leverage SDO coronal dimming results to indirectly detect and characterize stellar CMEs, as well as to characterize the exoplanet-host stars' EUV

irradiance in order to constrain the atmospheric chemistry models that determine habitability for those exoplanets. Furthermore, [Kay et al. \(2018\)](#) describe how solar CME observations can be adapted for studying the interaction of stars and their orbiting exoplanets.

1.5.7 PSG 7. Special Observing Opportunities and Rare Events

Solar eclipses. The total solar eclipse in August 2017 was supported by SDO team members at locations along the path and created a great deal of excitement in the public (Kirk et al. 2017). A prediction of the corona during the eclipse was very popular (Mikić et al. 2018). Ground-based data taken during the 2017 solar eclipse were compared with models of the corona (Riley et al. 2019; Mikić et al. 2018). They used HMI synoptic magnetograms for the bottom boundary condition of the Alfvén wave driven model and AIA images to identify regions requiring insertion of magnetic stress. The properties of a coronal cavity were determined from ground-based and AIA observations (Chen et al. 2019). Hanaoka et al. (2018) analyzed high-altitude features of polar jets during the eclipse and related them to AIA observations.

Planetary transits. The team ran special observation modes for the Mercury transit on 11 Nov 2019. This data event attracted a large audience and was featured by NASA HQ. SDO images were used as standard for an educational project using the transit to calculate the parallax of Mercury. The data can also be used for precise plate-scale determination and coordinate system validation, as well as for exoplanet research. The next transit of Mercury (13 Nov 2032) will occur during SDO's Seventh Extended Mission.

Sungrazing Comets. AIA observations of comets within the solar corona have revealed new physics in the formation of cometary tails and are a unique diagnostic of the corona magnetic field. SDO is prepared to slew and observe a newly-discovered sungrazing comet with less than 48 hours' notice.

1.6 Science Plans and Implementation for SDO's Third Extended Mission

Based on the success of the SDO mission and the excellent state of the observatory, we are proposing an over-guide science mission for SDO's EM-3. The broad goals of EM-3 are to:

- 1) Provide the science community with calibrated solar data;
- 2) Maintain an active data validation effort to verify that newly acquired data continues to meet scientific standards;
- 3) Assist science users and the public with access to and interpretation of SDO data;
- 4) Continue transferring data to the final archive at the SDAC;
- 5) Update and approve the EOMP & PDMP, write and approve CMADs;
- 6) Perform and publish science research related to the Scientific Objectives listed below.

The first four goals continue the work the SDO team has successfully done in EM-2 and represent the bulk of the in-guide proposal. Support for the CMAD goal is a line item in the over-guide budget. The updated PDMP required in the Call for Proposals (CfP) will be delivered by October 2021. We will continue to work with SSMO and other relevant parties to keep the End of Mission plan current (as described in the CfP). Goal #6 is partially supported by the cal-val efforts. We are asking for roughly one FTE per team to renew SDO as a science mission and increase the scientific output of the team.

For EM-3, we propose five comprehensive Science Objectives (SOs), several key questions for each SO, and specific tasks to address these questions. The relevance and importance of SDO for the HSO is discussed in Section 1.1 but are also intertwined with these SOs.

Table 1.1: Science Objectives (SOs) for SDO's Third Extended Mission

SO #1: Track Subsurface Flows and Structures as Activity Rises
SO #2: Unmask Magnetic Variability of the Solar Cycle
SO #3: Explore Magnetic Connections from the Sun Throughout the Heliosphere
SO #4: Reveal the Fundamental Physics of Solar Atmospheric Dynamics and Eruptive Events
SO #5: Understand Space Weather and Space Climate for Earth and Other Planets

These SOs trace directly to the Heliophysics Science Goals and Decadal Survey Key Science Goals in

Table 1.2. As in the past, SDO's SOs address a large number of these NASA goals. Our SOs are appropriate and mature. The summary of research results in EM-2 demonstrates that we selected appropriate science goals and were able to place research results from the SDO team and community into the tasks used in the earlier mission extensions.

The measurements needed for EM-3 research come from our current mode of operations. We do not anticipate having to change the SDO operations. The higher-level data products listed in the PDMP (App. A) are publicly available now. The team will continue to monitor and maintain the quantity and quality of the primary SDO data products throughout EM-3.

To accomplish these goals, we rely heavily on external support and partnerships. We highlight tasks to be performed by funded SDO team members with blue-colored text; all other tasks can only be addressed with outside sources of funding and support.

1.6.1 SO #1: Track Subsurface Flows and Structures as Activity Rises

Internal dynamics drive the solar cycle. As SC 25 begins, we can compare observed conditions at the start of the two cycles in a way that has never before been possible. We focus on these key questions:

- How will resolving variability of large-scale internal flows throughout the convection zone down to the tachocline enable us to better understand solar cycles?
- How do flow patterns during the early phases of SCs 24 and 25 differ, and what do the differences indicate about the activity level of SC 25?
- What is the structure of convection in the solar interior and how does it vary in time?
- What are the subsurface properties of magnetic nests? Can we understand their persistence?

Implementation Plan / Tasks

Task 1.1: Continue measurements of the Sun's internal rotation and meridional circulation. Helioseismic determinations of the latitude and depth dependence of rotation are robust; but measurements of the internal meridional circulation continue to face challenges. In order to reconcile results from various approaches, significant effort will be devoted to improving our understanding of center-to-limb systematic effect (Fig. 1.6). New measurements will provide the first and only data set of sufficient quality for the required local helioseismic analysis through the entire decay phase of one cycle and subsequent rise of the next. Evolution of the profiles of rotation and meridional circulation during the onset of the cycle will be studied, and their behavior during the rise of Cycle 25 will be compared with the same phase of Cycle 24.

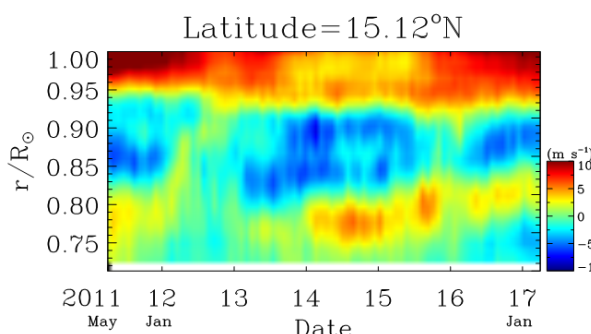


Figure 1.6: Temporal evolution of meridional circulation from 2010 to 2018 (2-year running average) at latitude 15° N, showing 3-layer flow structure most of the time. Positive flows are poleward and negative are equatorward.

helioseismic techniques and surface measurements; improved precision, especially at high latitudes; and novel algorithms for flow detection and characterization. SDO provides unique data for studying these features as they evolve over the course of a second solar cycle.

Task 1.3: Investigate subsurface properties of active nests. An active nest is a heliographic location where a series of flare productive ARs emerge over the course of several months or even years. Local

Task 1.2: Identify and characterize spatially-resolved flow structures and patterns. A variety of large-scale flow patterns and structures have been detected in the past few years, including non-axisymmetric high-latitude zonal flow anomalies (Hathaway et al. 2013, Bogart et al. 2015) and Rossby waves (e.g. Löptien et al. 2018). Little is understood about these phenomena, particularly their depth structure, their persistence, their contribution and relation to the evolution of global-scale flows associated with the Sun's activity cycles, such as torsional oscillations, and their hemispheric differences. Efforts to make progress in these areas will focus on cross-comparison of measurements from various

helioseismology will be used to investigate, during the relative quiet periods between the recurrences of active nests, what is different beneath such regions and the mechanism of their repetitive appearance. We will also explore whether it is possible to predict their re-appearance.

1.6.2 SO #2: Unmask Magnetic Variability of the Solar Cycle

We still cannot confidently predict the strength of a solar cycle or physically model why one cycle is unlike its predecessor. SDO provides unique and comprehensive visibility into the changing drivers of solar activity. Consequently SO #2 focuses on these key questions:

- How and where do solar dynamo(s) operate?
- What causes the long-term trends/differences between the solar cycle minima in 2008-2010 and 2019-2020 and for the rising phases of Cycles 24 and 25? (see also SO 5)
- How and why do large-scale magnetic field patterns vary during the cycle and from cycle-to-cycle?

Implementation Plan / Tasks

Task 2.1: Characterize the relationships between photospheric flows and the solar cycle. HMI will measure the long-term evolution of differential rotation, zonal flows, meridional motions, and convective flow patterns in the photosphere and below, and then determine their relationships to magnetic flux features and to subsurface conditions, including the subsurface shear layer (also SO #1). We will compare changes with solar cycle and phase.

Task 2.2: Determine how patterns of solar magnetic flux emergence and evolution constrain the mechanisms of the solar cycle. HMI, AIA, and EVE observations will provide quantitative characteristics of solar flux emergence, evolution, transport, and cancellation in early SC 25. We will compare with sub-photospheric features (Task 1.2) and the development of large-scale features (e.g., coronal holes, polar crown filaments, and field patterns) to find indicators and causes of hemispheric-scale asymmetries.

Task 2.3: Link detailed characteristics of magnetic features on small and large scales to other solar variations. One can identify, track, and measure photospheric and coronal features in HMI and AIA data to link structures at small and large scales and to better understand the causes of EVE's EUV spectral irradiance variability. One can perform comparative studies using SDO data with non-SDO observations (TIMED SEE irradiance, STEREO and GOES images, SOHO and GONG fields) and investigate secular changes with solar cycle and phase.

Task 2.4: Improve understanding of the dynamos that drive solar magnetic activity. Using HMI Doppler and magnetic field data over Cycles 24 and 25, one can compare flux generation at various scales to help determine the sites of solar dynamo activity by analyzing characteristics of flux emergence and flows, exploit quiet conditions at the current solar minimum to better understand measurements related to solar dynamo action, use measured variability in flow fields at various depths to improve models of magnetic field generation, and characterize the helicity of emergent flux and infer the constraints placed on dynamo models.

1.6.3 SO #3: Explore Magnetic Connections from the Sun Throughout the Heliosphere

The magnetic field structures the corona, solar wind, and heliosphere, but can presently only be measured accurately in the photosphere. To better understand the variability of the solar atmosphere and beyond we focus on these key questions:

- How do systematic and stochastic uncertainties of photospheric field measurements affect models of the solar corona and heliosphere?
- What metrics can be used to validate models of the corona?
- What are the causes and consequences of dynamic coronal magnetic field topology? E.g., how do ephemeral coronal holes form?
- How do photospheric oscillations in magnetic regions contribute to heating of the chromosphere and corona?

Implementation Plan / Tasks

Task 3.1: Explore how well observations and models of coronal conditions match. We will drive MHD and other simulations (e.g., MURaM, Rempel 2017; Cheung et al. 2019; and AWSoM, van der Holst et al. 2014) with HMI time series (E-field inversions; Fisher et al. 2020) to model coronal conditions and synthesize observables, and then compare synthetic observables to AIA imaging for simulated events from the same viewing angle/perspective. In addition to pixel-by-pixel comparisons, we will use computer vision techniques such as convolutional neural nets (e.g., Simonyan & Zisserman 2014) to extract features and to compute structural similarity indices.

Task 3.2: Explore how different methods for disambiguating vector magnetograms affect the field extrapolated in regions with high-gradient neutral lines. We will assess impact on several widely used extrapolation methods and data-driven modeling methods to quantify differences between extrapolated volumetric structures and observations, such as differences between current-density and high temperature morphological features in DEM maps. Then we will compare with observations from DKIST and SO.

Task 3.3: Investigate the association of coronal hole boundaries with supergranulation patterns. One can compare AIA coronal holes with supergranules derived by tracking the granules in HMI intensity images (Attie et al. 2018) to study the evolution of the boundary of the coronal hole. Short-lived ephemeral coronal holes (Inglis et al. 2020 ☺) will be used as an example.

Task 3.4: Explore how oscillations in photospheric magnetic regions heat the chromosphere and corona, and determine how phases of acoustic waves are affected. Various types of oscillation exist in photospheric magnetic regions, and magnetoacoustic waves of certain frequencies can travel upward along inclined magnetic field lines into the overlying atmosphere. By coupling HMI's photospheric observations and AIA's higher photospheric and chromospheric observations, we will track the propagation of magneto-acoustic waves and estimate the energy transport in this process.

1.6.4 SO #4: Reveal the Fundamental Physics of Solar Atmospheric Dynamics and Eruptive Events

Mechanisms of energy storage and release in the solar atmosphere are essential drivers of dynamics of the solar atmosphere, particularly of eruptive events. EM-3 research focuses on these key questions:

- How are magnetic energy and helicity injected into the corona by photospheric changes?
- Why do some ARs evolve to produce major activity?
- What is the impact of a multipolar global coronal field topology on the occurrence of EUV late-phase flares, eruptive events, and coronal rain?
- What role do solar global connections play in producing sympathetic events?
- How do abundances evolve in solar flares?

Implementation Plan / Tasks

Task 4.1: Study the coronal impact of the photospheric injection of magnetic energy and helicity. We will use 12-min HMI vector magnetic field observations to estimate the magnetic energy and helicity injected into the corona and compare with data-driven coronal models (e.g., Fisher et al. 2020; Toriumi et al. 2020). Those results, as well as DKIST flare observations, will be used for the other SO #4 tasks.

Task 4.2: Determine the triggers of Solar Eruptive Events (SEEs). Precursor activity is often observed in ARs before SEEs, such as brightenings of structures suggestive of pre-eruptive magnetic flux ropes seen in AIA 131 Å and DEM maps. We will perform a systematic study of well isolated events to determine whether the trigger is related to an ideal MHD instability, to a resistive process (e.g., runaway reconnection with topological features), or to the double arc instability (Ishiguro & Kusano 2017).

Task 4.3: Investigate the importance of emergence and magnetic cancellation in energizing ARs. Highly eruptive ARs have complex magnetic configurations, so one can study the evolution of complex flare/CME-productive ARs to measure the cumulative emerged and cancelled flux at polarity inversion lines (Chintzoglou et al. 2019) and relate these to AR energy/helicity build-up and SEE productivity.

Task 4.4: Explore the causality between PIL evolution / flares / eruptions. Chintzoglou et al. (2019) and Liu et al. (2019) correlated the onset of flare cluster activity and eruptions with collisional shearing

(strong magnetic cancellation events at PILs during the emergence phase). One can conduct a systematic study of more than 100 ARs to assess predictive potential for flare clusters and eruptive events from measurements related to collisional shearing (HMI) at PILs and formation of flux ropes in the corona.

Task 4.5: Constrain physical conditions in the early phases of shocks in SEEs that could produce SEPs. Magnetic topology of the source region may accelerate particles in different directions and with different efficiency than locations prescribed by the global magnetic topology and swept by traveling shocks. For this study, one can use a combination of global coronal modeling constrained by HMI and AIA observations (for shockwaves).

Task 4.6: Examine the relationship between global magnetic topology and the occurrence of eruptive flares, late-phase flares, sympathetic events, and coronal rain. The complexity of the Sun's magnetic field increases together with activity. More observations of SEEs will test the preliminary conclusions of DeRosa & Barnes (2018), who reported that ARs near open flux regions tend to produce more eruptive flares. We will examine whether EUV late-phase flares are more common in the rising phase of SC 25, as was reported by Woods et al. (2011) for SC 24.

Task 4.7: Examine the physics of late-phase EUV flares. Magnetic topology (e.g. quadrupolar configurations) may be key for explaining late-phase via continued magnetic reconnection during the long restoring phase of the magnetic system (Zhou et al 2019 ☀, Chintzoglou et al 2017 ☀). We will perform MHD modeling (using MURaM with Cartesian domains, and AWSOM with spherical domains) of eruptions in quadrupolar configurations to test whether this leads to late-phase EUV flares. We will further study the spatial distribution and evolution of late-phase flares in SC 25.

Task 4.8: Explore how abundance variations during solar flares behaves differently for various classes of flares and during different phases of the solar cycle. One can use EVE's solar EUV spectra to measure how the Fe, Ne, and other ion abundances change during solar flares observed in Cycles 24 and 25 and explore the cause for observed differences using HMI and AIA observations of magnetic field and corona configurations.

1.6.5 SO #5: Understand Space Weather and Space Climate for Earth and Other Planets

Solar activity drives space weather but understanding the limits of solar variability and how variations ultimately affect Earth and other planets remains uncertain. We must address these key questions:

- How does the location of an active region or eruptive event on the solar disk impact its capability for affecting space weather at Earth and other planets?
- Are long-term solar trends between the solar cycle minima in 2008-2010 and 2019-2021 also observed in Earth's ionosphere and thermosphere?
- How do we improve the far-side magnetic field determination for space weather forecasts?
- How are early-stage CME features (e.g., coronal dimming, EUV waves) observed by SDO related to CME properties in the heliosphere, and how can these be used to improve space weather forecasting models?
- What range of geospace effects results from the full variability of space weather sources on the Sun?

Implementation Plan / Tasks

Task 5.1: Characterize the center-to-limb variation (CLV) of EUV radiation as a function of wavelength for quiet-Sun, active-regions, and flares. The geoeffectiveness of solar photonic emissions is a strong function of wavelength due to the cross-sections of atmospheric species and to the viewing angle of the source (CLV). We will update existing models, such as the Flare Spectral Irradiance Model (FISM), to include CLVs based on EVE data.

Task 5.2: Compare solar EUV irradiance variability between cycle minima and corresponding temporal differences for ionosphere and thermosphere densities. The 2008-9 minimum had lower EUV irradiance levels than the one in 1996. In the EUV, the timing of minimum is a function of wavelength, so detailed spectral comparisons are necessary to investigate differences in the 2008-9 and 2019-20 minima.

Task 5.3: Refine DEM inversions to match soft X-ray observations. Su et al. (2018) reports AIA DEM inversions can infer plasmas up to T~30 MK. This motivates testing whether soft X-ray measurements

synthesized from AIA and EVE DEMs are in agreement with SDO EVE-ESP, GOES XRS, and MinXSS X-ray observations. Extend the Szenicer et al. (2019) deep learning model to output soft X-ray (in addition to EUV) band irradiance measurements.

Task 5.4: Improve global coronal field modeling for space weather predictions, and coordination with PSP & SO. We will perform quantitative comparisons between AIA observations and synthetic images to improve modeling of coronal conditions. The global electric-field derived from HMI vector magnetic field will drive the Coronal Global Evolutionary Model (CGEM, Fisher et al. 2015, Hoeksema et al. 2020) to simulate time-dependent coronal evolution. Important parameters needed for the Eruptive Event Generator Gibson-Low model (EEGGL, Jin et al. 2017) can be determined from SDO observations, such as flux rope helicity measured from HMI SHARPs. Estimating CME speeds using coronal dimming observations (Mason et al. 2016) can enable calculations to be initialized several hours earlier than waiting for LASCO observations.

Task 5.5: Investigate which information derived from SDO measurements is most useful for improving space weather predictions. We will extend coverage of SHARPs into SC 25 to provide training data critical for improving models of flare and CME predictions, and then examine whether additional input features (e.g. flux cancellation or UV brightening at PILs) can improve predictions. We will also investigate machine learning and other statistical methods to calibrate far-side helioseismic images into reliable magnetic flux maps for space weather prediction by comparing with SO far-side magnetograms.

Task 5.6: Characterize the range of solar drivers (EUV flux, solar wind, CMEs) on planetary space weather for different levels of solar activity. With a whole solar cycle of SDO observations available now and the rising phase of SC 25 over the next three years, it is timely to study the space weather effects for different levels of solar activity. One can validate global solar corona and solar wind models driven by SDO data and systematically investigate the solar cycle variability of coronal magnetic complexity, EUV irradiance, mass loss, and angular momentum transport.

The significance of SDO science to the Heliophysics Science Program is reflected in the 2014 Roadmap for Heliophysics³, which identifies SDO as important to 9 of its 13 Research Focus Areas and 11 of 12 Solar and Space Physics Decadal Survey Challenges⁴. SDO's full-disk, multi-domain, continuous coverage supports a extensive range of scientific areas in Heliophysics in general and in solar physics in particular. The traceability matrix in Table 1.2 (on following page) relates the SOs to the Roadmap Focus Areas and the Decadal Survey Challenges.

In summary, the five principle Science Objectives for the Third Extended Mission described above detail some of the critical science that can be performed with SDO data over the FY21-23 time frame.

1.7 Recommendations from the 2017 Senior Review Panel

Recommendation 1: It is recommended that for the next Senior Review the team provide a separate number for publications that derive scientific discoveries principally from SDO data, as opposed to papers in which SDO is referenced in general or as context. While the total number of annual publications associated with the SDO project is impressive, the Panel feels that in order to better evaluate the impact of SDO data on research in heliophysics that this recommendation should be implemented.

A random sampling of 50 papers in the SDO bibliography from 2012 to 2018 was used to determine how frequently SDO data were used in a general or only context. Each paper was examined and given a score between 0 and 3, where 0 meant SDO data were either not used or peripheral to the research and 3 meant SDO was essential to the research. Three of the papers (6%) fell into category 0. One of them was by an EVE Co-Investigator, another was a model study, and the third was a He II 304 study that advocated using AIA 304 in future studies. The other 47 papers had an average score of 2.5 and were judged to have used SDO data in a substantial way.

Based on this analysis, a large percentage of the SDO publications use SDO data in an essential way and there is no need to produce a breakdown of the publications. The SDO bibliography will be purged of these papers and others will be scrutinized before they are added to the publication database.

³ https://smd-prod.s3.amazonaws.com/science-blue/s3fs-public/atoms/files/2014_HelioRoadmap_Final_Reduced.pdf

⁴ <http://www.nap.edu/catalog/13060/solar-and-space-physics-a-science-for-a-technological-society>

SDO SO 1. Track Subsurface Flows and Structures as Activity Rises					
SDO SO 2. Unmask Magnetic Variability of the Solar Cycle					
SDO SO 3. Explore Magnetic Connections from the Sun throughout the Heliosphere					
SDO SO 4. Reveal the Fundamental Physics of Solar Atmospheric Dynamics and Eruptive Events					
SDO SO 5. Understand Space Weather and Space Climate for Geospace, Planets, and Exoplanets					
KEY: Blue X = Essential for Goal/Challenge, Green C=Contributes to Goal/Challenge -->					
NASA 2014 Science Plan Heliophysics Division (HPD) Science Goals					
HPD Goal 1. Explore the physical processes in the space environment from the Sun to the Earth	X	X	X	X	X
HPD Goal 2. Understanding the connections that link the Sun, Earth, planets, outer heliosphere	X	X	X	X	X
HPD Goal 3. Detect and predict extreme conditions in space to protect life and society	X	X	X	C	C
Heliophysics 2013 Decadal Survey (DS) Key Science Goals					
DS Goal 1. Determine origins of the Sun's activity and predict the space environment variations	X	X	X	X	X
DS Goal 2. Determine dynamics and coupling of Earth's magnetosphere, ionosphere, and atmosphere and their response to solar and terrestrial inputs	C		C		
DS Goal 3. Determine interaction of the Sun with the solar system and the interstellar medium	C		C		
DS Goal 4. Characterize fundamental processes within the heliosphere and the universe	X	X	X	X	X
Decadal Survey AIMI = Atmosphere Ionosphere Magnetosphere Interactions					
AIMI Challenge 4. Determine causes for long-term (multi-decadal) changes in the AIM system	C	C	C	C	
Decadal Survey SH = Solar Heliospheric					
SH Challenge 1. Understand how the Sun generates the quasi-cyclical magnetic field	C		C	X	X
SH Challenge 2. Determine how the Sun's magnetism creates its hot, dynamic atmosphere	X	X	X	X	C
SH Challenge 3. Determine how magnetic energy is stored and explosively released	X	X	X	C	C
Decadal Survey SWMI = Solar Wind Magnetosphere Interactions					
SWMI Challenge 1. Establish how magnetic reconnection is triggered and how it evolves to drive mass, momentum, and energy transport		C	C		
Heliophysics Observatory System (HSO) Collaborations					
	SO, Hinode TIMED, MinXSS	SO, PSP, STEREO, Hinode, IRIS	SO, PSP, STEREO, IRIS	SO	SO

Table 1.2: A traceability matrix of the proposed SOs to the Research Focus Areas of the 2014 Roadmap for Heliophysics and the 2013 Solar and Space Physics Decadal Survey Challenges. A **C** means the SO contributes to that research focus area; **X** means the SO is an essential part of that research focus area.

Recommendation 2: *The Panel recommends that an assessment of the mission requirements, including operations and data timeliness, be made with the intent of reducing mission costs. For example, assess the impact of relaxing the percentage of data that is required to be available in near real time. The panel expresses a concern regarding stated negative impacts of flat funding profile on spacecraft operations, data acquisition, data calibration and data processing described in the proposal under in-guide funding levels. This recommendation if implemented will alleviate the impact of the funding profile.*

This recommendation raises two topics, the near real time (NRT) data stream and the mission operations data completeness and requirements. The team discussed both topics. (1) The potential cost savings from reducing immediate availability of the NRT data stream are minor but the impact would be large. This data is not intended for scientific research; however, it is used to monitor instrument health and performance. It is also used to adjust some of the data-reduction parameters for the science level data that becomes available after 4-5 days. A subset of the NRT data is made available to the public, to those using it for space weather monitoring and prediction, such as the NOAA, Air Force, and NASA space weather facilities, and for mission planning. It is kept online for a few weeks for internal use but is not archived. (2) During the extended missions the SDO team reduced the most stringent data capture requirement from 95% of Dopplergrams to 90%. Dropping this requirement below 90% will reduce the accuracy and utility of the Dopplergram measurements. Unlike other data sets, Dopplergrams are not individually useful but are collectively analyzed to measure the properties of the solar interior. Both the spatial and temporal completeness enter into these calculations. The need for complete images drives the reliability requirement of the downlink over short times (approximately the one minute needed to accumulate a TLM file) while the temporal completeness requirement drives the reliability of the antenna-DDS system over longer timescales. Reducing the completeness requirement by small amounts does not similarly reduce the cost of the ground system. Without an onboard science data recorder, we must maintain the downlink at the current, reduced completeness requirement. The 24/7 coverage impacts not only the utility of helioseismology products but also detection and study of solar transient events.

2 Observatory Status and Performance

The SDO spacecraft, instruments, Mission Operations Center (MOC), Flight Operations Team (FOT) at GSFC, and the SDO Ground System (SDOGS) elements are all Green (see Figure 2.1). The only yellow is a redundant IRU, which still leaves the ACS subsystem green.

2.1 SDO Spacecraft Status

SDO Spacecraft Subsystem Status			
Subsystem	Life Rating	Life Expectancy	Discussed?
Command and Data Handling			
Electrical Power System			
Solar Array	5.25 yrs	> 22 years	Yes
Li Ion Battery	10 yrs	> 19 years	Yes
Relays	3850 cycles	100000 cycles	
High Gain Antennas			
Azimuth/Elevation Actuators	5.25 yrs	> 10.5 yrs	
Azimuth/Elevation Encoders	3 yrs	68.5 yrs	
Electrical Contact Ring Assembly	5.25 yrs	>10.5 yrs	
Azimuth/Elevation RF Rotary Joints	5.25 yrs	>10.5 yrs	
Elevation Cable Wrap	5.25 yrs	>10.5 yrs	
Attitude Control System			
Inertial Reference Unit (IRU) 1	5.25 yrs	> 10 yrs ***	Yes
- IRU 2	5.25 yrs	> 10 yrs ***	
- IRU 3	5.25 yrs	> 10 yrs ***	Yes
Star Tracker (ST) 1	5 yrs	> 20 yrs	
- ST2	5 yrs	> 20 yrs	
Coarse Sun Sensors (CSS)	5.25 yrs	> 2.525 yrs	
Digital Sun Sensors (DSS)	5.25 yrs	> 2.52 yrs	
Reaction Wheel (RW) 1	5 yrs	> 22.5 yrs **	Yes
- RW 2	5 yrs	> 22.5 yrs **	Yes
- RW 3	5 yrs	> 22.5 yrs **	Yes
- RW 4	5 yrs	> 22.5 yrs **	Yes
Propulsion			
Fuel	5.25 yrs	> 1200 yrs	Yes
Normally Closed Pyro Valves	10 yrs	20 yrs	
Normally Open Pyro Valves	10 yrs	20 yrs	
Helium Tank	11.5 yrs	> 184 yrs	
Fuel Tank	11.5 yrs	> 46 yrs	
Oxidizer Tank	11.5 yrs	> 46 yrs	
Latching Isolation Valves	5.25 yrs	> 31.5 yrs	
Series Parallel Check Valves	15 yrs	Unlimited	
Thrusters and Thruster Valves	10.5 yrs	Unlimited	
S-band RF			
Omni Antenna	5.25 yrs	> 2.52 yrs	
S-Band Transponders	5.25 yrs	> 2.52 yrs	
K-band RF			
Waveguide Transfer Switch	5.25 yrs	Unlimited	
Ka-band Transmitters	5.25 yrs	> 2.52 yrs	
Thermal			
DDS			
SDOGS			Yes

REF: 464-SYS-ANYS-0252 -- Solar Dynamics Observatory (SDO) Limited Life Items |
** 464-ACS-REVV-0148 -- SDO RWA DCR Presentation Package
*** 464-ACS-ANYS-0050_release -- Limited Life Analysis for the Inertial Reference Unit

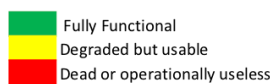


Figure 2.1: All major subsystems of SDO are green for the Extended Mission, with estimated remaining lifetimes exceeding five years. Discussed means system is mentioned in text.

algorithm such that it can be blended with valid gyro data and then as a full replacement to the gyro data if necessary. The development and test effort uses many of the same personnel involved in the LRO effort.

The observatory continues to meet all requirements (Fig. 2.1). All subsystems and components are nominal with the exception of IRU-1. IRU-1 was removed from the control laws and powered off late in 2013. Every quarter, IRU-1 is powered on for 4 days to verify alive ness. There were 3 minor anomalies on the ob servatory:

1) In December 2017, the B-side Power Supply Electronics unit (PSE-B) went through a warm software restart. During this event the application specific software on the unit was re started while the data was maintained. There were no impacts to operations or the observatory during the restart, as designed.

2) In May 2018 the Single Board Computer (SBC) went through a warm software restart. During this event the application specific soft ware on the unit was restarted while the data was maintained. There were no impacts to op erations or the observatory during the restart. It was designed as a “fly-through” event.

3) In March 2019, the IRU-3 current jumped up 19 mA. Both the original and cur rent value are inside the green limits established with the vendor during the investigation into the increase in the IRU-1 current.

SDO is preparing for reduced, and eventually zero, gyro operations. SDO will make use of the recent experience with gyro-less operations on LRO. LRO developed what is known as a complementary filter to replace the failing gyro. The complementary filter utilizes the star trackers and reaction wheels to produce an es timate of the spacecraft angular velocity. The rate estimate replaces the gyro measurement, leaving the onboard Kalman filter essentially unchanged. LRO has been operating successfully without gyros since the beginning of 2018. Initially, SDO will implement this algo rithm such that it can be blended with valid gyro data and then as a full replacement to the gyro data if necessary. The development and test effort uses many of the same personnel involved in the LRO effort.

The FOT performed a reaction wheel speed jitter test in January 2018. This test was designed to determine how fast the reaction wheels could spin before adversely affecting science data quality. In addition, the FOT and Science Teams conducted a “Simulated HGA Failure” scenario. During this event, all space-craft operations, including thruster maneuvers and instrument calibrations were performed as though the observatory only had one working High Gain Antenna.

The spacecraft has used 1 kg of propellant for station keeping and momentum management maneuvers over the last three years. The 382.9 kg of remaining propellant suffice to maintain the SDO orbit and pointing as long as the spacecraft is operational in addition to raising the spacecraft into the final disposal orbit. A review of the on-orbit aging of the solar panels and battery indicates that there is sufficient margin to operate past 2026 with the current power system load.

2.2 SDO End of Mission Plan

The SDO End of Mission Plan (EOMP) was reviewed and accepted by HQ (App. C). To update and further validate the EOMP, GMAT orbit propagation software was used to determine the maximum achievable semi-major axis (64,500 km) and maximum change to the inclination ($\sim 10^\circ$). These calculations were constrained only by the amount of propellant remaining on-board. The minimum disposal semi-major axis is 42,472 km (J4.6.5.11.1.1, NASA-STD-8719.14b). A matrix of semi-major axes and inclination angles was constructed, and a parametric analysis was performed to obtain viable disposal orbits. The orbit of each set of orbital elements was propagated for 100 years to model the long-term perturbations of each orbit. Orbit whose lifetime eccentricity values exceeded 0.0008 or were impossible to reach due to fuel limitations were discarded. As a result of this analysis, basic maneuver plans exist for all viable candidates.

2.3 Mission Operations Status

The FOT currently staffs the MOC 12 hours per day, Monday through Friday with personnel on call to support spacecraft and instrument issues. FOT support for the SDO was designed to make effective use of automation to reduce labor. While the observatory provides a continuous flow of solar data to the users, the spacecraft, the MOC and SDOGS are largely autonomous. The robustness and redundancies in the SDOGS, including some critical computer refreshes, have reliably provided the high-rate SDO data with very few losses over the 10 years of the mission so far.

2.4 SDO Ground System (SDOGS) Status

SDOGS continues to track the observatory 24x7. There were only two anomalies of note in EM-2:

- 1) Lightning strike of the SDO-2 antenna in June 2017. Due to the excellent work of our WSC Operations and Maintenance Team, along with an ample supply of spares, the antenna returned to operations in less than 2 weeks.
- 2) Failure of the Antenna Controller Assembly (ACA) Single Board Computer (SBC) in SDO-1 in April 2019. **Our only spare was installed**, and the antenna returned to operations the same day. Both ACAs have been in service since 2006. The spare SBC was installed in the antenna system in 2018 to verify its viability as a spare. An upgrade of the ACAs is included in the Over-guide Budget Proposal.

In 2018, the Range, Receive, Command Processors were refreshed with new plug-n-play units from the original vendor. These units receive, decode, and decommute the S-band (engineering & housekeeping) data; send commands to the observatory; and perform ranging operations with the observatory.

In 2019, the tracking receiver SBCs were refreshed with newer models. Two were installed in the operational units (one at each antenna) leaving three boards available as spares. The two SBCs removed from the tracking receivers were updated to become spare SBCs for the Antenna Controller Assemblies (ACAs). This is important as the lone, original spare was installed in SDO-1 in April 2019.

2.4.1 Data Distribution System

The SDO Data Distribution System (DDS) continues to receive, record, and forward the science data to the Science Operations Centers (SOCs) without interruption. The front ends of the DDS are the High Da-

tarate Receivers (HDRs). The HDRs receive, decode, and decommute the science data from the observatory. These HDRs were replaced in 2018 with newer plug-n-play hardware from the same vendor. The new HDRs have a life expectancy of at least 10 years before the vendor may not support their maintenance.

2.4.2 SDO MOC

The MOC continues to support all aspects of SDO flight operations without any problems. Looking ahead, all Linux machines in the MOC use the Red Hat 6 OS. To move away from Red Hat 6, the MOC will either have to update the hardware in the MOC to components that can support Red Hat 7 or move all workstations into the Virtual MOC (VMOC) 2.0 and replace the existing hardware with thin clients to access the virtualized machines.

2.5 Instruments and Science Operations Status and Performance

All SDO Instruments and Science Operations Centers (SOCs) have performed exceptionally well during EM-2 and are expected to perform well during EM-3. The only significant instrument anomaly, a shorted capacitor in the EVE MEGS-A CCD electronics, occurred in May 2014. This means there will be no MEGS-A science data during the rest of the mission. The EVE MEGS-B and ESP irradiance measurements continue during EM-3 and can address all of the original Level 1 requirements for EVE observations without MEGS-A.

2.6 AIA Instrument Status and Performance

AIA instrument health and performance are excellent; the instrument performance meets the requirements set by the original science goals and is expected to continue to do so throughout the mission extension. In seven of the nine UV/EUV wavelength channels, sensitivity has degraded by 10-60% (median: 30%) over the first 11 years of the mission, with degradation e-folding time scales greater than 15 years. Only the 304 Å and 335 Å channels have shown larger sensitivity loss; these are the wavelengths anticipated to be most affected by molecular contamination. The 304 Å channel throughput fell rapidly early in the mission, declining by a factor of three in the first 18 months of operation. Following a series of detector bakeouts in 2011 and one bakeout of the mirrors, the rate of sensitivity loss decreased substantially and leveled off in recent years; as of early 2020 the throughput is at approximately 6% of its initial value. The 335 Å channel sensitivity has fallen fairly steadily throughout the mission and is now at 15% of its initial value. Corrections to the response functions to account for throughput loss for all channels are regularly updated and are provided through SolarSoft for use by the community.

Throughput in the 304 Å and 335 Å channels is now decreasing with an e-folding time of approximately 3.5 years (Figure 2.2). In both channels, the signal-to-noise ratio remains ample for AIA to meet all of its science goals without a need to change the exposure durations or image cadence. The 304 Å channel is centered on the brightest EUV line in the solar spectrum, and still produces excellent, high-contrast images over the whole solar disk. The 335 Å line generally targets emission from flares and hot active regions with a high emission measure, and the data from such regions remains excellent.

Should instrument throughput become a concern during EM-3, we have the ability to perform CCD bakeouts. Six bakeouts were conducted between the start of operations and April 2012, and they produced a substantial recovery of the 304 Å and 335 Å channel sensitivities. We have not performed a bakeout since April 2012; the sensitivity is adequate, so it has been preferable to avoid complicating the instrument calibration by imposing discontinuous changes in throughput that can only be approximately calibrated through comparison with EVE and other spectroscopic information.

In all other respects, AIA remains entirely healthy. AIA uses 13 mechanisms (a shutter, filter wheel and focus mechanism on each of the four telescopes, and an aperture selector on one of them), each of which has performed approximately 54 million moves so far. The mechanism life tests covered 66 million moves for the focus mechanism, and over 80 million for the other mechanisms, without any failures. None of the mechanisms has shown any change in current draw, move time, or any other behavior while on-orbit. Therefore, we anticipate that these 13 mechanisms will continue to perform excellently throughout EM-3.

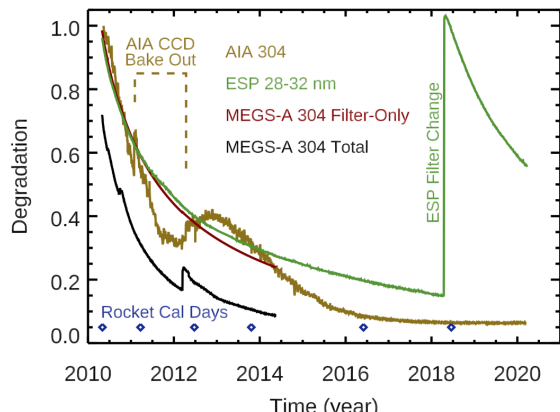


Figure 2.2: Degradation for He II 304 Å emission in the AIA and EVE channels over the SDO mission. The AIA degradation (gold) is based on transferring the EVE calibration to AIA. The ESP (green) and MEGS-A Filter-Only (red) degradation trends are based on the in-flight daily calibrations with the redundant filters. The MEGS-A total degradation (black) trend includes the filter-only degradation and long-term trending that is only possible with under-flight calibration measurements (diamonds).

nificant changes since our initial measurements during instrument commissioning. In summary, with none of its subsystems showing any sign of degraded performance, and with AIA having no consumables or limited-life items, there is every reason to expect that AIA will continue meeting its science requirements for another ten years.

Two classes of electronic upsets have caused brief interruptions in the steady flow of data from AIA. Both are likely attributable to cosmic ray hits, although it is difficult to establish this definitively. The first affects the camera interface board and causes corruption in the image data from the affected camera until a reset is performed. There have been 11 occurrences of this upset distributed across two of the four AIA cameras (and 14 on the two HMI cameras, which are identical). While the root cause has not been identified, the frequency is low and the recovery procedure is straightforward (the affected camera has been reset typically within a few hours), so this is not a threat to the data completeness budget. There have also been eight occurrences of single-bit errors in the data compression tables, which have the potential to cause minor errors in the image data but are again straightforward to clear and a large fraction of the affected images can also be corrected in the data processing pipeline later. Over the entire mission, these infrequent anomalies have caused the equivalent of six days of lost or degraded data.

2.7 EVE Instrument Status and Performance

The EUV Variability Experiment (EVE) continues to make solar SXR (0.1-10 nm) and EUV (10-122 nm) irradiance measurements. The EVE suite of instruments includes the Multiple EUV Grating Spectrographs (MEGS-B) covering 33.2-105 nm and the EUV SpectroPhotometer (ESP) with five bands in the 0.1-40 nm range. The MEGS-B also includes a photometer for H I 121.6 nm.

The ESP continues to provide accurate, high time-cadence (0.25-sec) irradiance data in five SXR-EUV bands. With its high reliability and low latency for its Level 0C space weather data product, ESP has proven useful for space weather operations at NOAA SWPC and Air Force Space Command as backup data for the GOES XRS (Hock et al. 2013) and SOHO Solar EUV Monitor (SEM) bands. Although the MEGS-A CCD failed in May 2014, EVE ESP and AIA cover the MEGS-A spectral range of 5-37 nm, but with less spectral resolution than MEGS-A.

The MEGS-B channel provides solar EUV spectral irradiance data at 0.1 nm resolution for the 33-105 nm range. Because there was unexpected degradation of the MEGS-B CCD at first light, MEGS-B

The image stabilization system (ISS) requires periodic calibration due to seasonal changes in the angular size of the Sun throughout the year, but the signal levels on the visible-light guide telescope have been steady and we have not had to retune the ISS for any degradation.

The optical performance of the four main telescopes has not changed noticeably, and the telescope focus has gradually settled to approximately half a depth-of-focus away from its initial value. The transmission of the thin-film entrance filters is gradually increasing due to micrometeorite strikes; this has resulted in the appearance of stray light in the 4500 Å channel. However, this channel is only used once per hour to verify alignment with other solar instruments. The nine EUV/UV channels use filters mounted in a wheel behind the optics to reject visible light, and stray light remains at least three orders of magnitude below the threshold of detection in those channels. Finally, the CCD characteristics (dark current, bad pixels, and flat-field pixel-to-pixel variation) are measured roughly quarterly and have not shown significant changes since our initial measurements during instrument commissioning.

observations have been limited to 3-6 hours per day since July 2010 in order to provide a long lifetime (>20 years) for MEGS-B observations. The MEGS-B cadence was 10-sec from 2010-2018 and is now 60-sec to improve the signal quality for low signals of solar EUV spectra during EM-2. The EVE team developed new flight software in 2015 to automatically activate MEGS-B observations when ESP measurements indicate that an M-1 or larger flare is starting. This autonomous flare detection algorithm has proven effective to allow the maximum coverage for the larger flares while still limiting MEGS-B exposure for a long mis-

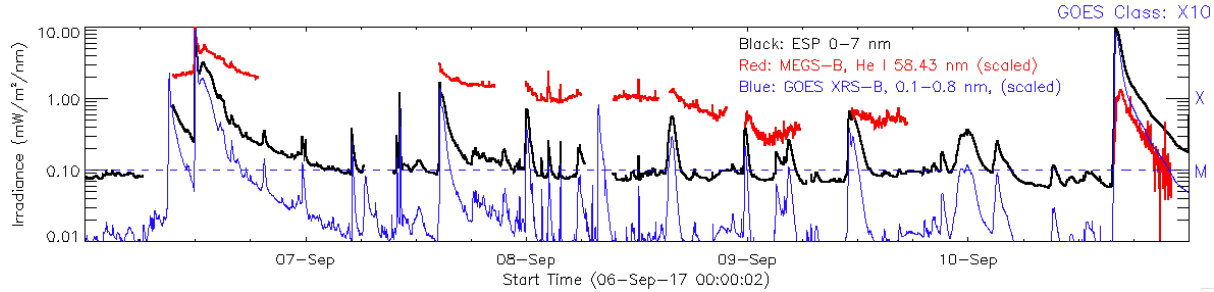


Figure 2.3: Example of EVE MEGS-B Flare Campaigns for the Many Flares on September 6-11, 2017. The MEGS-B campaigns are triggered realtime based on EVE ESP signal level and having a positive slope. EVE ESP (black) observed 17 M1.0 or larger flares during this period, and MEGS-B (red) campaigns observed 11 of those flares (65%). The gaps in the ESP are from seasonal SDO orbit eclipses (<70-min per day). The GOES XRS (blue) is also shown along with its M1.0 level (blue dashed line).

sion. Since being implemented, the algorithm has allowed EVE to observe 21 of the 32 M2-9.9 class flares (66%) and all 4 of the X-class flares (100%) that have occurred. An example of a MEGS-B autonomous flare campaign is shown in Figure 2.3.

It is critical for EVE to provide *calibrated* solar SXR-EUV irradiances for studying the solar influence on Earth's ionosphere and thermosphere. There are daily onboard EVE calibrations to track the degradation of the filters with redundant filters and to measure any relative changes of the CCD pixels with LED flatfield lamps. These onboard calibrations track exposure-related degradation effects, but they do not track all degradation effects seen in Figure 2.2. To address these effects, the EVE calibration plan includes underflight rocket calibrations using the prototype EVE. These occurred in 2010, 2011, 2012, 2013, 2016, and 2018; the next one is scheduled for Oct. 2020. In between each rocket underflight the instrument is calibrated at the NIST Synchrotron Ultraviolet Radiation Facility (SURF-III) in Gaithersburg, MD, achieving an accuracy of about 10%. During EM-3, we propose to continue flying an SDO underflight calibration rocket every two years, with a flight in June 2022 and with calibrations at NIST in 2021 and 2023. The EVE calibration underflights have also benefited the calibration and validation of 15 other SXR and EUV solar instruments aboard GOES, Hinode, ISS, PROBA2, SDO, SOHO, SORCE, STEREO, MAVEN, and TIMED.

2.8 HMI Instrument Status and Performance

Since the start of the science mission on 1 May 2010, HMI has been in almost continuous operation and has taken more than 150 million images. The vast majority of gaps in coverage are caused by planned spacecraft maneuvers and eclipses. Data recovery has been better than 99.95%, with losses caused primarily by issues at the SDO ground station (typically high winds). The science-quality 45-second cadence Dopplergram coverage is 97.7% over the entire mission and 97.7% in EM-2.

A variety of calibration data are taken at regular intervals to monitor and maintain the HMI performance. Twice daily, sets of images are taken to monitor the instrument throughput and image plate scale. Weekly and bi-weekly internal observing sequences are run to determine the optimal instrument focus and tunable-filter settings and update the small-scale image flatfield. The large-scale image flatfield is determined quarterly in conjunction with spacecraft off-point maneuvers. The HMI optics package has active thermal control that is monitored and adjusted to maintain an optimal operating environment. The HMI image focus is maintained at a roughly constant value by adjusting the thermal control of the HMI front window. On 16 October 2018, the best focus position was changed from focus step 11, where it had been maintained up to

that point, to focus step 10. This was achieved by increasing the temperatures on the front window and telescope tube. This was done because thermal control near perihelion was becoming difficult. The higher operating temperatures have allowed more consistent control of the HMI front telescope. Radiation darkening of the optics has caused an anticipated decrease in the end-to-end transmission of the instrument. The decrease through the Prime Mission was determined to be approximately 15%, but the rate of degradation has slowed, and the decrease in transmission to date is now 25%. There is still sufficient margin to increase exposure times to maintain uniform signal intensity as degradation continues. Due to the aging of the optical components, the optimal tunings of the Michelson interferometers change slowly with time, and this is corrected for every 6 to 12 months. The current trending plots for the HMI instrument can be found at http://jsoc.stanford.edu/doc/data/hmi/trend_plots/. The effort to better understand the source of the ~1% error in line position sensitivity that is the source of the 12- and 24-hour variations in Doppler and magnetic field measurements is continuing. The front window temperature daily variation has been reduced as part of compensation for window degradation increasing its temperature. In January 2020 during the semi-annual SDO 360° roll for solar shape measurements additional calibration data was obtained to verify the expected reduction in daily variation of the filter profiles.

On 17 Aug 2018, a diagonal dark band suddenly appeared at the upper-left edge of the image, visible in both cameras. Analysis of this anomaly has led us to believe that the artifact is likely caused by a fracture in element E4 of the Lyot filter. The primary effect of this artifact is a small decrease in image brightness at that location, which is corrected for with an updated flatfield. A secondary effect may be scattering of light from the affected area to other parts of the image, but this has not been detected. The artifact only affects the edge of the solar disk at high latitude and therefore has no impact on most science uses of the data. It is not known what caused the crack to form. No anomalies in instrument or spacecraft telemetry were noted at the time and we continue to monitor the situation.

HMI's normal operation has been interrupted a few times during EM-2. HMI experiences occasional anomalies due to corruption of onboard tables or software that results in corrupted data from one or the other camera. These issues are quickly dealt with by reloading the relevant tables and, if necessary, restarting the affected camera's electronics. There have been ten such events in EM-2.

Aside from these occasional interruptions, the HMI instrument continues to perform extremely well on-orbit. There is no indication that HMI will have any difficulty operating for five to ten more years.

2.9 Instrument Operations and Data Center Status

Table 2.1 provides a summary of the volume of SDO archived intermediate and final science data. Section 7 of the SDO PDMP (App. A) has additional details about the data volumes and status.

Data Products	Volume
AIA Level 1	2400 TB
AIA, higher level	1400 TB
HMI Level 1	3100 TB
HMI Level 1.5 and higher	3010 TB
EVE Level 0b	98 TB
EVE higher level	1.5 TB

Table 2.1: Data archived through FY 2020.

2.9.1 JSOC-IOC Operations

The SDO AIA and HMI instruments are run out of the JSOC Instrument Operations Center (JSOC-IOC) based at LMSAL. Both continue to run smoothly. The JSOC team performs weekly calibrations of the HMI instrument and bi-weekly calibrations for the AIA instrument. These calibrations include flatfields, long exposures, focal plane filter and entrance filter checks, as well as detunes for the HMI instrument. Monthly calibrations include AIA focus sweeps and AIA/HMI

diagnostic data collection. In addition, a bi-monthly AIA guide telescope/PZT calibration is conducted. The onboard clocks for both instruments require routine monitoring and adjustment. Eclipse season occurs twice a year for SDO and requires thermal adjustments for both AIA and HMI. The team meets before each eclipse season to discuss strategy, and after eclipse season to discuss lessons learned. Both the MOC and EGSE Alert Notification Systems (ANS) continue to function well and provide remote and continual monitoring for the instruments.

The JSOC team conducts internal weekly planning meetings and participates in the weekly GSFC FOT telecon. The health of both the AIA and HMI instruments is closely monitored with twice-daily checks. In

addition, the health and safety and the long-term trending websites have proven beneficial for monitoring not only the instruments, but in helping to monitor the health of the SDO spacecraft. The JSOC team works closely with the FOT in monitoring the health of the AIA and HMI instruments by conducting regular, roughly every six months, reviews of the trending data. The JSOC team monitors the instrument not only during normal working hours, but also on weekends and provides emergency support 24/7 for both the AIA and HMI instruments. For the foreseeable future, the operation of the HMI and AIA instruments from the JSOC should continue to be straightforward. The AIA team has continued to bring on new members to the operations team with the intent of increasing the depth of coverage and knowledge.

Health & Safety: <http://jsocstatus.stanford.edu/hk/SDOStatus/index.jsp>

Long-Term Trending: http://jsocstatus.stanford.edu/hk/long_term_trending/aia/temperatures.html

2.9.2 EVE Operations

The current EVE operations are ready to support the EM-3 science goals. EVE operations include weekly planning uploads, daily data processing, and data distribution; these are mostly automated at the EVE SOC at CU/LASP. The EVE public data products (currently Version 6) include photometer irradiances at a 0.25-sec cadence as Level-1 products, the MEGS spectra and extracted emission lines with 10-sec and 60-sec cadence as Level-2 products, and daily averages of these Level 1-2 products as the Level-3 products. The EVE team also provides NRT Level-0C products of ESP data and MEGS spectra with latency as low as 5 minutes to NASA, NOAA, and Air Force space weather operations. The next version of EVE products will be released soon and will include the latest rocket calibration measurements.

2.9.3 JSOC-SDP Operations

The JSOC Science Data Processing (JSOC-SDP) center at Stanford University receives HMI and AIA raw telemetry from the DDS and archives two copies to LTO6 tapes. The raw data are processed to reconstructed images (Level-0) then to corrected images (Level-1) for both HMI and AIA, all of which is archived. The Level-1 data are the primary science data for AIA and are provided to the JSOC-AVC at LMSAL. HMI science data consists of magnetograms, Dopplergrams, etc., that are generated from the Level-1 and then archived. Most HMI science data are available for space weather use 15 minutes after receipt and in final form within five days. Additional higher-level processing is required for some HMI science data products, including helioseismic subsurface flow maps, global internal rotation, meridional flows, and vector field products including the detailed analysis of the disk passage of each emerging magnetic patch. Most higher-level products are available a day or so after the input data is available.

A processor cluster is available for research computing by local and remote users. On-line storage is provided by file servers totaling 4100 TB. The 18,000 TB of archived data reside on 2200 LTO4/LTO6 tapes in an automated library and the rest stored nearby. An additional 4600 TB of redundant telemetry data are archived offsite. The SDO tape archive grows at ~6 TB/day. The JSOC system stores image and processing metadata in a PostGreSQL database. The JSOC-SDP also houses the SOHO/MDI resident archive, the IRIS mission archive, and the DSX/BBR instrument archive (not supported with SDO funds).

The JSOC-SDP distributes the HMI and AIA science data to the community. In 2019, the JSOC-SDP automated web services processed, each month, approximately 41 K export requests for 25 TB of image data in approximately 7.7 million FITS files. 5.4% of these export-system requests involved additional user-requested processing. Including the data distributed to remote NetDRMS data centers, the SDP distributed about 100 TB each month. The JSOC web portal supported requests from approximately 275 K distinct IP addresses. Remote NetDRMS systems have been set up at 19 sites in eight countries (USA, Germany, France, Belgium, UK, South Korea, Sweden, and United Arab Emirates). The distribution rate to remote NetDRMS sites averages approximately 2.5 TB/day. The remote centers distribute the SDO data as well. Two of them, NASA GSFC's Solar Data Analysis Center and The National Solar Observatory, serve as Virtual Solar Observatory (VSO) data providers of SDO data. Each month, the VSO serves approximately 13 TB of SDO data via 1.3 million file requests. AIA data images and movies and cutouts are also available via web and SolarSoft services from the JSOC-AVC at LMSAL.

A system comprising over 1000 processors, 4100 TB of disk, >13000 tapes, and that manages several billion files occupying 18,000 TB of storage requires continual care and maintenance. In accordance with the ongoing maintenance plan, as the mission has progressed and computing hardware has aged, the hardware has been upgraded and replaced. Currently, the various subsystems (data capture system, processing clusters, database servers, file servers, tape drives, web servers, and infrastructure hardware) are at varying stages in their lifespans. A major upgrade of storage (hard drives and solid-state drives) will be needed in the next two to four years. At that time, 2000 TB of new storage will be needed to replace 1000 TB of aging disks, and to provide 1000 TB for data growth. The four database servers are expected to last another three years, at which time they will be replaced as well. Replacement of the 11-year-old web server is imminent. Other infrastructure servers are needed as well – one or two machines hosting multiple virtual machines will suffice. Finally, the home-directory server plus backup system needs to be replaced.

A proactive approach to hardware maintenance is critical. Occasional and unexpected disruptions due to file server and other hardware failures, and power and cooling outages, among other events, occur. JSOC-SDP staffing is limited – a support staff of eleven members at launch is now only five at present, and certain critical skills are possessed by only a single member. As such, recovery from hardware failures can cause data-availability delays that range in time from several hours to over a week. A single file-server crash requiring restoration of data from tapes could require near full-time attention from a single operator for a period of a couple of months. Although no data have ever been lost, downtime due to hardware failure stretching thin staffing can be significant. Keeping hardware in good condition is essential to keeping data flowing promptly.

2.9.4 JSOC-AVC Operations

The JSOC AIA Visualization Center (JSOC-AVC) exists to help researchers find data sets relevant to their topics of interest; to serve as an open forum where solar/heliospheric features and events can be reported and annotated; to facilitate discovery of statistical trends and relationships between different classes of features and events; and to avoid overloading the SDO data systems. To achieve these goals, the HEK consists of registries to store metadata pertaining to observational sequences (Heliophysics Coverage Registry, or HCR), heliophysical events and informatics data products (Heliophysics Events Registry, or HER), and browse products such as movies. Interfaces for communications and querying between the different registries are also provided by web services. The Event Detection System (EDS) autonomously orchestrates a variety of feature and event detection modules in order to populate the HEK with events from SDO data. The AIA science team also inspects all AIA data to add events that are missed by the automated methods.

The Helioviewer tools at <https://www.helioviewer.org> provide access to HMI and AIA data through the 36-second cadence jpeg2000 images generated at the JSOC-AVC and stored in the JSOC-SDP and Helioviewer archives. Web-based and local Java tools are provided to examine and combine solar data in a convenient form. They also have interfaces to query the HEK and display the solar events captured there. Some science and a great deal of public access are accomplished using these tools including 3.5M screenshots and 95k movies made in 2019.

3 Budget

We propose an over-guide budget for SDO's Third Extended Mission that accounts for the expected 3% inflation over the mission and for addition of one junior scientist at each institution to support highly needed calibration/validation efforts, restoration of some of the daily operations support lost during EM-1, and partial support of the new SunPy software library being developed for NASA solar data sets. The new requirements placed on the missions to support the science plan, write CMADs, and update the PDMP have also contributed to an over-guide budget request.

3.1 Plan for Requested Over-guide Scenario

Mission Operations: During the extended missions the data completeness requirement has been reduced to 90%. The minimum advisable level will be maintained for the FOT and system administration team that will staff the MOC one 8-hour shift each day. One person will be on-site at the SDO ground station Monday

through Friday. Nights and weekends will be supported in an unattended mode, and handovers and eclipses will not be staffed. SDO has been running in a robust and reliable unattended mode since soon after launch. The Alert Notification Service (ANS) has been used to notify essential people in the event of an anomaly within the observatory. Anomalies are assigned according to established and agreed-upon guidelines. Spacecraft anomalies receive a more urgent response than ground system anomalies.

The MOC will continue to produce mission support data products (e.g., orbital files, instrument and spacecraft timelines), and distribute them via the web. Routine health and status monitoring and trending of spacecraft housekeeping data will remain the same. Instrument commanding will be restricted to Monday–Friday, as it is not supported in unattended mode. Engineering team support is on an as-needed basis.

Ground System: The SDO ground system will continue to provide the services and level of reliability needed to meet the SDO science objectives during EM-3. The SDOGS and DDS will continue to provide primary ground station services; **the cost of their services must be completely covered by the SDO budget.** No significant changes are planned to the computer infrastructure used to operate the mission and process data; however, normal upgrades to disk space and tape backup capacity are planned to continue to provide a reliable system for the operations and science teams. System administration and ground software support are planned to provide ongoing maintenance for the operational systems. Maintenance contracts will be continued for critical hardware and software elements.

SDO Data Delivery System (DDS): During EM-3, the DDS will continue to receive and forward telemetry files to the SOCs. Necessary and required upgrades and replacements continue to be made with a minimal impact on operations.

Instrument Teams: The instrument teams will operate the instruments, accept data from the DDS and continue the automated processing and distribution of SDO data products. Science data analysis will be supported to perform the science plan, concentrating on the SOs described in Section 1.5, but recognizing that most of the SO progress will need to come from outside funding sources. Funding to replace aging computer systems and to buy more tapes and disks is included in the budget. The rocket underflight calibrations with the prototype EVE are planned to fly in Oct. 2020 and June 2022.

SDO Science Data Archive: Final delivery of SDO science data to a long-term NASA archive will be conducted as part of the completion of the mission data analysis period and is described in the Mission Archive Plan submitted as part of this proposal.

3.2 In-guide Scenario and Impact Assessment

The Extended Mission investigation described above is for the over-guide mission scenario. The in-guide scenario would continue the flat budget of \$12M per year in place since the end of Prime Mission. With a flat budget, the work effort must be reduced each year. Combining a flat budget and a 3% inflation rate, then the work effort reduction would be 20% over six years. There would need to be a reduction in force (RIF) of one FTE of effort out of five every six years. The over-guide budget includes a 3%/year inflation rate so that additional RIF action is not required during EM-3.

The in-guide scenario would also not support the addition of four post-docs for the SDO project (one per institution) as planned in the over-guide budget. This modest addition over the in-guide budget would support highly needed calibration/validation efforts, restoration of some of the daily operations support lost during the previous extended missions, and for partial support of the new SunPy software library being developed for NASA solar data sets. The required writing of CMADs is also budgeted for each instrument team. The impacts without this support are described more in the following subsections.

3.2.1 Mission Operations Over-guide Impact

An upgrade of the ACAs at both SDO1 and SDO2 is proposed in the Overguide Budget Request. We evaluate the ACAs to be the most likely source of unexpected SDOGS downtimes and SDO science data losses in the coming years if they are not refreshed. Discussions with vendors have been occurring over several years to assess the feasibility of various upgrades and replacement options. It is our judgement that the time to address this issue is at hand, since a suitable hardware system is now available from the original

vendor that is compatible with the SDOGS hardware and that has been successfully installed at other facilities. A quote from the ground station manufacturer indicates that each ground station will require one year from receipt of order to final testing, with approximately three weeks of antenna downtime during installation. The cost will be approximately \$850,000 per antenna, for a total of \$1,700,000. If the requested funding is approved, we would upgrade the SDO2 antenna first in one fiscal year, and then upgrade the SDO1 antenna in the following fiscal year.

3.2.2 AIA Over-guide Impact

The AIA over-guide request consists of two parts. The first is to establish an AIA *Science Lead* position. The Science Lead will be the principal developer of the AIA team's open-source software to support scientific data analysis. In this role, they will coordinate with the SunPy consortium to develop and maintain the SunPy affiliate software package *aiapy*. They will also be responsible for developing data analytics solutions for high performance computing (e.g. at NASA supercomputing facilities) and commercial cloud computing systems. The Science Lead will also work closely with the SDAC to support prototyping and testing of the end-of-mission archive. The Science Lead will be trained by the AIA PI (Mark Cheung) and Instrument Scientist (Wei Liu). The AIA team proposes to hire Will Barnes for this position. Barnes is a core member of the SunPy consortium, has led the initial development of *aiapy* and has worked with NASA High-End Computing (ARC) staff to develop SDO processing tools that scale to thousands of CPUs (Barnes, Cheung & Bobra 2019 ☺). The second component of the over-guide request includes a growth of the budget to include yearly inflation at 3% per annum and enables the AIA investigation to maintain an experienced core team, whose main tasks are operating the AIA and HMI instruments, data calibration, some science (SDO science is mostly supplemented by external grants) and the production of AIA CMADs (budgeted at 0.7 FTE/year). Under the in-guide budget, the continued erosion of FTE support will eventually lead to a reduction in operational experience and institutional memory.

3.2.3 EVE Over-guide Impact

The over-guide budget includes 3%/year for inflation; support for the writing, updating, and approval of the EVE CMADs; moving toward an open source code environment, and 1.0 FTE of support for the EVE science team. The science support would cover the conversion of EVE SolarSoft IDL code to Python code for the SunPy project, support the EVE team in daily operations and calibration rocket underflights, and work on additional science tasks addressing the newly proposed Science Objectives but not scoped in the in-guide budget. For example, this EVE science team could explore new models of the solar EUV irradiance based on HMI magnetic field images for SO 2 & 5, study EUV late-phase flares for SO 5, compare solar cycle minima irradiances for long-term solar changes for SO 2 & 5, and/or evaluate abundance changes in the EVE spectral lines for studying coronal heating and flare magnetic reconnection physics for SO 4. The impact for being funded at the in-guide budget is the loss of the SunPy conversion, the inability to produce the updated EVE CMADs and open source code, stress on the EVE team to perform the daily operations and calibration rocket activities with less funding every year, and/or RIF of one of the current EVE team members to account for an essentially decreasing funding profile with the loss of the inflation adjustment.

3.2.4 HMI Over-guide Impact

The HMI over-guide budget has three components: 1) inflation adjustments to maintain the size of the core operations and science team at present levels (e.g. the HMI PI is cut to < 50% for the in-guide budget); 2) additional post-doc support to ensure that personnel retirements expected in the next three years do not compromise the integrity of HMI science goals and JSOC operations; and 3) effort to develop the now required CMAD to be developed in FY 21 and FY 22. The present minimum effort-level required for the SDO-JSOC and for HMI-team support of instrument operations is about 7.2 FTE. Even at this level the team is stretched thin for critical tasks. The in-guide FY 21 budget supports 5.8 dropping to 5.0 FTE for ops and < 4 FTE of science staff and 2 post-docs for SO science including scientific validation of the data products. Without inflation adjustments, two team members must be cut over the 5-year budget. Even after accounting for accelerated retirements of senior personnel, the JSOC staffing must decrease below a long-term sustainable level in FY 21 and a layoff is required in FY 23. This would mean that some of the SOs

will not be completed with SDO support. In the over-guide plan one additional junior staff member joins the team in FY 21 to allow time for training and to assume increasing responsibility for data-user support, to enable tailored data products for Parker, Solar Orbiter, DKIST, and other HSO elements, help with calibration improvements of HMI science data, and contribute to Solar Orbiter science goals.

3.3 GSFC Science Over-guide Impact

GSFC requests support for a post-doc in the over-guide budget. We have been supporting a graduate student, who has finished their PhD and moved on, some part-time research scientists, and the development of Helioviewer. We want to hire a NASA Postdoctoral Program Fellow to work on a project relating coronal holes to supergranulation that uses SDO data. Allowing for inflation helps retain the workforce used to run SDO, the SDO website, and special data events as they arise. Effort is requested to support the writing and review of the CMADs related to data served by GSFC and to assist the instrument teams.

3.4 Budget Detail Explanation

This proposal is an over-guide submission. Section 3.2 details how the small requested over-guide budget yields a large science reward. As shown in Table 3.1, we have asked for over-guide budgets increases from 14-24% for the EM-3 described by this Senior Review and WYE increases of 18-21%. This small increase in funding results in a significantly larger group of scientists working on SDO data validation studies and forefront scientific research, as well as to reduce attrition of the highly trained team members from the SDO team. Inflation, enhanced science research, CMAD production, and the ACA upgrade are shown as separate items. No Work Effort is included for the ACA upgrade as it will be procured.

Table 3-2 shows the anticipated HEC resources. The AIA resources have been requested; the HMI resources will be requested later this year.

Table 3.1: Budget Details (\$1000k)						
		FY21	FY22	FY23	FY24	FY25
In-guide		\$12,000.0	\$12,000.0	\$12,300.0	\$12,300.0	\$12,300.0
Over-guide		\$156.0	\$421.3	\$703.2	\$991.2	\$1,289.3
Inflation		\$717.0	\$742.2	\$764.4	\$787.1	\$810.3
Science		\$810.9	\$830.8	\$609.4	\$0.0	\$0.0
CMAD		\$850.0	\$850.0	\$0.0	\$0.0	\$0.0
ACA		\$2,537.9	\$2,850.3	\$2,086.3	\$1,791.8	\$2,115.5
Subtotal		\$14,538	\$14,850	\$14,386	\$14,092	\$14,415
Total						
Difference		21%	24%	17%	15%	17%
Work Effort (Work-Year Equivalents)						
In-guide		37.0	36.3	35.6	34.9	34.2
Over-guide		0.00	0.71	1.42	2.08	2.73
Inflation		4.20	4.20	4.20	4.20	4.20
Science		2.60	2.60	1.90	0.00	0.00
CMAD		6.80	7.51	7.52	6.28	6.93
Subtotal		43.8	43.8	43.1	41.2	41.2
Total						
Difference		18%	21%	21%	18%	20%
Table 3.2: HEC Resource Requests (Estimated Standard Billing Units [SBUs])						
		FY21	FY22	FY23	FY24	FY25
SMD-20-99125391 (AIA)		100000	120000	144000	172000	200000
HMI		80000	80000	90000		

SDO is unique in having its own dedicated ground system. Over 10% of the Mission Operations budget is for anticipated repairs of equipment related to the antennas and ground system at the WSC. All of these fixed costs and mission services can only be managed and are included in the budget.

Even with a constant budget for almost five years, the SDO team collected, archived, and served one of the largest scientific data sets in the world. The team produced excellent research and supported research by scientists around the world. We believe this over-guide proposal will keep SDO producing world-class science for another three years during EM-3.

4 Data and Code Management Plans

4.1 Data Management Plan

The SDO science data is a treasure trove of solar information that will be used by researchers for many years to come. The published research encompasses only one sunspot cycle, which will be enhanced by comparing the SDO data with those from missions yet to come. During the SDO mission, SDO science data is safely stored at the JSOC and EVE SOC. It is available to all members of the public through web interfaces and services. The SDO data will be delivered to the SDAC following the plan negotiated with the Heliophysics Directorate.

SDO has included the current draft of the PDMP as Appendix A to this proposal. We have begun updating the PDMP as required in the Call for Proposal. We anticipate the PDMP will be approved by September 2021 (the end of the first year of EM-3.)

SDO science data uses standard data formats that are designed for permanent access. Most of the metadata needed is contained within the exported files. An extensive database of metadata at the JSOC allows quick searching of the AIA and HMI data for desired time intervals and other parameters. By adhering to standards, the data will be accessible for all time. By taking detailed data over more than one solar cycle, SDO adds to our knowledge of the long-term variations of the solar dynamo.

The total data volumes accumulated through 2019 are listed in Table 2.1. A more detailed version is included in Section 7 of the draft PDMP attached as App. A.

4.2 Calibration and Measurement Algorithm Document (CMAD)

SDO has published data algorithms in the scientific literature. We are working to translate those papers into Calibration and Measurement Algorithm Documents (CMADs). Based on the EVE's team pre-launch effort and their updates to similar documents on SORCE, each team has provided estimates for the times to complete these documents over the next three years. See App. C for an example of an EVE CMAD.

4.3 Code Management Plan

The SDO team is committed to allowing anyone to access the programs needed to read and analyze SDO data. All of the programs needed to decommute the telemetry files and create the Level-0 files will be included in the delivery to the SDAC. Some of these codes may include proprietary code or be subject to ITAR or EAR restrictions; these codes will be described by CMADs, so changing to an open-source license is not required.

Basic routines to read the FITS-formatted science data files are available in the publicly accessible and freely available cfitsio and SolarSoft code packages. During EM-2 many analysis routines were ported into the SunPy distribution and are freely available under that package's Open-Source license. The AIA routines (aiapy) are served at https://gitlab.com/LMSAL_HUB/aia_hub/aiapy as a GitLab repository under a BSD 3 license. HMI code is available in a CVS repository at <http://jsoc.stanford.edu/cvs/JSOC/>. Applying an Open-Source license to code will become part of the software development cycle and does not add cost at this time.

5 References

Aschwanden, Markus J. (2019), ApJ, 880, 105.
Attie, R., et al. (2018), Space Weather, 16, 1143-1155.

Barnes, W. et al. (2019), Fall AGU Abs., SH41C-3317.
Basu, S., & Antia, H.M. 2019, ApJ, 883, 93.

- Bi, Y., et al. (2018), ApJ, 865, 139.
- Bjørgen, J. P., et al. (2019), A&Ap, 631, A33.
- Bobra, M., & Mason (2019), *Machine Learning, Statistics, & Data Mining for Heliophysics*, <http://helioml.org/title.html>.
- Bogart et al. (2015), ApJ, 807, 125, 12 pp.
- Böning, V. G. A., et al. (2017), ApJ, 845, 2.
- Chen, R. PhD thesis, (2019), Stanford University.
- Chen, R., & Zhao, J. (2018), ApJ, 853, 161.
- Chen, Y., Tian, H., et al. (2018), ApJ, 856, 21.
- Cheung, M. C. M., et al. (2019), Nature Astron., 3, 160.
- Chintzoglou, G., et al. (2019), ApJ, 871, 67.
- Couvidat, S., et al. (2016), Solar Phys., 291, 1887-1938.
- Dai, Yu, & M. Ding (2018), ApJ, 857, 99.
- DeRosa, M. L., & G. Barnes (2018), ApJ, 861, 131.
- Dissauer, K., et al. (2018), ApJ, 863, 169, 20pp.
- Dissauer, K., et al. (2019), ApJ, 874, 123, 15 pp.
- Effenberger, F., et al. (2017), ApJ, 835, 124, 13 pp.
- Fisher et al. (2015), Space Weather, 13, 369-373.
- Fisher, G., et al. (2020), ApJS, 248, 2.
- Fontenla, J. M., et al. (2017), ApJ, 834, 54.
- France, K. (2019), AAS, Extreme Solar Systems 4, id. 330.03. BAAS, Vol. 51, No. 6.
- Galvez, R., et al. (2019), ApJS, 242, 7, 7 pp.
- Gitiaux, X., et al. (2019), in *2nd Workshop on ML and the Physical Sci.*, <https://arxiv.org/abs/1911.01490>, 6 pp.
- Graham, D. R., et al. (2019), ApJLett, 880, L12
- Grava, C., et al. (2018), A&Ap, 616, A159.
- Guo, J., (2018), Sp. Wea., 16, 1156–1169.
- Guo, Y., et al. (2019), ApJLett, 870, L21.
- Hanaoka, Y., et al. (2018), ApJ, 860, 142.
- Harra, L. K., et al. (2016), Solar Phys., 291, 1761–1782.
- Hathaway, D.H. et al. (2013), Science, 342, 1217-1219.
- Hock, R. A., et al. (2013), Space Weather, 11, 262–271
- Hoeksema, J. T., et al. (2014), Solar Phys., 289, 3483.
- Hoeksema, J. T., et al., (2017), AAS/SPD, #48, id.301.05.
- Hoeksema, J. T., et al. (2020), ApJ, submitted, May 2020.
- Houston, S. J., et al. (2018), ApJ, 860, 28, 13 pp.
- Howe, R., et al. (2018), ApJL, 862, L5.
- Inglis, A. et al. (2020), ApJ, 880, 98, 9 pp.
- Ishiguro, N., & K. Kusano (2017), ApJ, 843, 101, 8pp.
- James, A. W., et al. (2018), ApJLett, 855, L16.
- Jin, M., et al. (2017), ApJ, 834, 173, 9 pp.
- Jin, M., et al. (2018), ApJ, 867, 122.
- Jungbluth, et al. (2019), in *2nd Workshop on ML and the Physical Sci.*, <https://arxiv.org/abs/1911.01490>, 8 pp.
- Kay, C. et al. (2018), 2018 SDO Science Workshop held October 29 - November 2, 2018 in Ghent, Belgium.
- Kazachenko, M.D., et al. (2014), ApJ, 795, eid 17, 19 pp.
- Kazachenko, M. D., et al. (2017), ApJ, 845, 49 13 pp.
- Keenan, F. P., et al. (2017), MNRAS, 468, 1117-1122.
- Kirk, M. S., et al. (2017), AGU Fall Meeting Abstracts, 2017, ED34B-07.
- Kleint, L. (2018), COSPAR Sci. Assem., 42, E2.3-1-18.
- Kosovichev, A. G., & V. Pipin (2019), ApJLett, 871, L20.
- Kowalski, A. F., et al. (2017), ApJ, 836, 12, 27 pp.
- Leamon, R. J., et al. (2020), Solar Phys., 295, 36, 18 pp.
- Lekshmi, B., et al. (2018), ApJ, 861, 121.
- Li, Jing (2018), ApJ 867, eid 89.
- Liang, Z.-C., et al. (2018), A&Ap, 619, A99.
- Liang, Z-C. et al., (2019) A&Ap, 626, A3
- Lin, C.-H., & Chou, D.-Y. 2018, ApJ, 860, 48.
- Lin, Y. C., & Y. H. Chu (2017), JGR, 122, 2505–2529.
- Liu, W., et al. (2018), ApJLett, 864, L24.
- Liu, Y., et al. (2017), ApJ, 846, L6.
- Liu, Y. (2019), AAS Meeting Abstracts, 51, 402.03.
- Löptien, B. et al. 2018, Nature Astronomy, 2, 568
- Loukitcheva, M. A., et al. (2019), ApJL, 877:L26 (5pp).
- Lumme, E., et al. (2019), Solar Phys., 294, 84.
- Mason, J. P., et al. (2019), ApJS, 244, A13.
- McIntosh, S.W., et al., (2019), Solar Phys., 294, 88.
- Mikić, Z., et al. (2018), Nature Astronomy, 2, 913.
- Namekata, K., et al. (2017b), ApJ, 851, 91, 14 pp.
- Namekata, K., et al. (2017a), PASJ, 69, 7, 10 pp.
- Neuberg et al. 2019, in *2nd Workshop on ML and the Physical Sci.*, <https://arxiv.org/abs/1911.04008>, 6 pp.
- Nitta, N. V., & T. Mulligan (2017), Solar Phys., 292, 125.
- Norton, A. A., et al. (2017), ApJ, 842, 3.
- O’Kane, J., et al. (2019), ApJ, 882, 85.
- Panesar, N. K., et al. (2018), ApJ, 853, 189.
- Park, E., et al. (2020), ApJ, 891, L4.
- Pesnell, W.D., & K. Schatten (2018), Solar Phys., 293, 112.
- Polito, V., et al. (2018), ApJ, 856, 178.
- Price, D. J., et al. (2019), AAp, 628, A114.
- Qian, L., et al. (2019), JGR, 124, 2298-2311.
- Quinn, S., et al. (2019), ApJ, 881, 82.
- Rajaguru, P. S., et al. (2019), ApJ, 871, 155.
- Ratnam, V., et al. (2019), JGR, 124, 7320–7331.
- Reale, F., et al. (2019), ApJ, 882, 7.
- Reep, J. W., et al. (2018), ApJ, 856, 149.
- Rempel, M. (2017), ApJ, 834, 10, 23 pp.
- Riley, P., et al. (2019), ApJ, 874, L15, 6 pp.
- Salvetelli et al. (2019) in in *2nd Workshop on ML and the Physical Sci.*, <https://arxiv.org/abs/1911.04006>, 5 pp.
- Sato, H., et al. (2019), Space Weather, 17, 816-826.
- Schonfeld, S. J., et al. (2019), ApJ, 884(2), 141.
- Shmolter, E., et al. (2018), Adv. Radio Sci., 16, 149-155.
- Simonyan & Zisserman (2014), arXiv: 1409.1556 [cs.CV].
- Solomon, S. C., et al. (2019), JGR, 124, 3799–3809.
- Su, Y., et al. (2018), ApJ, 856, L17, 10 pp.
- SunPy (2020), <https://sunpy.org>
- Szenicer, A., et al. (2019), Sci. Adv., 5 (10), eaaw6548.
- Thalmann, J. K., et al. (2019), ApJ, 880, L6.
- Thiemann, E. M. B., et al. (2017), JGR, 122, 2748–2767.
- Thiemann, E. M. B., et al. (2018), GRL, 45, 8005–8013.
- Thiemann, et al. (2019), J. Sp. W. Sp. Cl., 9, A43, 19 pp.
- Toriumi, S., et al. (2017), ApJ, 834, 56.
- Toriumi et al. (2020), ApJ, 890, 103.
- van der Holst, B., et al. (2014), ApJ, 782, 81, 15 pp.
- Wang, T., & L. Ofman (2019), ApJ, 886 2, 14 pp.
- Woods, T. N., et al. (2011), ApJ, 739, 59.
- Zhao, J., & Chen, R. 2018, ApJ Lett, 860, L29
- Zhao, J., et al. (2019), ApJ, 887, 216 14 pp.
- Zhou, Z., et al. (2019), ApJ, 878, 46, 11 pp.

Appendix A: Project Data Management Plan (PDMP) (Factor D-3, informational)

The SDO Project Data Management Plan (464-SCI-PLAN-0052.pdf) was released in December 2009. It describes the data products and volumes that existed before the launch of SDO. The PDMP has been updated by appending a Mission Archive Plan (MAP) at both of the previous Senior Review proposals.

Instead of a MAP, the Call for Proposals in this Senior Review cycle asked for an updated PDMP to be released. We have begun that process. A draft of the revised PDMP is attached that includes the data volumes in the requested tables and some updated language.

A project-controlled document must go through a review process before it can be released. We plan that the revised PDMP will be released before the end of FY 2021.

We will move toward a web-based version of as much of the PDMP as can be published, including the data products and CMADs. The text portions of the PDMP will be served in a pdf document that is posted at the SDO website.

A draft of the revised SDO PDMP is attached after this page.

Solar Dynamics Observatory

Project Data Management Plan

464-SCI-PLAN-0052
Revision - A

Effective Date: December 15, 2009

Prepared By: W. Dean Pesnell

DRAFT



Goddard Space Flight Center
Greenbelt, Maryland

May 29, 2020

i

CM FOREWORD

This document is a Solar Dynamics Observatory Project controlled document. Changes to this document require prior approval of the SDO Project CCB Chairperson. Proposed changes shall be submitted to the SDO Project Configuration Management Office (CMO), along with supportive material justifying the proposed change.

Questions or comments concerning this document should be addressed to:

*SDO Configuration Management Office
Mail Stop 464
Goddard Space Flight Center
Greenbelt, Maryland 20771*

DRAFT

Signature Page

Prepared by:	Approved by:
<u>Original Signed By</u> 12/10/ W. Dean Pesnell SDO Project Scientist (GSFC)	<u>Original Signed By</u> 12/07/ Dale Fink SDO Mission Director (GSFC)
Approved by:	Approved by:
Phil Scherrer HMI Instrument Principal Investigator	<u>Original Signed By</u> 12/08/ Mark Cheung AIA Instrument Principal Investigator
Approved by:	Approved by:
<u>Original Signed By</u> 12/14/ Madhulika Guhathakurta Program Scientist (HQ)	<u>Original Signed By</u> 12/13/ Tom Woods EVE Instrument Principal Investigator
Approved by:	Approved by:
Jeffrey Hayes Program Executive for MO & DA (HQ)	Jack Ireland Manager of Archive

Project Data Management Plan

DOCUMENT CHANGE RECORD

Sheet: 1 of 1

REV/ VER LEVEL	DESCRIPTION OF CHANGE	APPROVE D BY	DATE APPROVED
-	Released following approval of SDO-CCR-1067.	<i>R. Lilly</i>	12/15/2009
A	Changes required by the Senior Review 2020 Call for Proposal	<i>in draft</i>	

Table of Contents

1.0	INTRODUCTION	7
1.1	PURPOSE AND SCOPE	7
1.2	PDMP DEVELOPMENT, MAINTENANCE, AND MANAGEMENT RESPONSIBILITY	7
1.3	CHANGE CONTROL	7
1.4	RELEVANT DOCUMENTS.....	8
2.0	PROJECT OVERVIEW.....	9
2.1	SCIENCE OBJECTIVES	9
2.2	MISSION SUMMARY.....	10
3.0	SCIENCE INSTRUMENTATION	13
3.1	ATMOSPHERIC IMAGING ASSEMBLY (AIA).....	13
3.1.1	<i>Instrument Description</i>	13
3.1.2	<i>Capabilities and Requirements</i>	13
3.1.3	<i>Data Acquisition</i>	14
3.1.4	<i>Changes in AIA Operation</i>	14
3.2	EUV VARIABILITY EXPERIMENT (EVE)	14
3.2.1	<i>Instrument Description</i>	14
3.2.2	<i>Capabilities and Requirements</i>	15
3.2.3	<i>Data Acquisition</i>	15
3.2.4	<i>Changes in EVE Operations</i>	16
3.3	HELIOSISMIC AND MAGNETIC IMAGER (HMI)	16
3.3.1	<i>Instrument Description</i>	16
3.3.2	<i>Capabilities and Requirements</i>	16
3.3.3	<i>Data Acquisition</i>	17
3.3.4	<i>Changes in HMI Operations</i>	17
4.0	DATA PRODUCTS	18
4.1	AIA SCIENCE DATA PRODUCTS	18
4.2	EVE SCIENCE DATA PRODUCTS.....	20
4.2.1	<i>EVE Data Products Functional Description</i>	20
4.2.2	<i>EVE Science Data Distribution</i>	21
4.3	HMI SCIENCE DATA PRODUCTS.....	23
5.0	GROUND SYSTEM.....	25
5.1	MISSION OPERATIONS	25
5.2	PROJECT DATA	26
5.2.1	<i>Project Data Repositories</i>	26
5.3	CONTINUED ACCESSIBILITY	27
5.3.1	<i>Directories and Catalogs</i>	27
5.3.2	<i>Standards and Policies</i>	28
5.3.3	<i>Scientific Computing Resources</i>	28
5.3.4	<i>Networking Requirements</i>	28
5.4	MISSION SUPPORT DATA	28
6.0	DATA FLOW.....	29
6.1	OVERVIEW OF END-TO-END DATA FLOW	29
6.1.1	<i>Data Flow to Spacecraft</i>	29
6.1.2	<i>Data Flow from Spacecraft</i>	29
6.2	DATA HANDLING AND TIMELINE	30
7.0	ARCHIVING AND DATA ACCESS.....	31
7.1	CURRENT ARCHIVE LOCATIONS.....	33
7.2	DATA ACCESS AND PROCESSING TOOLS	34
7.3	DOCUMENTATION AND METADATA	34
7.4	FINAL ARCHIVE/MISSION ARCHIVE PLAN.....	34
7.4.1	<i>Data Products</i>	35
7.4.2	<i>Analysis Tools</i>	35
7.4.3	<i>Documentation</i>	35

7.4.4	<i>Final Archive Access and Distribution</i>	35
8.0	GLOSSARY	36
9.0	ACRONYM AND ABBREVIATION LIST.....	38
10.0	APPENDIX A. DATA RIGHTS AND RULES FOR DATA USE	39

Figures

Figure 5-1. Summary of SDO Project Data Flows	25
Figure 4-1. Summary of SDO Project Data Flows	25

Tables

Table 2-1. SDO Mission Summary.....	10
Table 4-1. Science data product summary parameters for AIA.....	20
Table 4-2. EVE Data Products.....	22
Table 5-3. HMI Science Data Products	22

1.0 Introduction

This document describes the Project Data Management Plan (PDMP) for the Solar Dynamics Observatory (SDO) mission. SDO is a National Aeronautics and Space Administration (NASA) Living With a Star (LWS) mission scheduled for launch in November 2009. This PDMP is designed to be consistent with the SDO Level-1 Requirements in the LWS Program Plan (Reference 1) and the Level-2 SDO requirements as defined in the SDO Mission Requirements Document (MRD, Reference 2).

1.1 Purpose and Scope

This document describes the generation, delivery, and serving of SDO mission data and science data products and associated responsibilities for the provision of data access and data analysis.

Covered in this plan are:

1. Summaries of the SDO mission and instruments
2. Description of the data flow
3. Description of the science data products
4. Processing requirements and facilities
5. Data service requirements
6. Policies for access and use of SDO data

1.2 PDMP Development, Maintenance, and Management Responsibility

The SDO Project Scientist, currently Dr. William D. Pesnell at the Goddard Space Flight Center (GSFC), is responsible for the development, maintenance, and management of the PDMP through the life of the mission. The PDMP applies to the “Science” or “nominal” mission phase, which begins when the instruments are on orbit, checked-out, and gathering science data.

1.3 Change Control

The SDO PDMP will be modified and updated as required in accordance with the Configuration Management Plan for the SDO mission and the NASA Science Mission Directorate's Heliophysics Division requirements for the contents and revisions of PDMP.

The original PDMP was signed at the time of the Flight Operations Readiness Review, which was held 21-22 July 2009.

The Call for Proposals of the 2020 Heliophysics Senior Review mandated that a new version of

the PDMP must be prepared.

1.4 Relevant Documents

- Reference 1. SDO Level-1 Science Requirements, NASA Headquarters Living With a Star Program Plan, Appendix A.
- Reference 2. SDO Mission Requirements Document, NASA-GSFC, 464-SYS-REQ-0004, November 18, 2005.
- Reference 3. NASA Science Mission Directorate, Heliophysics Division Program Data Management Plan.
- Reference 4. SDO Project Operations Concept Document, NASA-GSFC, 464-GS-PLAN-0010, March 2, 2004.
- Reference 5. SDO Configuration Management Plan, 464-PROJ-PROC-0010. January 18, 2005.
- Reference 6. Guidelines for Development of a Project Data Management Plan (PDMP), NASA Office of Space Science and Applications, March 1993.
- Reference 7. The SDO Science Definition Team Report, October 2001.
- Reference 8. Interface Control Document between the SDO Mission Operations Center and the Science Operations Centers. 464-GS-ICD-0001, April 27, 2006.
- Reference 9. Interface Control Document between the SDO Data Distribution System (DDS) and the Science Operations Centers. 464-GS-ICD-0010, June 16, 2006.
- Pesnell, W. D., B. J. Thompson, and P. C. Chamberlin, (2012) The Solar Dynamics Observatory (SDO), *Solar Physics*, **275**, 3-15, <http://adsabs.harvard.edu/abs/2012SoPh..275....3P>
- Lemen, J. R. , A. M. Title, C. Akin, J. F. Drake, D. W. Duncan, F. M. Edwards, G. F. Heyman, N. L. Hurlburt, G. D. Kushner, M. Levay, D. P. Lindgren, E. L. McFeaters, R. A. Mitchell, C. J. Schrijver, R. A. Springer, T. D. Tarbell, C. J. Wuelser, C. Yanari, P. N. Bookbinder, D. Caldwell, R. Deluca, L. Golub, S. Park, R. I. Podgorski, P. H. Scherrer, P. Gummin, G. Auker, P. Jerram, R. Pool, D. L. Windt, S. Beardsley, J. Clapp, N. Waltham, (2012), The Atmospheric Imaging Assembly (AIA) on the Solar Dynamics Observatory (SDO), *Solar Physics*, **275**, 17-40, <http://adsabs.harvard.edu/abs/2012SoPh..275...17L>.
- Schou, J., P.H. Scherrer, R.I. Bush, R. Wachter, S.Couvidat, M.C. Rabello-Soares, R.S. Bogart, J.T. Hoeksema, Y. Liu, Jr. T.L. Duvall, D.J. Akin, B.A. Allard, J.W. Miles and R. Rairden, R.A. Shine, T. D. Tarbell, A. M. Title, C. J. Wolfson, D. F. Elmore, A. A. Norton, S. Tomczyk, (2012), Design and ground calibration of the Helioseismic and Magnetic Imager (HMI) instrument on the Solar Dynamics Observatory (SDO), *Solar Physics*, **275**, 229-250, <http://adsabs.harvard.edu/abs/2012SoPh..275..229S>.
- Woods, T. N.; Eparvier, F. G.; Hock, R.; Jones, A. R.; Woodraska, D.; Judge, D.; Didkovsky, L.; Lean, J.; Mariska, J.; Warren, H.; McMullin, D.; Chamberlin, P.; Berthiaume, G.; Bailey, S.; Fuller-Rowell, T.; Sojka, J.; Tobiska, W. K.; Viereck, R. (2012), Extreme Ultraviolet Variability Experiment (EVE) on the Solar Dynamics Observatory (SDO): Overview of Science Objectives, Instrument Design, Data Products, and Model Developments, *Solar Physics*, **275**, 115-143, <http://adsabs.harvard.edu/abs/2012SoPh..275..115W>

2.0 Project Overview

The Solar Dynamics Observatory (SDO) is the cornerstone mission within the LWS program. SDO's mission is to understand the nature and source of the solar variability that affects life and society. It must make accurate measurements of those solar parameters that are necessary to provide a deeper physical understanding of the mechanisms that underlie the Sun's variability on timescales ranging from seconds to centuries. Using remote sensing techniques, it will monitor and record those aspects of the Sun's variable outputs that have the greatest impact on the terrestrial environment and the surrounding heliosphere.

An Announcement of Opportunity (AO 02-OSS-01) to provide instruments for the SDO mission was published on January 18, 2002 by NASA Headquarters. The SDO Project office at GSFC has overall responsibility for the mission. For the purposes of this document, "spacecraft" refers to the bus subsystems without instruments, while the spacecraft plus instruments will be referred to as an "observatory."

Three science investigations were selected for development:

- Atmospheric Imaging Assembly (AIA) led by Lockheed Martin Solar and Astrophysics Laboratory (LMSAL), Palo Alto, CA.
- EUV Variability Experiment (EVE) led by the Laboratory for Atmospheric and Space Physics (LASP) at the University of Colorado, Boulder, CO.
- Helioseismic and Magnetic Imager (HMI) led by Stanford University, Stanford, CA.

The SDO implementation schedule was based on a launch date of November 2009. The Phase A study began in September 2002, and the Mission Systems Requirements and Concept Reviews were held in April 2003. The Phase B study began in September 2003 and the Preliminary Design Review was held in March 2004. The Critical Design Review was held in April 2005, while individual instrument Pre-Environmental Reviews were held in late 2006. The Mission Readiness Review was held December 18, 2009. SDO was launched February 11, 2010. The Flight Operations Readiness Review was held July 21-22, 2010, during which SDO was declared an operating mission with a start date of May 1, 2010.

2.1 Science Objectives

SDO has four science goals:

1. Understand how magnetic fields appear, distribute, and disappear from their origin in the solar interior
2. Understand the magnetic topologies that give rise to rapid high-energy release processes
3. Study and gauge the dynamic processes that influence space weather phenomena
4. Study the variations in irradiance and solar structure that occur on short timescales, as well as over the solar cycle

Seven key science questions, first listed in the SDO Science Definition Team Report (Reference 7), are the Level 1 Science Questions for SDO:

1. What mechanisms drive the quasi-periodic 11-year cycle of solar activity?
2. How is active region magnetic flux synthesized, concentrated, and dispersed across the solar surface?
3. How does magnetic reconnection on small scales reorganize the large-scale field topology and current systems? How significant is it in heating the corona and accelerating the solar wind?
4. Where do the observed variations in the Sun's EUV spectral irradiance arise, and how do they relate to the magnetic activity cycles?
5. What magnetic field configurations lead to the Coronal Mass Ejections (CME), filament eruptions, and flares that produce energetic particles and radiation?
6. Can the structure and dynamics of the solar wind near Earth be determined from the magnetic field configuration and atmospheric structure near the solar surface?
7. When will activity occur, and is it possible to make accurate and reliable forecasts of space weather and climate?

SDO will address these objectives with helioseismic and magnetic field measurements, EUV images, and EUV spectral irradiances.

2.2 Mission Summary

The SDO mission will observe the Sun from an inclined geosynchronous orbit. A summary of the mission is presented in Table 2-1

Table 2-1. SDO Mission Summary	
Orbit Description	Geosynchronous Circular, inclined at 28.5 degrees
Launch Date	February 11, 2010
Launch Vehicle	Atlas-V 401 EELV
Nominal Mission Duration	5 years after check-out and commissioning
Potential Mission Life	10 years (assuming a 5-year margin on fuel)
Mission Duty Cycle	Continuous observations with 2 eclipse seasons per year with max duration of 23 days and daily shadows of < 72 minutes
Spacecraft + Instrument Mass	3200 kg at launch (wet)

SDO was launched into a geosynchronous transfer orbit by an Atlas-V expendable launch vehicle. Mission check-out and commissioning activities, including deployments, outgassing,

instrument check-out, and subsystem commissioning, and other early-orbit checkout activities, were completed. Some of these activities will be concurrent with the orbit circularization phase, which will raise the orbit to geosynchronous.



Figure 2.1: Simplified Orbital Configuration of SDO. The orbital radius is scaled to the radius of the Earth, the distance and size of the Sun are not to scale.

Table 2-2. SDO Data Acquisition Parameters

Continuous Data Acquisition Rates	129 Mbps for science data 55 Mbps for HMI 67 Mbps for AIA 7 Mbps for EVE 32 to 64 Kbps for Housekeeping data (nominally)
On-Board Data Storage Capacity	Minimal for Housekeeping data (24 hours) None for Science data
Target Pointing Duration	Continuous Sun center pointing
Target Re-orientation Period	N/A
Attitude Control Accuracy	Sun center pointing with an absolute accuracy of 10 arcsec in the Y and Z axis
Attitude Determination	Roll angle from star trackers Fine pointing from Guide Telescope as part of AIA investigation

SDO is designed to operate with a continuous science downlink and no on-board science data storage. The continuous nominal science data return from the observatory will be approximately 130 Mbps. A ground system designed and allocated specifically for SDO will be receiving data continuously throughout the nominal mission.

Instrument operations will be routine for the majority of the mission with each instrument continuously running in its primary science mode. Periodic interruptions to routine science operations are expected. These would include spacecraft maneuvers for momentum dumping and station keeping and instrument calibration maneuvers. Two eclipse seasons of about 23 days per year cause the science instruments to be occulted from the Sun on a daily basis for periods of up to 72 minutes. Data outages are expected due to rain at the ground site and other causes. However, these data interruptions are budgeted to satisfy the high-level mission requirements for data completeness.

Onboard communication for commanding, and health and safety telemetry between the spacecraft subsystems and the instrument electronics boxes is through a MIL-STD 1553 bus. Science data is placed on a MIL-STD 1355 bus. All data is formatted into CCSDS packets. Each spacecraft subsystem and each instrument have an assigned range of Application Identifiers (ApID) to identify science data as well as housekeeping data. Before downlink, all data packets are formatted into Virtual Channel Data Units (VCDU) and assigned to certain Virtual Channels (VCs).

The science telemetry will be downlinked on the Ka-band to the SDO ground tracking station and routed to the Data Distribution System (DDS), which distributes it to the Science Operations Centers (SOC). To compensate for dropouts in the transfer of data on the ground network, the SDO ground system will maintain temporary archives at the antenna site and at the DDS.

Housekeeping telemetry data is downlinked on the S-band and transferred directly from the antenna site to the Mission Operations Center (MOC), which then distributes it to the appropriate SOC. The MOC archives all the observatory housekeeping data for the life of the mission. Flight dynamics products, such as ephemeris information, are generated at the MOC and forwarded to the SOCs as needed. The predicted ephemerides and the tracking data are stored in the MOC for the life of the mission. The SOCs are expected to archive any other products that may be needed for future science data processing.

3.0 Science Instrumentation

The SDO observatory includes a complement of three instruments:

- 1- Atmospheric Imaging Assembly (AIA), Principal Investigator (PI) Alan Title, at LMSAL in Palo Alto, CA.
- 2- EUV Variability Experiment (EVE), PI Tom Woods, at LASP, in Boulder, CO.
- 3- Helioseismic and Magnetic Imager (HMI), PI Philip Scherrer, at Stanford University in Stanford, CA.

Table 3-1: Summary Properties of Instruments				
	Mass (kg)	Size (LxWxH) (in)	Data Rate (Mbps)	Power (W) Normal/eclipse
AIA	155	60.1 x 64.6 x 19.3	67	190/207
EVE	55	33.1 x 23.9 x 15.4	7	76/76
HMI	77	48.0 x 25.2 x 12.0	55	111/122

3.1 Atmospheric Imaging Assembly (AIA)

3.1.1 Instrument Description

AIA consists of four multi-wavelength telescopes with the spatial resolution of the TRACE heritage telescopes (0.6 arcsec/pixel) with a full-Sun view. AIA will provide images of the solar chromosphere and corona at 10 wavebands (or temperatures). Three of the telescopes have 2 sectors with 2 different mirror coatings which center on a particular waveband, while the fourth telescope has four sectors. To capture all ten wavebands, the telescopes each cycle through one waveband sector then proceed to another, so that eight of the ten wavebands are imaged within ten seconds, and all ten wavebands are imaged within a nominal 30 second interval. The time cadence of less than 10 seconds will capture the initiation and progression of dynamic processes in the solar atmosphere.

3.1.2 Capabilities and Requirements

The summary parameters of AIA are shown in **Table 3-2**.

Table 3-2. Summary Parameters for AIA

Parameter	Value
Parameters Measured	Images of the Sun in seven EUV wavelengths every 12 seconds, with 3

	UV and visible channels every 30 seconds
Number and Type of Detectors	Four 4096×4096 CCDs
Sensitive Area	4096×4096 pixels
Field of View	$40'$ (solar disk has a diameter of $32'$)
Energy/Wavelength Range	10 channels with central wavelengths of 94, 131, 171, 193, 211, 304, 335, 1600, 1700, and 4500 \AA
Energy/Wavelength Resolution	
Time Resolution	≤ 12 sec for EUV wavebands
Positioning	
Sensitivity	
Data Rate	Science data (Ka-band): 67 Mbps HK data (S-band): 2 kbps

3.1.3 Data Acquisition

AIA will return full-disk images of the Sun with a pixel resolution of $0.6''$. These images are taken every 12 seconds through most of the filters, although the three long-wavelength filters are exposed less frequently such that images in eight of the 10 possible wavelengths are collected each interval. The image is transferred into the camera electronics, where it is compressed, and then transmitted to the ground. There are no special requirements for data acquisition. Special operating modes will be used occasionally that will increase the data rate but decrease the areal coverage on the sun or decrease the number of wavelengths collected each cycle.

3.1.4 Changes in AIA Operation

AIA has reduced the cadence of the visible light channel to once per hour, the two UV wavelengths are observed alternately for a 24 sec cadence.

3.2 EUV Variability Experiment (EVE)

3.2.1 Instrument Description

EVE will measure the EUV spectral irradiance from 0.1 to 105 nm, plus hydrogen Lyman-alpha at 121.6 nm at a cadence of one spectrum every 10 seconds. EVE will measure the spectral irradiance with a sensitivity that allows us to gauge and model the energy input into the complex processes of the Earth's atmosphere and near-Earth space. Its temporal resolution will allow us, for the first time, to understand the flare-induced impacts on these processes.

EVE combines the measurements from two grating spectrographs (MEGS-A, MEGS-B) to produce a EUV spectrum covering the 5-105 nm wavelength range. A pinhole camera with single photon detection (MEGS-SAM) obtains a 1-nm spectrum of the 0.1-7 nm wavelength region, and it also makes a low-resolution image of the Sun at wavelengths between 0.1 and 7 nm, while the MEGS-P photometer provides measurements from 120-122 nm covering the hydrogen Lyman-alpha line.

Several broadband (3-20 nm) photometer measurements (ESP) provide calibrations for the spectrographs and provide information at a higher time cadence (0.25 seconds).

3.2.2 Capabilities and Requirements

The summary parameters are EVE are shown in Table 3-3.

Table 3-3: Summary Parameters for EVE

Parameter	Value
Parameters Measured	Spectral irradiance covering 0.1-105 nm and 121.6 nm every 10 seconds [Baseline] Spectral irradiance covering 37-105 nm and 121.6 nm every 10 seconds [Updated 27 May 2014]
Number and Type of Detectors	2 1024 × 2048 CCDs 2 Si photodiodes in MEGS; 9 Si photodiodes in ESP
Sensitive Area	2048 (wavelength/spectrum) × 1024 (slit image) for each CCD
Field of View	$2^\circ \pm 1^\circ$
Energy/Wavelength Range	0.1 to 105 nm [Baseline] 37-105 nm [after 27 May 2014]
Energy/Wavelength Resolution	0.1 nm (5-105 nm); 1 nm (0.1-5 nm) [Baseline] 0.1 nm (37-105 nm); 1 nm (0.1-5 nm) [Updated 27 May 2014]
Time Resolution	≤ 20 sec between spectra
Positioning	Uncertainty $< 60''$ over 10 second intervals
Sensitivity	
Data Rate	Science data (Ka-band): 7 Mbps HK (S-band): 2 kbps

3.2.3 Data Acquisition

EVE data are obtained using observation sequences that define the time cadence and filter positions in the filter wheel mechanism. The primary mode is to take solar observations every 10 seconds for the spectrographs. The calibration modes include flat-field measurements of the CCDs using on-board LEDs, dark measurements, and solar measurements using order-sorting filters. The photometer data are taken at a constant rate of 0.25 seconds without any software control of their time cadence. All of the EVE science data is sent to the SDO High-Speed Bus, which is directly transmitted to the SDO ground station.

3.2.4 Changes in EVE Operations

EVE lost the MEGS-A channel due to a power failure driving a CCD May 2014. The MEGS-B channel has changed its cadence to 60 sec. *Need a description of the proton-induced losses in MEGS-B.*

3.3 Helioseismic and Magnetic Imager (HMI)

3.3.1 Instrument Description

HMI will observe “filtergrams” of the Sun through a series of optical filters that are combined to produce 5 or 6 filter positions straddling a spectral absorption line of Fe I at 6173 Å. Each filtergram is a measurement of the spectral line radiance at a known polarization. Combinations of these filtergrams will provide measurements of the line-of-sight Doppler velocity of the solar photosphere and the Stokes parameters needed to create the line-of-sight and vector magnetic field in the photosphere. Analysis of time series of filtergrams using techniques of helioseismology can provide information about sub-photospheric dynamics with the goal of a better understanding of magnetic field growth and decay processes on time scales of hours to years.

3.3.2 Capabilities and Requirements

HMI is required to obtain Dopplergrams, which measure the Doppler shifts due to oscillation velocities over the entire visible disk, and to make high-resolution magnetograms, measurements of the longitudinal and vector magnetic field over the whole visible disk of the Sun. The summary parameters are shown in Table 3-4.

Table 3-4. Summary Parameters for HMI	
Parameter	Value
Parameters Measured	Line-of-sight velocity and magnetic field (vector and longitudinal.)
Number and Type of Detectors	2 4096 × 4096 CCDs
Sensitive Area	4096 × 4096
Field of View	2000"

Energy/Wavelength Range	Spectral line of Fe I (6173 Å), at least five positions on and off-band
Energy/Wavelength Resolution	Filter width of 76 mÅ (FWHM)
Time Resolution	Dopplergrams, 50 secs; Line-of-sight magnetograms, 50 secs; Vector magnetograms, 10 min; Continuum proxy, 50 secs.
Positioning	Uncertainty < 0.1" over 0.5 sec intervals
Sensitivity	
Data Rate	Science data (Ka-band): 55 Mbps HK (S-band): 2 kbps

3.3.3 Data Acquisition

HMI will continually acquire filtergrams that are sent to the ground and combined to give the listed observables. The data acquisition modes are expected to have little variation during the operational phase of the mission.

3.3.4 Changes in HMI Operations

Vector magnetograms are released at a cadence of 135 s.

4.0 Data Products

Science data products include data sets generated by the project. This section of the PDMP identifies and describes all data sets expected to be generated, and how these data sets are to be made available to the user community. This includes the science data itself, associated ancillary data, and orbit/attitude data of the spacecraft. The science data products for each of the instruments on SDO are summarized in sections 5.1 through 5.3 below.

4.1 AIA Science Data Products

This section summarizes the science data products produced by AIA. The AIA/HMI Joint Science Operations Center (JSOC), supported by Stanford University and LMSAL, serves the data to the science community and other users. Nominally, all AIA and HMI data will be served from Stanford University.

AIA data levels are defined below in Table 4-1. The AIA routine processing for Level 0 data will consist of steps that are considered to be well understood and which are reversible. The Level 0 data, combined with the AIA metadata and calibration data, are stored on the JSOC data server.

Level 1 data products will be assembled by the data system to suit the user requests. This is because we anticipate a wide range of data requests, and because the characterization of the instrument itself and therefore the calibration will change throughout the mission. The data server will assemble each data product request from the Level 0 data and the metadata using the most recent calibration information. All possible pixel-level calibrations are applied to generate Level 1 data. The only exception is that the bad pixel maps are created, but not applied at this stage. These maps include both those due to detector imperfections and cosmic rays. All higher products are based on Level 1 data. Levels 1.5 and 1.6 have all geometric corrections with all images sharing common plate scales and centers and rotation angle from Solar North. In addition, Level 1.6 has a quick FFT-based PSF correction to provide the cleanest images for browse products. Higher-level products for general distribution are reductions of these three series. Browse and synoptic products are generated from Level 1.5. Research data cubes are subsets of Level 1.5. These levels are maintained as data series in the JSOC DRMS/SUMS environment. These calibrated data products will be distributed as part of normal data operations, and only to the extent that existing facilities and resources will allow. Large data requests may be delayed or may require the requestor to supply media or other resources.

Higher-level data products can be divided into two main areas: more-highly processed images, such as Differential Emission Measure maps (with temperature inversions) or field extrapolations, and metadata which can be used to locate and interpret the data. The latter could include processed movies, event and feature catalogues, and derived coronal structures. AIA Level 2 data products will generally be generated and archived by the LMSAL.

Browse data, consisting of summary images and movies, will be available to assist users in

identifying subsets of the data for analysis. Additionally, the AIA data system will serve some Assembled Data products, chiefly data cubes of image subsets tracking regions of interest, or assemblies of popular data subsets. Assembled Data products that are not accessed on a regular basis will be migrated off the server.

To aid researchers in finding appropriate data, and to reduce the demand on the Level 1 archive, a variety of metadata products will be generated and maintained. These include descriptions of observed events, along with associated thumbnails and compressed movies, and pointers to the Level 1 archive (including bracketing time intervals and region of interest) and associated modeling or higher-level products. These events are described in XML documents based upon the VOEvent standard (for further detail see <http://www.ivoa.net/twiki/bin/view/IVOA/IvoaVOEvent>), with extensions developed by the Heliophysics Knowledgebase project. These events are ingested into a separate database server maintained at LMSAL.

The AIA data server is continually populated with the most recent Level 0 data and browse data. After receipt from the DDS, AIA Level 1 near-realtime data will be available with a latency of less than one hour; browse data will be available within two hours. Once the DDS confirms all data has been received, nominally within 24 hours of the original downlink, Level 1 data will be generated, released for general distribution, and used to generate higher-level products. These products will be available within three days.

Table 4-1. Science data product summary parameters for AIA						
Level	Description	File Format	Rate (Gb/day)	Rate (TB/year)	Cache (day)	Archived (%)
Raw	Telemetry	Packets	674	250	30	100
0	Raw images with header information, in instrument units (DN)	FITS	1200	440	100	100
1.0	Calibrated images (using best-available calibrations)	FITS	1200*	0	60	0
1.5	Scaled, registered, and aligned images (DN)	FITS	0*	0	0	0
2	Irradiance curves, reconstructed temperature maps, etc.	FITS	1	0.4	0	100
Browse Data	Compressed images and movies	jpeg, mpeg	10	4	0	100
Synoptic	Low-resolution images	FITS	10	4	0	100
Data Cubes	Resampled, cropped data samples	FITS	Var.	100	30	100

Table 5- 1: **Data level definitions, with anticipated volume for the AIA instrument. A *** indicates that individual data products are not stored on the server; it is assembled from the Level 0 data and metadata by the data system upon request.

4.2 EVE Science Data Products

4.2.1 EVE Data Products Functional Description

This section describes the public science data products produced by the EVE SPOC (Science Processing Operations Center).

Level 0C

Level 0C products include MEGS photometer, ESP, MEGS-A and MEGS B products,

The Level 0C processing produces Space Weather products that are intended to be “quick & dirty.” With this understanding, these products will be uncalibrated and contain only engineering units (counts). These shall only be minimally processed since products must be produced in near-real-time.

Level 1

Level 1 processing is performed on an hourly basis for all channels (SAM, MEGS-P, ESP, MEGS-A, MESG-B). The result of a single Level 1 processing task is a file containing data

from individual integrations from the nominal operating mode over one UT hour. Data are fully calibrated, degradation corrected, 1-AU corrected irradiance.

Level 2

Level 2 processing is performed on an hourly basis for only MEGS-A and MEGS-B channels. The result of a single Level 2 task is a file containing data from the individual integrations from the nominal operating mode over one UT hour. Data are integrated using the trapezoid method onto a fixed wavelength scale to allow meaningful comparisons between integrations. Specific solar emission lines will be extracted from the fixed wavelength spectra.

Level 3

Level 3 processing is performed on a daily basis. Level 3 merges the data from each channel into a daily averaged EVE measurement. The following data are used to create the Level 3 product: Level 1 SAM, Level 1 ESP, Level 1 MEGS-P, Level 2 MEGS-A, and Level 2 MEGS-B. The result of the Level 3 task is a file containing averaged data from all EVE channels from the nominal operating mode over one UT day. Two spectra will be produced: a 0.1 nm spectrum from merged MEGS-A and MEGS-B spectrum, and a 1 nm spectrum that includes the SAM spectral measurement. Daily averages from the ESP, SAM total irradiance, MEGS-A extracted lines, MEGS-B extracted lines, and MEGS-P will also be reported.

For Level 3 the units will be watts per square meter for photometer and SAM total band pass irradiance measurements, and watts per square meter per nanometer for spectral measurements.

All measurement will contain the date and at least three different types of uncertainty:

- Precision: fractional Poissonian statistical uncertainties ($1/\sqrt{\text{counts}}$)
- Accuracy: fractional total uncertainty including propagated calibration uncertainties
- Standard deviation: one-sigma statistical spread of the measurement over the day

4.2.2 EVE Science Data Distribution

EVE Science Data Storage

All data stored on the RAID is redundant except for the plots, catalog files, database files, and user registration information. This information is backed up periodically to the Archival subsystem. Approximately 500 GB of additional hard drive space will be required per year. Only the newest version/revision combination will be kept online. A weekly purge routine will automatically delete old versions/revisions.

Data product files will be stored in a compressed form (like gzip) to reduce the download time for users and reduce storage costs. Plots will be stored in a format that is highly compressible, and widely recognized by most web browsers (likely PNG).

EVE Science Data Catalog

Table 4-2. EVE Data Products

Level	Components	Time resolution	Time span	Processing cadence	Daily Volume (MB)	Public release of day N data
L0A	All	Highest	~1 min	N/A	75000	N/A
L0B	All	Highest	~1 min	1 min	75000	N/A
L0C	ESP MEGS-P MEGS-A, B	1-sec 1-sec 10-sec	~1-min	Each TLM file (~1/min)	2.2 1.1 34	~15 min after receipt
L1	ESP SAM MEGS-P	1-sec 1.5-min 1-sec	1-hour	24-hour	13 0.075 9	Hour 1-2 on day N+1
L1	MEGS-A, B	10-sec	1-hour	24-hour	1100	NA
L2	MEGS-A, B	10-sec	1-hour	After L1	1200	Hour 23-24 on day N+1
L3	ESP, SAM, MEGS-A, MEGS-B, MEGS-P	1-day	1-day	1/day	0.026	Hour 0-1 on day N+2

Catalog files are flat ASCII files that contain a list of data product files that are available in sequential time order. There will be one catalog file per data product type. This allows users to search and identify specific data product file names that were collected at certain times of interest. Additional information may be determined through the database. This structure will allow queries to be performed through most virtual observatories, including the Virtual Solar Observatory.

4.3 HMI Science Data Products

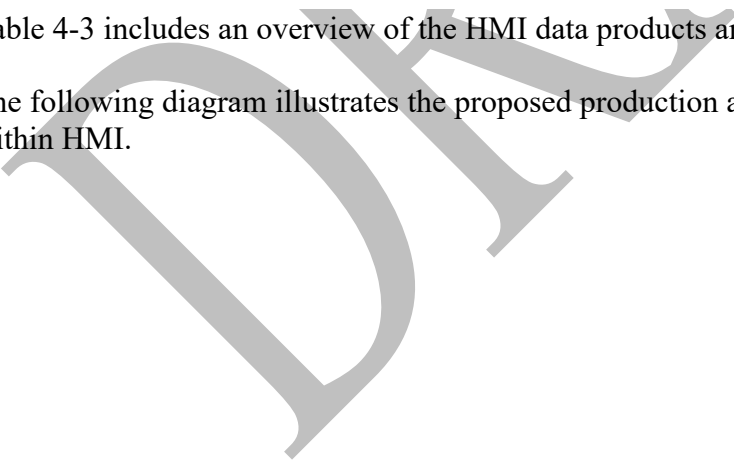
This section summarizes science data products to be generated by HMI. This data is archived at the JSOC located at Stanford University, along with the AIA data. For a full listing of HMI data see <http://jsoc.stanford.edu>.

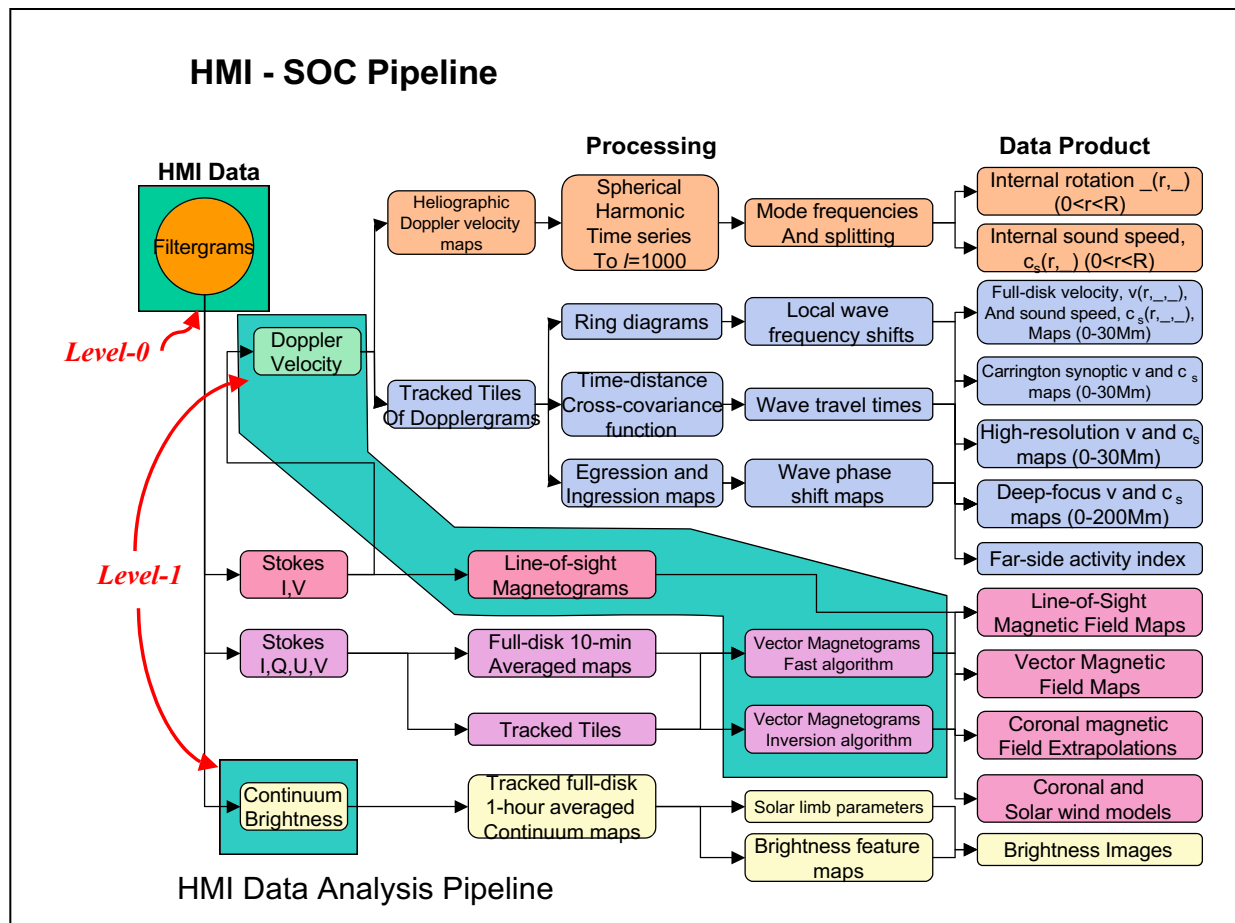
Table 4-3: HMI Science Data Products

Level	Description	Examples	Cadence	Rate (Gb/day)	Rate (TB/year)	Cache (day)	Archived (%)
Raw	Telemetry	—		553	220	30	100
0	Filtergrams	—		530	200	100	100
1	Observables	Doppler velocity, line-of-sight magnetic field, continuum proxy	45 sec.	130	15	600	30
1	Observables	Vector field parameters	10 min.	130	15	600	30
2	Higher Level Data Products	Spatial/temporal averages, synoptic maps, spherical harmonic decomposition, frequencies	Var.	20	8	3000	100

Table 4-3 includes an overview of the HMI data products and their expected data volumes..

The following diagram illustrates the proposed production and relationship of data products within HMI.





5.0 Ground System

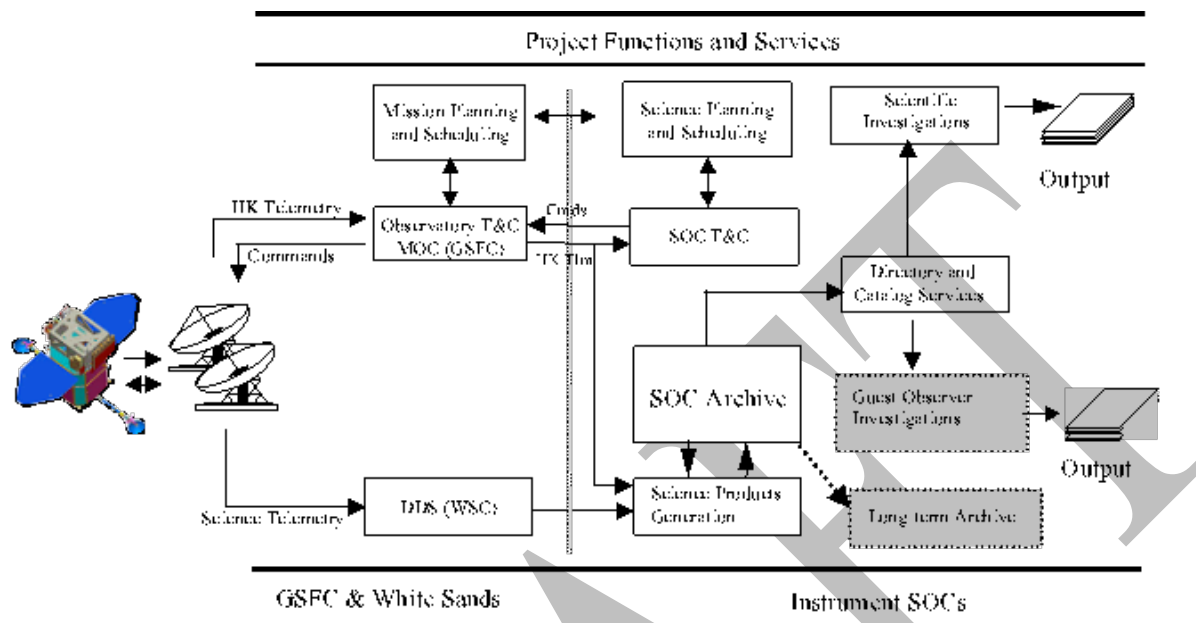


Figure 5-1. Summary of SDO Project Data Flows

This section will summarize the data flow within the project. A diagram of the generalized architecture for Mission Operations and Data Analysis is shown in Figure 5.1.

Shaded areas in Figure 5-1 represent activities that are not directly supported by the SDO Project.

5.1 Mission Operations

This section summarizes the responsibilities of each SDO Ground System facility.

SDO Ground Tracking Stations responsibilities

- Receive Ka-band telemetry from spacecraft and forward it to DDS
- Receive S-band Housekeeping telemetry and forward it to the MOC.
- Receive commands from the MOC, uplink them to the spacecraft and monitor uplink.

DDS responsibilities

- Capture science telemetry and distribute science telemetry files to SOCs in near-real time
- Maintain a thirty-day archive of science telemetry data and associated metadata
- Retransmission of science telemetry upon request by SOCs

MOC responsibilities

- Monitor and control observatory health and safety
- Route instruments commands from SOC to antenna for uplink
- Receive housekeeping telemetry from the antennas and distribute to the appropriate SOCs
- Maintain archive of housekeeping telemetry and trending data for the life of the mission.
- Maintain activity timelines for spacecraft and instruments.
- Provide Flight Dynamics products for use within the project
- Provide mission support data for use within the project

SOC responsibilities

- Produce, serve, and archive Level 0-3 science products for the instrument. This includes producing calibrated radiance and irradiance data as well as the derived data products.
- Provide data processing support, including hardware and software, for the science team associated with their instrument.
- Maintain an accessible database containing the instruments planned and as flown status information.
- Maintain an accessible database containing science metadata, instrument calibration data and analysis tools.
- Maintain an accessible database containing data product generation status information.
- Serve and archive analysis products generated by the science team associated with the instrument. Requests for large volumes of AIA or HMI data will be handled as feasible given the resources at the JSOC, which may delay data delivery or dictate that the data be delivered via mass-storage hardware rather than via the internet.
- Develop and support the Web-based interface that provides access to the instrument data products by the science community
- Participate in the design of the final archive.

5.2 Project Data

5.2.1 Project Data Repositories

Project data repositories are located at and maintained by the instrument SOCs. HMI and AIA will maintain a Joint SOC (or JSOC) that will ingest the data from the DDS and process the TLM files into Level 0 and Level 1 files.

Table 5-1 summarizes storage requirements by instrument over the prime mission. The data sets are identified as Level 0, Level 1, and higher-level products. The first two columns of values represent the estimated amount of storage without compression. The next two columns show the requirements if the CCD images (the Level 0 and Level 1 data) are compressed by 50%. Products with a “0 TB*” are generated from lower level data upon request. In addition to the data

shown in Table 5-1 the SOCs will maintain two copies of the raw telemetry data amounting to up to AIA: 528TB/yr, EVE: 55TB/yr, and HMI: 435 TB/yr.

Table 5-1. Estimated Storage Requirements (Pre-Launch)				
Instrument/Data Set	Annual	5-Year Total	Annual (Compressed)	5-Year Total (Compressed)
AIA				
<i>Level 0 Data</i>	805 TB	4025 TB	403 TB	2015 TB
<i>Browse Data</i>	3 TB	15 TB	3 TB	15 TB
<i>Level 1 Data</i>	0 TB*	0 TB*	0 TB*	0 TB*
<i>Higher level Products</i>	0 TB*	0 TB*	0 TB*	0 TB*
AIA TOTAL	808 TB	4040 TB	406 TB	2030 TB
EVE				
<i>Level 0 Data</i>	54 TB	270 TB	27 TB	135 TB
<i>Level 1 Data</i>	0.5 TB	2.5 TB	0.25 TB	1.25 TB
<i>Space Weather Data</i>	0.028 TB	0.14 TB	0.028 TB	0.14 TB
<i>Higher level Products</i>	0.5 TB	2.5 TB	0.25 TB	1.25 TB
EVE TOTAL	55 TB	275 TB	27.5 TB	137.5 TB
HMI				
<i>Level 0 Data</i>	512 TB	2560 TB	256 TB	1280 TB
<i>Level 1 Data</i>	150 TB	750 TB	75 TB	375 TB
<i>Higher level Products</i>	15 TB	75 TB	15 TB	75 TB
HMI TOTAL	677 TB	3400 TB	346 TB	1655 TB
Total	2.450 PB	12.25 PB	1295 TB	6.4 PB

5.3 Continued Accessibility

5.3.1 Directories and Catalogs

This section of the PDMP addresses metadata and the associated mechanisms for the identification and location of data sets and data analysis tools.

1. Metadata: Instrument observation parameters and ancillary information that is needed for the analysis of the data
2. Catalogs: A web-searchable compilation of relevant metadata, combined with additional indexing for available data products, calibration data, and (if applicable) analysis tools. SDO data will be available for searching through the Virtual Solar Observatory (VSO), as well as by user interfaces hosted at the PI SOCs.
3. Browse Products: Web-accessible catalog of data compiled from a subset of the science data that allows the user to quickly browse and perform a preliminary assessment of the data. Browse data are typically used to determine a time or wavelength range for a request of higher-level science data.

4. Calibration Data and Analysis Tools: Additional derived or calibration data, software routines, version numbers and information that are necessary for the quantitative analysis of the data
5. Inclusion in the NASA Master Directory (MD) or other directories and catalogs at the time of, or prior to, the delivery of data to the archives.

5.3.2 Standards and Policies

Projects and investigators will archive data conforming to those standards and policies that will facilitate subsequent data access and use. The specifics of each data set are provided in section 5. SDO will use FITS formatted files to serve science data.

5.3.3 Scientific Computing Resources

Each SOC is responsible for providing computing resources sufficient for achieving the goals of their scientific investigation(s). The resources will be sited at the PI institutes and controlled by the PI teams. External resources, such as those provided by the NASA Center for Computational Sciences (NCCS) at GSFC, and non-NASA resources, such as those available from the National Science Foundation and the Department of Energy, can be utilized if they are obtained at no additional cost to the project and do not delay the delivery of data projects to the user communities. However, these external resources will not be used to create the standard data products.

5.3.4 Networking Requirements

SDO uses dedicated commercial links to transfer the data from White Sands to the SOCs and from GSFC to the SOCs. The network configuration is defined in the applicable SDO Ground System Design documents. Each SOC has sufficient network capability to serve the requested data.

5.4 Mission Support Data

The availability, distribution, format and archiving of mission support data is described in the DDS-to-SOC ICD (Reference 8) and MOC-to-SOC ICD (Reference 8).

The MOC-to-SOC ICD also defines the FDS products that are made available to the SOCs.

6.0 Data Flow

This section provides details on the transfer of data between [flight and ground] mission elements.

The SDO instruments produce about 1.5 TByte of science data every day. Because SDO is in continuous contact with the ground station there is no onboard recorder for the science data. Instead, the science data are downlinked in Ka-band (26.5 GHz) through two high-gain antennas (HGAs) at a data rate of 150 Mbps. These redundant HGAs are mounted at the end of rigid booms (must be rigid due to required waveguides) that are attached via hinges to the bus module. The TT\&C data are sent down in S-band (2220 MHz) using two onboard omni-directional antennas. Commands to SDO are sent via an S-band link at 2044 MHz.

SDO's dedicated ground station is located at the White Sands Complex near Las Cruces, NM. It has two 18-m dual-band antennas in continuous contact with the spacecraft. Two 1-m high-gain antennas on SDO transmit the science data at 150 Mbps with 2.5 W on a frequency of 26.5 GHz (Ka band). Two omni antennas for transmit and receive the S-band H/K telemetry with 5~W on frequencies of 2.220 GHz/R and 2.044 GHz/T \citep{2005Tann}. Science data accumulates at 1.5 TB per day (roughly 1.5 PB per year.) The ground transmitter has a maximum output of 300 W.

6.1 Overview of End-to-End Data Flow

6.1.1 Data Flow to Spacecraft

This subsection describes the transfer (e.g., Guest Observer Office-to-Science Office, Science Office-to-POC, POC-to-MOC, MOC-to-Network) of information as it evolves from a desired observation to a spacecraft command, including the development of intermediate products (e.g., objects of interest, candidate target lists, pixel masks, target tables, instrument and spacecraft commands).

SDO makes a series of measurements with only limited capacity for changing the observing sequence. Changing the observing sequence is done on a case-by-case basis. The Science Team and Flight Operations Team must agree on the necessity and timing of the changes. Only six changes have been approved and executed, three planetary transits, two sun-grazing comets, and one off-point to look for Regulus. The SDO Teams have asked the community for other possibilities but none have been received.

6.1.2 Data Flow from Spacecraft

This subsection describes the transfer (e.g., Network-to-FDF, Network-to-POC, POC-to-SOC, etc.) of return data and the development of products along each step (e.g., raw telemetry, Level 0 data, light curves, calibrated images, etc.) as well as transfer timeframe and expected processing time.

6.2 Data Handling and Timeline

This section summarizes the flow of data from the spacecraft as well as the transfer method (e.g., TCP/IP over Restricted IONet, FTP, etc.) along with the timeline for delivery to/from each element (see sample below).

DRAFT

7.0 Archiving and Data Access

This section describes the process for archiving data and how those archives may be accessed. An estimate of instrument data storage requirements over the nominal life of the mission should be provided. Revised estimates for extended mission phases shall be provided at the Senior Review.

The tables in this section reflect the state of the SDO mission science data archives at three points in the mission: the ends of the prime, first extended, and second extended missions. This information supersedes any listed above in the pre-launch tables of data.

No “Uncompressed” data volumes are presented for AIA and HMI because the bulk of the AIA and HMI science data is stored as compressed FITS files. AIA Level 1.5 data is marked with a ‘*’ as it is created only upon receiving an export request.

The SDO operating mode is extremely consistent and we anticipate the science data volume will grow at the same rate during the third extended mission. The JSOC and EVE SOC are successfully managing almost 20 PB of science data.

Table 7-1: Data Volumes at End of Prime Mission (01 May 2010 – 30 Sep 2015)				
Instrument/Data Set	Annual (Uncompressed)	5.5-Year Total (Uncompressed)	Annual Compressed (TB)	5.5-Year Total (Compressed)
AIA				
Telemetry	N/A	N/A	193	1.1 PB
Level 0	N/A	N/A	206	1.1 PB
Browse Data	N/A	N/A	69	380 TB
Level 1	N/A	N/A	224	1.2 PB
Level 1.5*	0	0	0	0
Higher-level Products	N/A	N/A	124.5	0.725 PB
AIA Total	N/A	N/A	804	4.6 PB
EVE				
Level 0	N/A	N/A	13 TB	66 TB
Level 1	15 GB	78 GB	0.26 TB	1.3 TB
Space Weather Data	0.2 GB	1 GB	N/A	N/A
Higher level Products	0.058 GB	0.3 GB	0.073 GB	0.37 TB
EVE Total	15 GB	80 GB	13 TB	68 TB
HMI				
Telemetry	N/A	N/A	202	1.1 PB
Level 0	N/A	N/A	264	1.5 PB
Level 1	N/A	N/A	298	1.5 PB

Level 1.5	N/A	N/A	99	0.54 PB
Higher-level Products	N/A	N/A	188	1.0 PB
HMI Total	N/A	N/A	1.05 PB	5.8 PB
SDO Total	15 GB	80 GB	1.9 PB	10.5 PB

Table 7-2: Data Volumes at End of First Extended Mission (01 Oct 2015 – 30 Sep 2017)

Instrument/Data Set	Annual (Uncompressed)	7.5-Year Total (Uncompressed)	Annual (Compressed) (TB)	7.5-Year Total (Compressed)
AIA				
Telemetry	N/A	N/A	193	1.5 PB
Level 0	N/A	N/A	206	1.5 PB
Browse data	N/A	N/A	69	518 TB
Level 1	N/A	N/A	224	1.7 PB
Level 1.5*	0	0	0	0
Higher-level Products	N/A	N/A	124.5	1.0 PB
AIA Total	N/A	N/A	804	6.2 PB
EVE				
Level 0	N/A	N/A	6.3 TB	78 TB
Level 1	14 GB	112 GB	20 GB	1.1 TB
Space Weather Data	0.2 GB	1.5 GB	N/A	N/A
Higher level Products	0.058 GB	0.45 GB	0.073 GB	0.4 TB
EVE Total	14 GB	114 GB	6.4 TB	80 TB
HMI				
Telemetry	N/A	N/A	202	1.5 PB
Level 0	N/A	N/A	264	2.0 PB
Level 1	N/A	N/A	298	2.2 PB
Level 1.5	N/A	N/A	99	0.75 PB
Higher-level Products	N/A	N/A	188	1.4 PB
HMI Total	N/A	N/A	1.05 PB	7.9 PB
SDO Total	15 GB	114 BG	1.9 PB	14 PB

Table 7-3: Data Volumes at End of Second Extended Mission (01 Oct 2017 – 30 Sep 2020)

Instrument/Data Set	Annual (Uncompressed)	10.5-Year Total (Uncompressed)	Annual Compressed (TB)	10.5-Year Total Compressed
AIA				
Telemetry	N/A	N/A	193	2.0 PB
Level 0	N/A	N/A	206	2.2 PB
Browse Data	N/A	N/A	69	725 TB
Level 1	N/A	N/A	224	2.4 PB
Level 1.5*	0	0	0	0
Higher level Products	N/A	N/A	124.5	1.4 PB
AIA Total	N/A	N/A	805	8.7 PB
EVE				
Level 0	N/A	N/A	6.3 TB	97 TB
Level 1	14 GB	154 GB	2.2 GB	1.1 TB
Space Weather Data	0.2 GB	2 GB	N/A	N/A
Higher level Products	0.058 GB	0.62 GB	0.073 GB	0.41 TB
EVE Total	15 GB	160 GB	6.4 TB	99 TB
HMI				
Telemetry	N/A	N/A	202	2.1 PB
Level 0	N/A	N/A	264	2.8 PB
Level 1	N/A	N/A	298	3.1 PB
Level 1.5	N/A	N/A	99	1.0 PB
Higher-level Products	N/A	N/A	188	2.0 PB
HMI Total	N/A	N/A	1.05 PB	11.0 PB
SDO Total	15 GB	160 GB	1.9 PB	20 PB

7.1 Current Archive Locations

This section describes each of the locations/repositories for science data products, any mirroring locations, and archival roles and responsibilities. Any requirements or restrictions for accessing the archives (e.g., accounts) are identified.

The EVE SPOC retains all science data files on site at LASP. Public products are available on the LASP website <http://lasp.colorado.edu/home/eve>. Non-public products are made available for special cases upon request.

The lowest level 0a (telemetry file) data are copied to Amazon Glacier to support disaster recovery. All data are also copied to two separate LTO-6 tapes on site and stored in separate buildings to support more rapid recovery from accidental data deletion or a single building problem.

7.2 Data Access and Processing Tools

This section identifies any software available to help users search the archive catalog, access data, and further process the data. Minimum system requirements needed to install (if needed) and use the software shall be provided. This section identifies the capabilities of the software (e.g., browsing, generating light curves, performing analyses, etc.), the language it was developed in, and the file types it can be used with.

EVE data can be accessed in multiple ways. One method is through the LASP Solar Irradiance Data center (LISIRD) at <http://lasp.colorado.edu/lisird> where users have access to all of the tools available to all of the other irradiance datasets. This includes interactive plotting, zooming, panning, data selection, and download in other formats. LISIRD uses REST and has an API to support more advanced user needs.

Another access method is through the EVE web page. This access method supports directory browsing of individual product files and a calendar view for access to public data products. Users can take advantage of standard tools like wget and curl with this method to retrieve multiple files.

7.3 Documentation and Metadata

This section describes how the project will make documentation of data products and format available. Listings of any software documentation or user guides shall indicate when they were last updated as well as the version of the software they are applicable to. This section also identifies any metadata schemes to be employed (e.g., SPASE).

The EVE data product documentation is distributed from the EVE web site through a file of Release Notes, and a README file for each data product. The EVE FITS metadata keywords are a subset of the conventions used by AIA.

7.4 Final Archive/Mission Archive Plan

This section describes the tasks needed to adapt products/data sets in order to maintain their long-term utility with minimal (or no) support from the mission or instrument team. The details of this section will be updated at each Senior Review in preparation for extended mission phases and to leverage advances in Information Technology.

The Solar Data Archive Center (SDAC) at NASA Goddard Space Flight Center in Greenbelt, MD, has been designated as the final archive for SDO data products and software. The SDO team is working with the Jack Ireland, the lead of the SDAC, on transferring Level 0 AIA and HMI data to the SDAC. These files are invariant in time. Higher-level data products are subject to revisions as the knowledge of the calibration and data-reduction algorithms improve.

7.4.1 Data Products

This subsection describes the classes of data products to be contained within the Final Archive including, but not limited to catalog data, calibrated data, and ancillary products. A summary list or table of final products and their formats shall be included.

This subsection also includes details on each instrument team's archiving plan.

Science data and the ancillary data needed for its analysis will be held and served at the JSOC and EVE SOC during the SDO mission lifetime. A list of the data products and how to access them is contained in the spreadsheet SDO_Data_Products.xlsx.

7.4.2 Analysis Tools

This subsection describes the set of analysis tools to be archived for the research community.

Analysis tools are contributed to the SolarSoft IDL tree and the SunPy distribution. This allows free and unfettered access to the analysis tools by the scientific community.

7.4.3 Documentation

This subsection describes the process of reviewing existing mission documentation and downselecting to a core set that has been scrubbed to remove obsolete and/or conflicting material.

The plan for this activity will be developed during the Third Extended Mission.

7.4.4 Final Archive Access and Distribution

This subsection describes how data, tools, and documentation are to be served and maintained for the long term.

SDO and the Heliophysics Director have agreed to host the final data archive for SDO data at the Solar Data Archive Center (SDAC) at Goddard Space Flight Center. The plan for this activity will be developed during the Third Extended Mission.

8.0 Glossary

Ancillary Data	Non-science data needed to generate Level 1 data sets. Consists of instrument gains, offsets; pointing information for scan platforms, etc.
Browse Data	Web-accessible subset of the science data that allows the user to quickly browse and perform a preliminary assessment of the data. Browse data are typically used to determine a time or wavelength range for a request of higher-level science data.
Catalog	The instrument source catalog is a compilation of derived parameters and scientific results about observed sources.
Continued accessibility	The derivation and dissemination of useful science knowledge and insight resulting from the data collected. The functions and services provided during continued accessibility include directory and catalog services, scientific computing resources, discipline data archives, and other archives and databases.
Correlative data	Other science data needed to interpret space-based data sets. May include ground-based data such as H α images or other space-based measurements of the solar irradiance.
Data Analysis	Process by which higher-level data products are derived from basic data acquired by instruments. Data analysis functions include modeling, manipulation, data interpretation, and data presentation.
Data Directory	Top-level index containing information about location, ownership, contents of data. Used as first step in determining what types of data exist for given time, period, location, etc.
Data Handling	The process of data acquisition including onboard encoding and compression of data generated by flight sensors, data preprocessing on the ground to remove the artifacts of data transmission and conversion of raw data to Level 0 data, and management of this process to assure completeness and accuracy of the science data.
Data Set	The accumulation of data products, supplemental data, software, and documentation that will completely document and support the use of those data products. A data set can be part of a data set collection; can reside on a single physical volume or across multiple volumes.
Decommutation	Process whereby the downlink data stream is split into data streams that contain data from only one or from select payloads or systems.
Discipline Data Archive	Long-lived collections of science, operational and related ancillary data, maintained as a national resource at a discipline data center, supported with adequate cataloging, protection, and distribution functions. It provides long-term access to data by the general space science community.
Guest Observer	Has access to observation, to generate specific space science data to conduct independent investigations, although seldom participate in initial mission planning or instrument design.
High-Level Processed Data	Products of detailed processing including instrumental calibrations and background corrections.
Level 0 Data	Reconstructed unprocessed instrument data at full resolution. Edited data corrected for telemetry errors and split or decommutated into a data set for a given instrument. Sometimes called Experimental Data Record. Data are also tagged with time and location of acquisition.
Low-Level Processed Data	Data products of "automatic" pipeline processing. These data are generally produced within a few months of acquisition.
Metadata	Descriptions of database contents in sufficient detail to allow retrieval of subsets of data.
Mission Operations	The safe and efficient operation of the spacecraft and associated payloads during the active flight portion of the investigation. The principal functions and services associated with

mission operations include telemetry services, mission planning and scheduling, and mission control.

Non-Science User	General public, Public Affairs/Outreach or curious individuals seeking data for information purposes rather than for scientific investigation.
Primary User	Includes science investigators who plan and design the experiments, and have an immediate need for access to the data being generated. This includes principal investigators, guest observers, and investigator team members. They represent the first scientists with access to the data.
Principal Investigator (PI)	Often work with co-investigators, are responsible for planning, development, and integration of experiments and instruments, data analysis, and the selection and preparation of the analyzed data for archiving. Principal Investigators are usually tied to a particular instrument.
Production Time	This is the processing time required to generate a data product in usable form after data acquisition.
Project Data Repository	Short-term database that serves as a way station or clearinghouse for data - such as a mission data base to support operations and compilation of initial results. Temporary buffers for new data, usually existing only as long as the mission producing the data.
Public Release Time	This is the time when a data product becomes public domain after its production and can be accessed by a researcher without exclusive rights to the data.
Raw Data or raw telemetry	Telemetry data with data embedded
Science Operations	The functions and services required to ensure the production of valuable science data or samples during the active flight portion of the investigation. Principal functions and services provided as science operations include science planning and scheduling, science control, project data archive, and science data analysis.
SDO Science Working Group	This group is responsible for scientific direction of the SDO mission. It is composed of the project scientist, the principal investigators of each of the SDO instruments, and one representative from the Space Weather community.
Secondary User	A member of the general science community, which could include discipline peers or interdisciplinary scientists, who usually conduct their analysis using data that has been archived, as well as data provided or published by the PI. Secondary users also work in collaboration with primary users. A researcher not involved with instrumentation design, development, or data acquisition. A secondary user would normally go to a data archive to obtain the required data set. Also referred to as retrospective investigator.
Status	Data products that contain information about the SDO spacecraft or data products
Telemetry Services	Those activities required to convert the spacecraft downlink into data that is useful to the experimenter or investigator.
Test SOC	Science Operations Center employed during integration and test.

9.0 ACRONYM AND ABBREVIATION LIST

See also <http://sdo.gsfc.nasa.gov/resources/acronyms.php>

AIA	Atmospheric Imaging Assembly
CCB	Change Control Board
CCSDS	Consultative Committee for Space Data Standards
CI	Collaborative Investigator
CME	Coronal Mass Ejection
Co-I	Co-investigator
DDS	Data Distribution System
EELV	Evolved Expendable Launch Vehicle
EVE	Extreme ultraviolet Variability Experiment
EUV	Extreme Ultraviolet
FITS	Flexible Image Transport System
FOT	Flight Operations Team
FTP	File Transfer Protocol
GB	Gigabyte
GSFC	Goddard Space Flight Center
HMI	Helioseismic and Magnetic Imager
I&T	Integration and Test
ICD	Interface Control Document
LASP	Laboratory for Atmospheric and Space Research
LMSAL	Lockheed Martin Solar and Astrophysics Laboratory
MB	Megabyte
MOC	Mission Operations Center
PB	Petabyte (10^{15} bytes)
PI	Principle Investigator
SDAC	Solar Data Archive Center
SDO	Solar Dynamics Observatory
SOC	Science Operations Center
SWG	Science Working Group
T&C	Telemetry & Control
TBD	To Be Determined
TLM	Telemetry
TRACE	Transition Region and Coronal Explorer
VCDU	Virtual Channel Data Unit
VSO	Virtual Solar Observatory
WSMR	White Sands Missile Range

10.0 Appendix A. Data Rights and Rules for Data Use

The SDO science investigators agree to abide the Rules of the Road developed for the Sun-Earth Connection and its successor, the Heliophysics Division. These are:

1. The Principal Investigators (PI) shall make available to the science data user community (Users) the same access methods to reach the data and tools as the PI uses.
2. The PI shall notify Users of updates to processing software and calibrations via metadata and other appropriate documentation.
3. Users shall consult with the PI to ensure that the Users are accessing the most recent available versions of the data and analysis routines.
4. Browse products are not intended for science analysis or publication and should not be used for those purposes without consent of the PI.
5. Users shall acknowledge the sources of data used in all publications and reports.
6. Users shall include in publications the information necessary to allow others to access the particular data used.
7. Users shall transmit to the PI a copy of each manuscript that uses the PI's data upon submission of that manuscript for consideration of publication.
8. Users are encouraged to make tools of general utility widely available to the community.
9. Users are also encouraged to make available value-added data products. Users producing such products must notify the PI and must clearly label the product as being different from the original PI-produced data product. Producers of value-added products should contact the PI to ensure that such products are based on the most recent versions of the data and analysis routines. With mutual agreement, Users may work with the PI to enhance the instrument data processing system, by integrating their products and tools.
10. The editors and referees of scientific journals should avail themselves of the expertise of the PI while a data set is still unfamiliar to the community, and when it is uncertain whether authors have employed the most up-to-date data and calibrations.

Appendix B: Calibration and Measurement Algorithm Documents (CMAD) (Factor D-4, informational)

The Call for Proposals in this Senior Review cycle has asked for a Calibration and Measurement Algorithm Documents to be produced for each data product served by the missions.

The SDO team is working to inventory the approximately 150 data products that we currently produce. Once that inventory exists, the data products will be grouped into families that share a similar data pipeline. The need to produce a CMAD for each data product (or family of data products) will then be assessed.

We will move toward a web-based version of as much of the CMADs as possible. This allows an easier update process and facilitates distribution to the public. Due to complexity of the algorithms we plan to release the CMADs as project-controlled documents served at the SDO public-facing website.

We have determined that producing the CMADs will require a significant amount of work. The author of a CMAD must be familiar with the instrument, the data used in the product, and the algorithms used to generate the data product. Members of the EVE Team recently produced Algorithm and Theoretical Basis Documents as they prepared for the final delivery of their data products from the SORCE satellite. Based on the work that of effort, we estimated each CMAD will take a total of three months of effort, from the initial writing, to review, and project acceptance. This work effort estimate was used to generate the over-guide budget requests.

Attached to this appendix is the EVE pre-launch CMAD, which shows the format and style we anticipate for these documents.

B.1: EVE Level 0-3 CMAD

Laboratory For Atmospheric and Space Physics

LASP Engineering Division
University of Colorado
Boulder, Colorado



**Solar Dynamics Observatory
EUV Variability Experiment
(SDO EVE)**

Calibration and Measurement Algorithms Document (CMAD)

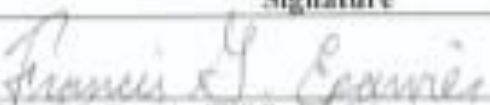
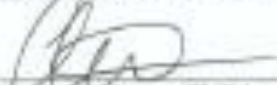
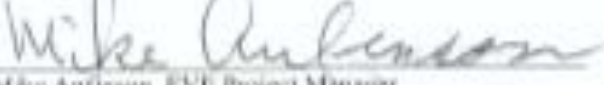
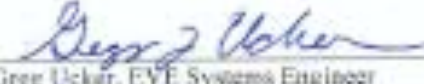
Document No. **EVE-T-11003** Rev. A

Date: 01/31/2005

Prepared By: Francis G. Eparvier, EVE Project Scientist

Revision History				
Rev	Description of Change	By	Approved	Date
1	Draft for PDR	FGE	TNW	12/13/2003
A	Revised Draft for CDR	FGE	TNW	1/31/2005

CHECK TO VERIFY THAT THIS IS THE CURRENT VERSION PRIOR TO USE

Authority	Signature	Date
Approved by	 Francis G. Espenier, EVE Project Scientist	01-Feb-2005
Approved by	 Thomas N. Woods, EVE Principal Investigator	01-Feb-2005
Approved by	 Andrew R. Jones, EVE Instrument Scientist	2/2/2005
Approved by	 Mike Antilinson, EVE Project Manager	2/1/05
Approved by	 Greg J. Uckar, EVE Systems Engineer	2/1/05

CM FOREWORD

This document is a Solar Dynamics Observatory EUV Variability Experiment project controlled document. Changes to this document require prior approval of the EVE project. Proposed changes shall be submitted to EVE Configuration Management, along with supportive material justifying the proposed change.

Questions or comments concerning this document should be addressed to:

EVE Configuration Manager
Laboratory for Atmospheric and Space Physics
University of Colorado
1234 Innovation Dr.
Boulder, CO 80303

Table of Contents

1	Scope.....	1
2	Related Documentation.....	1
2.1	Applicable Documents.....	1
3	Overview and Background Information	1
3.1	Science Objectives	1
3.2	EVE Instrument Description.....	2
3.2.1	Overall EVE Measurement Concept.....	2
3.2.2	EVE Instrument Subsystem Descriptions	4
3.2.2.1	Multiple EUV Grating Spectrographs (MEGS).....	4
3.2.2.1.1	MEGS Channel A (MEGS-A) Design	4
3.2.2.1.2	MEGS Channel B (MEGS-B) Design.....	6
3.2.2.1.3	MEGS Solar Aspect Monitor (MEGS-SAM) Design	8
3.2.2.1.4	MEGS Photometer (MEGS-P) Design	9
3.2.2.1.5	EUV SpectroPhotometers (ESP) Design.....	9
3.2.3	EVE Heritage	10
3.2.3.1	Instrument Heritage	10
3.2.3.2	Algorithm and Calibration Heritage	10
4	EVE Calibration Plan.....	10
4.1	Overall Calibration Scheme	10
4.2	Pre-flight Calibration Plans.....	11
4.2.1	MEGS Pre-flight Calibrations	11
4.2.2	ESP Pre-flight Calibrations	12
4.3	In-flight Tracking of Short-Term Changes	12
4.4	Long-term Absolute Calibration Tracking (Re-Calibration)	12
4.5	Validation.....	13
5	EVE Measurement Algorithm Descriptions	13
5.1	Theoretical Basis.....	13
5.2	Conversion of Instrument Signals to Irradiance Units.....	14
5.2.1	MEGS-A and MEGS-B Measurement Equations.....	14
5.2.2	MEGS-SAM Measurement Equation	15
5.2.3	ESP and MEGS-P Measurement Equation	15
5.3	Signal Estimates and Error Analyses for Subsystems	15
5.3.1	MEGS Signal Estimates and Error Analysis.....	15
5.3.2	MEGS-SAM Signal Estimates and Error Analysis.....	18
5.3.3	ESP Signal Estimates and Error Analysis.....	20
5.4	Preflight Calibration Algorithms	20
	APPENDIX A: List of EVE Variable Definitions.....	21

List of Tables

Table 1: List of Applicable Documents	1
Table 2: EVE Science Requirements	2
Table 3: MEGS-A and MEGS-B Uncertainty Estimate and Error Budget	18
Table 4: MEGS-SAM Uncertainty Estimate and Error Budget.....	19
Table 5: ESP Uncertainty Estimate and Error Budget.....	20

List of Figures

Figure 1: EVE redundant wavelength coverage diagram.	3
Figure 2: MEGS-A optical layout with MEGS-SAM.....	5
Figure 3: MEGS-A simulated detector image with MEGS-SAM image. Slit 1 is on top and Slit 2 is on the bottom. Note that the image has been contrast-enhanced to show weaker lines. The corresponding solar signal estimate is shown below the image.	6
Figure 4: MEGS-B optical layout.	7
Figure 5: MEGS-B simulated detector image. The primary sceince (1.1) order spectrum falls diagonally across the detector from the upper right to lower left. Note that the image has been contrast-enhanced to show weaker lines. The corresponding solar signal estimate is shown below the image.....	7
Figure 6: MEGS-SAM optical layout withing the MEGS-A housing.....	8
Figure 7: MEGS-P optical alyouth withing the first chamber of MEGS-B. The photometer is placed on the opposite side of the the 0 th order as the primary spectrum from the MEGS-B first grating.....	9
Figure 8: ESP optical layout.	10
Figure 9: MEGS-A Slit 1 signal estimates for solar minimum, maximum, and flare conditions.	16
Figure 10: MEGS-A Slit 2 signal estimates for solar minimum, maximum, and flare conditions.	16
Figure 11: MEGS-B signal estimates for solar minimum, maximum, and flare conditions.	17
Figure 12: MEGS-SAM irradiance signal estimates for solar minimum conditions.....	18

1 Scope

The Calibration and Measurement Algorithm Document (CMAD) describes the overall concept for calibrating the EUV Variability Experiment (EVE) instrument for the Solar Dynamics Observatory (SDO), including preflight and inflight calibrations, and details the algorithms for converting instrument signals to solar spectral irradiances, including signal estimates, error analyses, and error budgets. In addition, the document gives a brief overview of the scientific goals of EVE and an introduction to the instrumentation, but it is not designed to be the only reference for these aspects of EVE and gives only enough detail to understand the calibration plan and measurement algorithms. Other, more detailed, documents describe the EVE instrument design, operations, ground system, and data products. All plans and algorithms are described as they are envisioned or known during the design phase of the EVE project. Future changes in instrument design and understanding of calibrations and algorithms may require modifications to this document.

2 Related Documentation

2.1 Applicable Documents

The following documents and drawings in effect on the day this document was signed shall apply to the extent specified herein. In the event of conflict between this document and any referenced document, this document will govern.

The following is a list of the applicable specifications and publications.

Table 1: List of Applicable Documents

DOCUMENT NUMBER	TITLE	Revision/Date
EVE-T-11001	EVE Science Requirements Document	
EVE-T-11002	EVE Systems Requirements Document	
EVE-S-11314	EVE Science Data Processing Requirements Document	
EVE-T-13010	EVE Performance Verification Plan	
EVE-T-11004	EVE Solar Emission Line Measurement List	

3 Overview and Background Information

3.1 Science Objectives

The Extreme Ultraviolet Variability Experiment (EVE) program for the SDO measures the solar extreme ultraviolet (EUV) irradiance with unprecedented spectral resolution, temporal cadence, accuracy, and precision. In addition, the EVE program incorporates physics-based modeling to advance the understanding of the solar EUV irradiance variations based on magnetic features. The science objectives for EVE are fourfold: (1) Specify the solar EUV spectral irradiance and its variability on multiple time scales (seconds to years); (2) Advance current understanding of how and why the solar EUV spectral irradiance varies; (3) Improve the capability to predict

(nowcast and forecast) the EUV spectral irradiance variability; and (4) Understand the response of the geospace environment to variations in the solar EUV spectral irradiance and the impact on human endeavors.

3.2 EVE Instrument Description

3.2.1 Overall EVE Measurement Concept

In order to fulfill the science objectives of EVE, the measurements of solar EUV irradiance must have high spectral resolution, high accuracy and long-term stability throughout the SDO mission. The science requirements are summarized in Table 2. For the origins of the specific requirements, see the EVE Science Requirements Document, EVE-T-11001. To achieve these requirements, the EVE instrumentation includes multiple channels with different optical designs and detectors and with different techniques for pre-flight calibration and in-flight monitoring of relative sensitivity changes, plus regular sounding rocket flights with nearly identical instruments to track absolute sensitivity changes.

Table 2: EVE Science Requirements

Parameter	Minimum Success Requirements	Comprehensive Success Criteria	Design Goals
λ Range	6 or more emissions to specify the chromosphere, TR, and corona, plus the He II 30.4 nm emission	0.1-105 nm	0.1-105 nm
$\Delta\lambda$ Resolution	0.2 nm for these lines	0.1 nm for 18 or more emissions to specify the chromosphere, TR, and corona, and 5 nm or better elsewhere	0.1 nm
Time Cadence	60 sec	< 20 sec	10 sec
Accuracy	35% for 5 nm intervals and daily average	25% for 5 nm intervals and daily average	20% for brighter emissions
Mission Life	3 years	5 years	5 years, long enough to sample low and high solar activity

The EVE instrument subsystems are described in more detail in the following subsections. The overall concept is illustrated in Figure 1, which shows the wavelength coverage of each of the channels of the EVE instrument suite along with a sample solar spectrum.

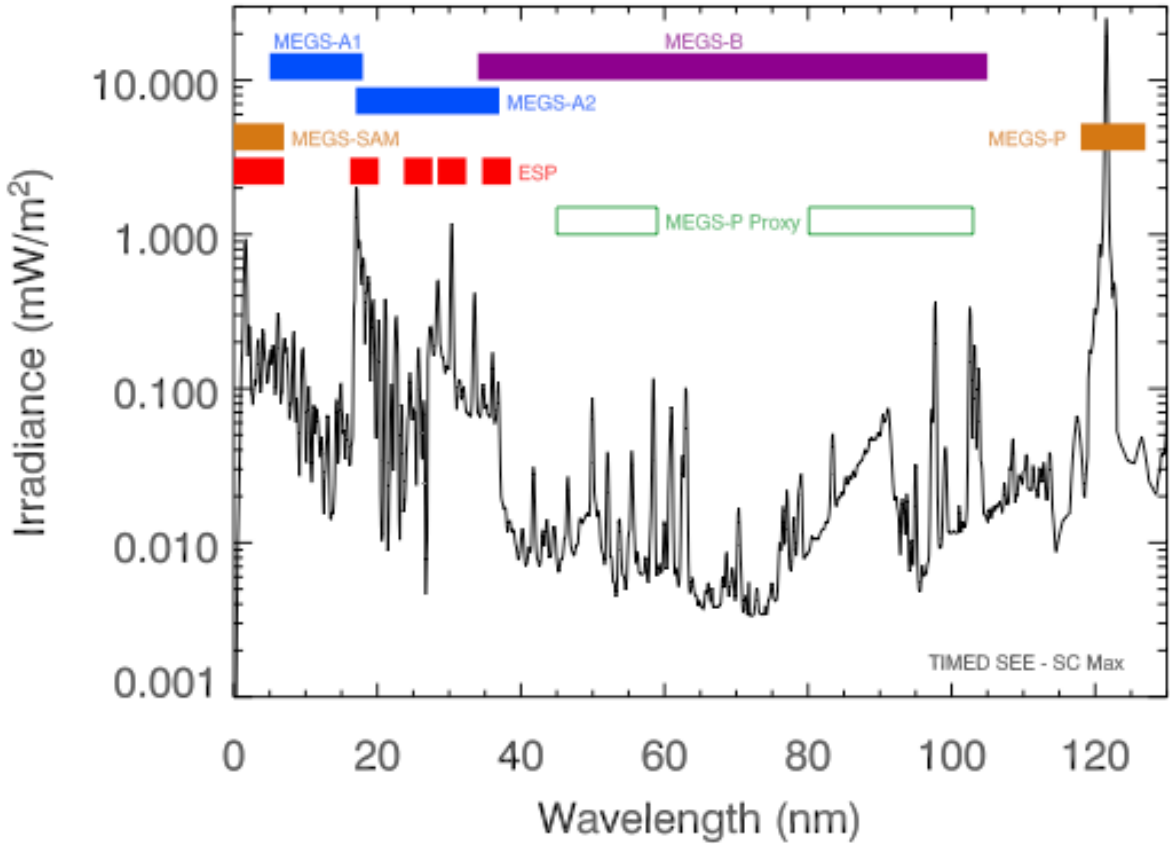


Figure 1: EVE redundant wavelength coverage diagram.

The primary, high spectral resolution irradiance measurements are made by the Multiple EUV Grating Spectrographs (MEGS). The MEGS is composed of two spectrographs: MEGS-A is a grazing incidence spectrograph covering the 5 to 37 nm range, and MEGS-B is a two-grating, cross-dispersing spectrograph covering the 35 to 105 nm range. Included as part of the MEGS-A package, is a pinhole camera to be used as a solar aspect monitor (MEGS-SAM). The MEGS-SAM will provide a pointing reference for the EVE channels. It will also make a spectral measurement of the solar irradiance in the 0.1 to 5 nm wavelength range at approximately 1 nm resolution. In addition, as part of the MEGS-B, is a photodiode with a filter to isolate Lyman- α at 121.6 nm (MEGS-P). This measurement is used for short-term calibration tracking. While Lyman- α is not within the spectral range of the rest of MEGS, it is a proven proxy for other EUV emissions and will be used in conjunction with a spectral model to track potential changes in the sensitivity of the MEGS on the timescale of weeks and months. Longer-term changes in the sensitivity of the EVE channels will be tracked by annual sounding rocket underflights of similar instruments.

Also, for short-term calibration tracking purposes, redundant, lower spectral resolution measurements at select bandpasses will be made by the EUV Spectrophotometer (ESP). The ESP is a transmission grating and photodiode instrument similar to the SOHO SEM. ESP has four channels centered on 18.2, 25.7, 30.4, and 36.6 nm that are each approximately 4 nm in spectral width. The ESP also has a central, zeroth-order diode with a filter to make the primary irradiance measurement in the 0.1 to 7 nm range. The ESP measurements are made at a high time-cadence (0.25 sec) and so are useful as quick indicators of space weather events such as flares.

The redundant wavelength coverage from ESP, the MEGS-P (along with the HI Ly- α proxy) and the MEGS-SAM, all provide EVE with the ability to track any relative sensitivity changes that may occur in the MEGS primary spectral measurements. Absolute sensitivity changes will be provided by sounding rocket underflights of EVE prototype instruments at regular intervals throughout the SDO mission life. The sounding rocket instruments can be calibrated on the ground before and after each rocket flight, and that calibration can be transferred to the EVE instruments on the SDO spacecraft through simultaneous observations.

3.2.2 EVE Instrument Subsystem Descriptions

3.2.2.1 Multiple EUV Grating Spectrographs (MEGS)

The MEGS is an improved version of the EUV Grating Spectrograph (EGS) that is part of the highly successful TIMED SEE instrument [Woods et al., 1998]. The MEGS has two channels: MEGS-A and MEGS-B. Both the EVE MEGS-A and the SEE EGS have spherical grating spectrograph designs that are highly desirable for the EUV range as they require only one reflection. MEGS-A covers the wavelength range from 5 to 37 nm. Unlike the SEE EGS, the EVE MEGS-B uses two normal incidence gratings and covers the wavelength range from 35 to 105 nm. In all these instruments array detectors provide for rapid integration times over the full spectral range. The main improvements over the EGS for MEGS include higher spectral resolution (4 times improvement) that is achieved by having two channels, better sorting of the grating orders, extension to shorter wavelengths, and the use of EUV sensitive CCDs that are more stable with long-term exposures than the MCP-based CODACON detectors used for TIMED EGS.

Both MEGS channels are integrated into the same housing. Each channel is optimized for its respective wavelength range by implementing specific grating angles, coatings on the grating, ruling densities, and filters used in front of the entrance slits. The filters define the desired wavelength ranges and reject out of band contributions, such as visible light. The grating rulings are laminar to suppress higher orders. The MEGS field-of-view (FOV) is 2.0° , which is more than sufficient to measure the off-limb contributions to the irradiance. A study of SOHO EIT images indicates that a FOV of 0.9° is required to measure $> 98\%$ of the solar EUV irradiance. The CCD cameras for MEGS use the MIT LL CCID-28, which is a backside illuminated 2048x1024 CCD.

Each MEGS channel has LED lamps to allow for flatfield characterization of the CCD detectors before and during flight. Each MEGS channel also has a filter wheel to place special filters, instead of the primary science filters, in front of the aperture allowing for characterization of higher order signals before and during flight. The filter wheels also contain dark, or closed aperture, positions to allow for determination of detector dark signals.

In addition to the two spectral channels for MEGS, a Solar Aspect Monitor (MEGS-SAM) has been incorporated into the MEGS-A channel to provide pointing information both during calibration and in-flight. The MEGS-SAM will also provide spectral information between 0.1 and 7 nm.

3.2.2.1.1 MEGS Channel A (MEGS-A) Design

The optical layout of the MEGS-A is shown in Figure 2. It is a 80° grazing incidence, off-Rowland circle spectrograph with a CCD detector to measure the solar spectrum between 5-37

nm at a resolution just less than 0.1 nm. MEGS-A has two entrance slits, each 20 microns wide and 2 mm high, oriented top-to-bottom. In front of the slits is a filter wheel mechanism with bandpass-limiting thin foil (filters made by Luxel). The primary science filters are Zr/C for slit 1 to isolate 5 to 18 nm and Al/Ge/C for slit 2 to isolate 17-37 nm. Secondary filters are available to further limit the bandpasses of each slit to provide an occasional check on higher orders (Zr/Si/C for slit 1 to pass 13 to 18 nm, and Al/Mg/C to pass 25 to 37 nm for slit 2). The filter wheel mechanism also has a blanked-off position for dark measurements. The grating, produced by J.-Y., is a spherical holographic grating with a radius of curvature of 600 nm, platinum coating, and 767 grooves/mm with a laminar groove profile to suppress even orders. The detector for MEGS-A is a back-thinned, back-illuminated, split-frame transfer CCD with 1024x2048 pixels and is being designed and built by MIT-LL. The CCD is maintained at -90°C to suppress noise and to minimize radiation damage in the geosynchronous environment.

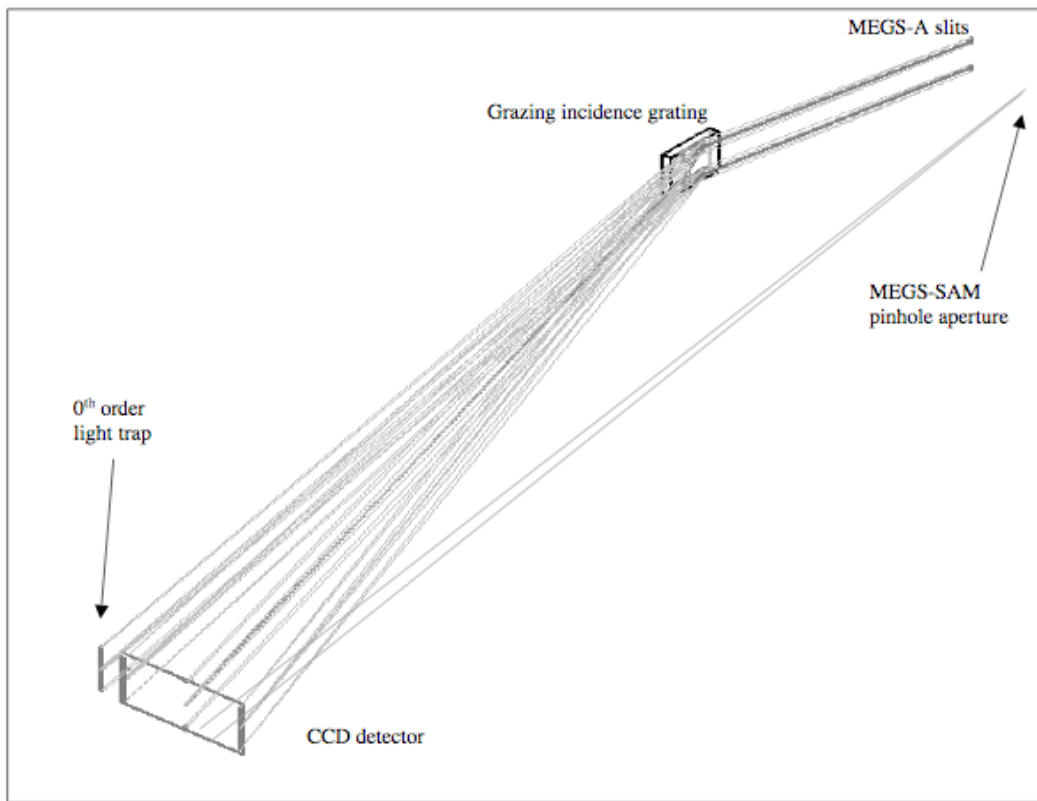


Figure 2: MEGS-A optical layout with MEGS-SAM.

A simulated CCD image of a solar spectrum taken with MEGS-A is shown in Figure 3. The contrast has been enhanced to show dim lines. Wavelengths go from right to left, as indicated on below the image. MEGS-A Slit 1 (upper portion) will be used to cover 5 to 20 nm, and Slit 2 (lower portion) will be used to cover 17 to 37 nm.

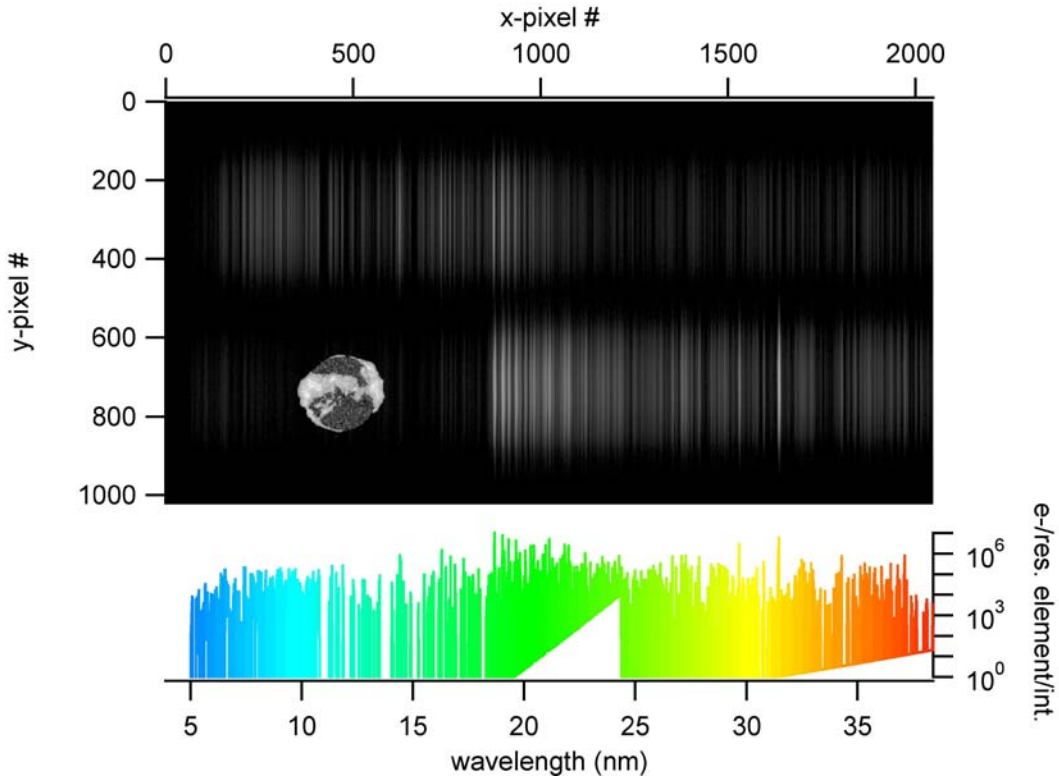


Figure 3: MEGS-A simulated detector image with MEGS-SAM image. Slit 1 is on top and Slit 2 is on the bottom. Note that the image has been contrast-enhanced to show weaker lines. The corresponding solar signal estimate is shown below the image.

3.2.2.1.2 MEGS Channel B (MEGS-B) Design

The optical layout for MEGS-B is shown in Figure 4. MEGS-B is a normal incidence, double-pass, cross-dispersing Rowland Circle spectrograph with a CCD detector to measure the solar spectrum between 35-105 nm at a resolution just less than 0.1 nm. MEGS-B has a single entrance slit, 35 microns wide and 3.5 mm high. The double-pass grating design is needed for MEGS-B to block out unfiltered visible solar light entering the instrument (stable foil filters that pass wavelengths longward of 80 nm do not exist). Reflection gratings typically have 10-5 to 10-8 rejection of out-of-band light, with holographically-ruled gratings performing better than mechanically-ruled gratings. The two gratings in MEGS-B reject 10-10 or better of the visible light. The MEGS-B gratings are cross-dispersed giving a spectrum diagonally across the detector with higher order spectra parallel to the main (1st order) spectrum. Both MEGS-B gratings are also produced by J.-Y., and are spherical holographic gratings with platinum coating, and laminar groove profiles to suppress even orders. The first grating has 900 grooves/mm and the second has 2140 grooves/mm. The detector for MEGS-B is identical to the MEGS-A detector. While MEGS-B does not have a primary bandpass filter, it does have a filter wheel in front of the slit. The filter wheel provides an open position for solar measurements, a closed position for detector dark measurements, and a higher order contributions filter (Sn/Ge/SnO₂) for pre-flight calibrations and in-flight checks.

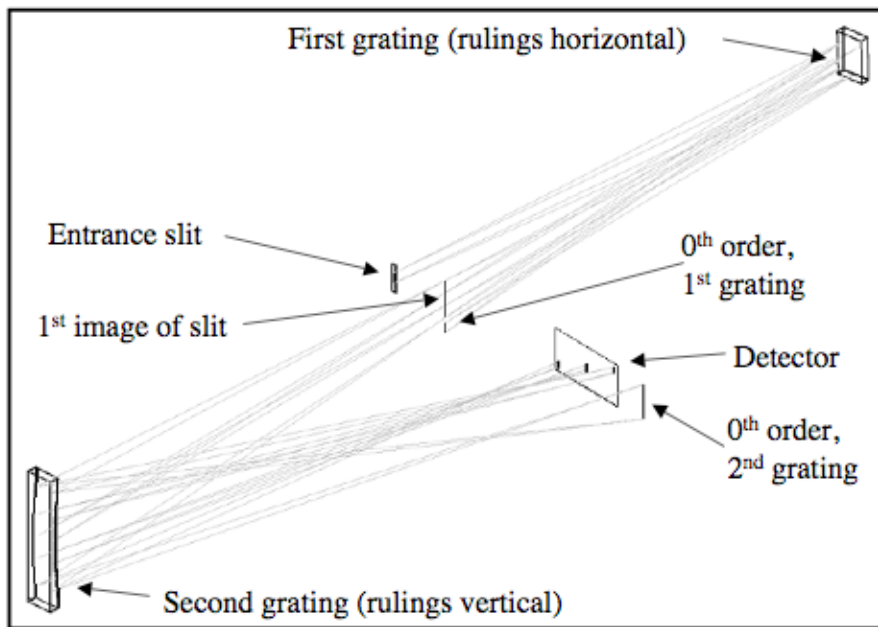


Figure 4: MEGS-B optical layout.

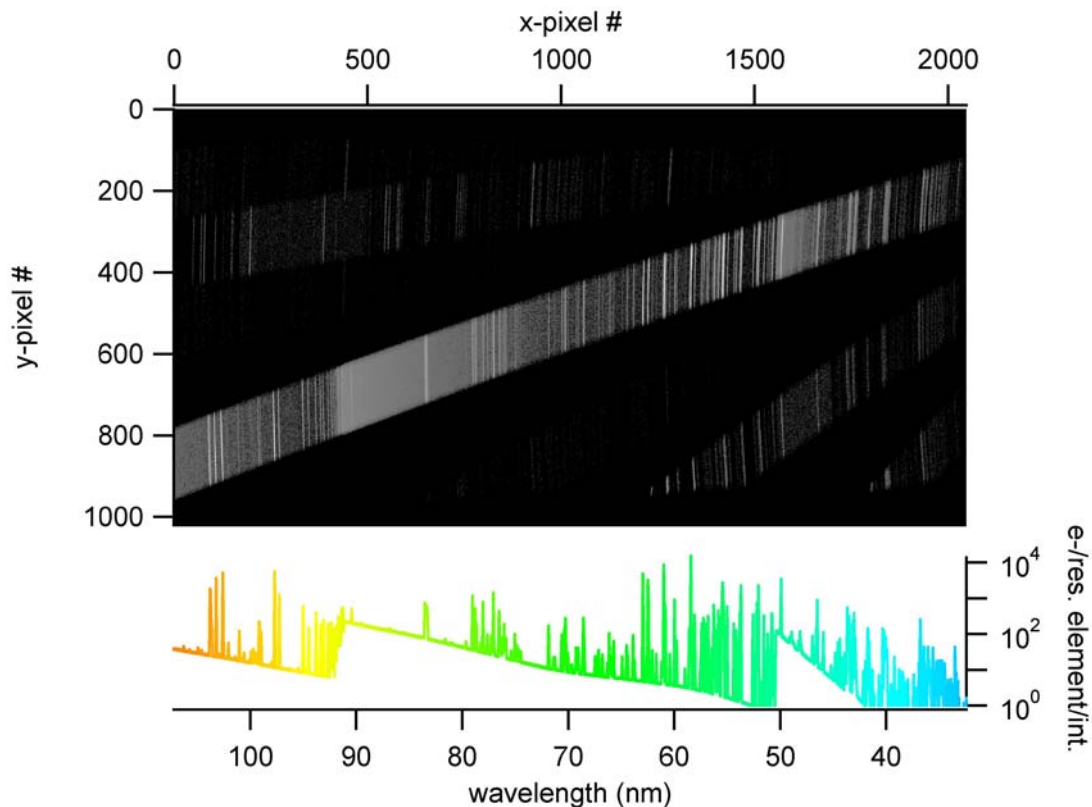


Figure 5: MEGS-B simulated detector image. The primary science (1.1) order spectrum falls diagonally across the detector from the upper right to lower left. Note that the image has been contrast-enhanced to show weaker lines. The corresponding solar signal estimate is shown below the image

A simulated CCD image of a solar spectrum taken with MEGS-B is shown in Figure 5. Again, the contrast has been enhanced to show dim lines. Wavelengths go from right to left, as indicated on below the image. The primary spectrum falls diagonally across the detector from the lower left to the upper right. Higher order spectra fall to either side of the primary spectrum. MEGS-B will be used to cover the 35 to 105 nm wavelength range.

3.2.2.1.3 MEGS Solar Aspect Monitor (MEGS-SAM) Design

The requirement for knowledge of EVE's alignments for preflight calibrations, spacecraft mounting, and solar observations is 1 arc-minute. Quadrant diodes have been used as solar aspect sensors on the TIMED SEE EGS and SORCE SOLSTICE instruments to provide pre-flight and in-flight alignment information. The Solar Aspect Monitor (SAM), although it is not a quadrant diode, serves the same purpose for MEGS. The SAM is a simple addition to the MEGS-A channel that provides alignment information for pre-flight calibration and tests and in-flight solar measurements. The optical layout of the MEGS-SAM is shown in Figure 6. SAM is a pinhole camera within the MEGS-A housing, using a separate aperture, but focusing an image of the Sun onto a portion of the MEGS-A CCD where the bandpass filter for slit 2 allows essentially no light to fall. The SAM aperture has a separate filter wheel mechanism allowing three modes. In aspect monitor mode a UV filter is in place and the resultant image of the Sun can be centroided to give pointing information for all of EVE relative to the boresights found during pre-flight calibrations to roughly 1 arcminute accuracy. In XUV photon-counting mode a Be foil filter is in place to isolate 0.1 to 5 nm. The pinhole and filter are optimized so that in this mode only single photon events occur per pixel per 10-sec CCD integration. This allows for the determination of the energy (or wavelength) of each photon event. Binning photon events from over the entire image of the Sun gives a low (~ 1 nm) spectral resolution for the SAM XUV bandpass. Summing consecutive integrations over minutes will give XUV images of the Sun. The third mode for SAM has the filter wheel in a blanked off position for dark measurements. The location and a simulated image for SAM are shown in Figure 3.

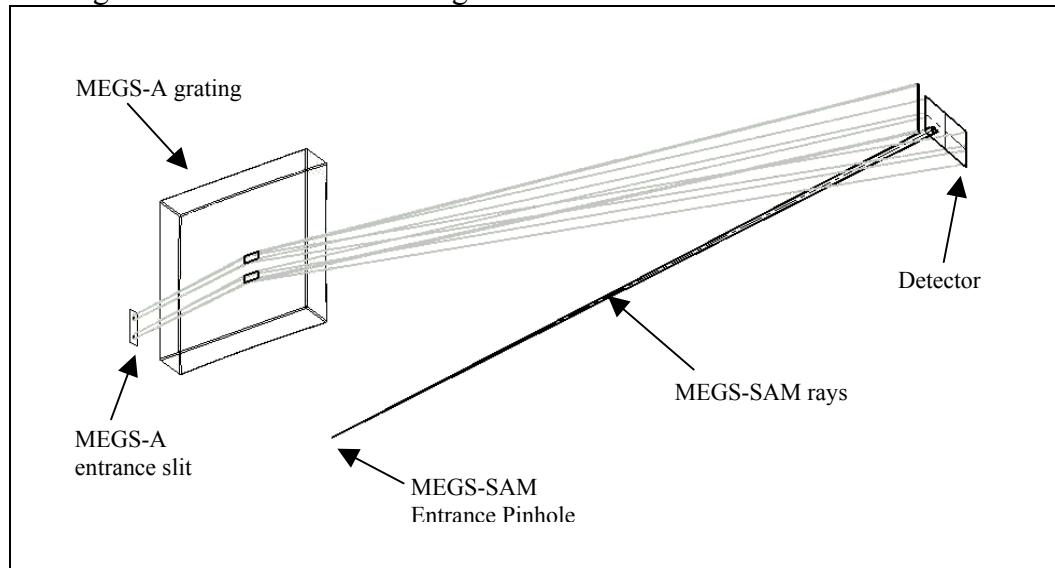


Figure 6: MEGS-SAM optical layout within the MEGS-A housing.

3.2.2.1.4 MEGS Photometer (MEGS-P) Design

The optical layout of the MEGS-P is shown in Figure 7. MEGS-P is an IRD silicon photodiode placed at the -1st order of the first MEGS-B grating. In front of the diode is an Acton interference filter to isolate the solar hydrogen Lyman- α line at 121.5 nm. The filter has a bandwidth of 10 nm, but the solar spectrum is such that greater than 99% of the signal will be due to Lyman- α . Next to the primary MEGS-P diode is an identical diode that is masked off to give simultaneous dark information that is used to correct the MEGS-P measurements for background noise induced by particle radiation.

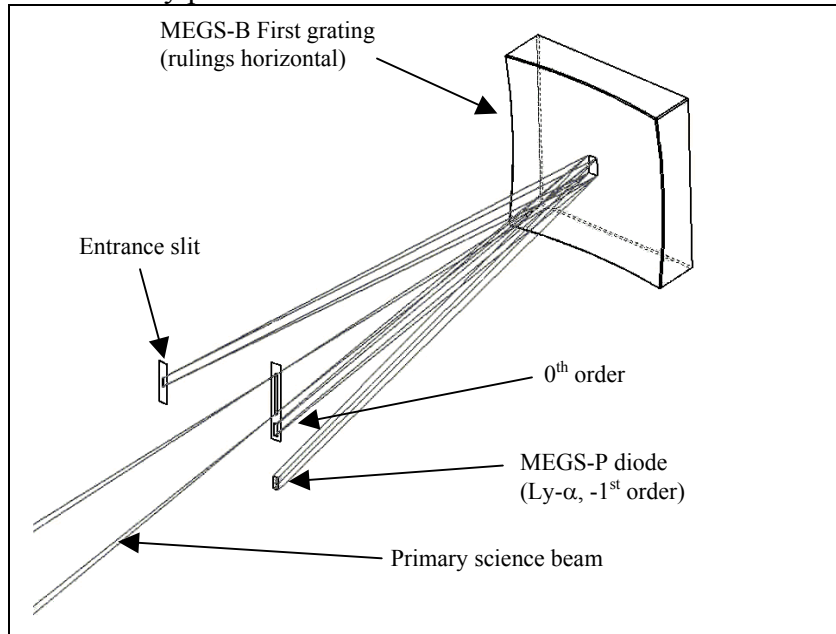


Figure 7: MEGS-P optical layout within the first chamber of MEGS-B. The photometer is placed on the opposite side of the 0th order as the primary spectrum from the MEGS-B first grating.

3.2.2.1.5 EUV SpectroPhotometers (ESP) Design

The EUV Spectrophotometer (ESP) is a small, lightweight instrument based on the successful design of the SOHO SEM spectrometer [Judge et al., 1998]. The optical layout of the ESP is shown in Figure 8. The ESP is a non-focusing, broadband spectrograph with a transmission grating and IRD silicon photodiodes. In front of the entrance slit is an Al foil filter made by Luxel to limit the out-of-band light that gets into the instrument. The transmission grating, made by X-Opt, is essentially a set of thin wires with no substrate spaced so that there are 2500 lines/mm. Silicon photodiodes are placed at both plus and minus first orders and positioned so that the centers are at 18.2, 25.7, 30.4, and 36.6 nm. The diodes are sized to give approximately 4-nm bandpasses centered on each of these wavelengths. The central, zeroth order position has a silicon quadrant photodiode with an additional thin foil filter to isolate 0.1 to 7 nm. The sum of the quadrants gives the solar irradiance in this bandpass. Differencing the quadrants allows for determination of the pointing of the ESP. The ESP has a filter wheel mechanism with open and blanked off positions for solar and dark measurements. The ESP has the fastest measurement cadence of all of the instruments in the EVE suite at 0.25 seconds.

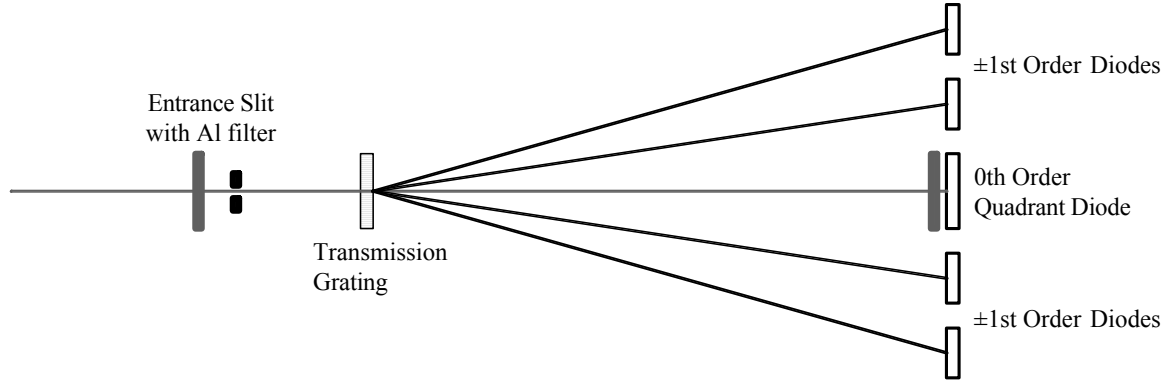


Figure 8: ESP optical layout.

3.2.3 EVE Heritage

3.2.3.1 Instrument Heritage

The MEGS Channels A and B have evolved from the successful TIMED SEE EGS instrument and from sounding rocket versions of the EGS, designed and built by LASP. The CCD cameras for MEGS consist of space-flight CCDs and associated signal processing electronics developed at the MIT Lincoln Laboratory (MIT LL). The CCD cameras have excellent heritage based upon devices flown on the Chandra ACIS instrument, Astro-D CIS instrument, and the Space Based Visible (SBV) instrument on the MSX spacecraft (DoD). Similar cameras will be flown on the HETE-II and Astro-E spacecraft. The MEGS-SAM in spectral irradiance mode utilizes a technique used for astronomical X-ray spectroscopy. The ESP is a direct descendent of the highly successful Solar EUV Monitor (SEM) built by USC and flown on the Solar Heliospheric Observatory (SOHO) and on many sounding rocket flights.

3.2.3.2 Algorithm and Calibration Heritage

The algorithms to convert spectroscopic measurements from detector signal to solar irradiances for both MEGS and ESP are essentially the same as those used in the current TIMED-SEE and SOHO-SEM data processing. LASP has extensive experience in calibrating both high resolution and broadband instruments.

4 EVE Calibration Plan

4.1 Overall Calibration Scheme

Solar EUV irradiance instruments are notoriously difficult to calibrate absolutely. Until recently there have been disagreements as large as a factor of four over the absolute irradiance at some wavelengths (particularly in the XUV). While spacecraft instruments may have good relative measurement stability (precision) that allow for comparisons between measurements made by the same instrument at different times, there has been a problem of knowing the absolute value of the irradiance being measured. The calibration philosophy for EVE has evolved from the experiences of the EVE team with measuring solar spectral irradiances from space-borne instrumentation over several decades, particularly the recent TIMED-SEE instrument.

The essentials for any absolutely calibrated spectral irradiance instrument are to 1) Calibrate pre-flight to an appropriate radiometric standard, 2) Track in-flight any changes that will affect the measurements, 3) Re-calibrate in-flight both as close as possible after launch and at regular intervals thereafter to track absolute changes, and 4) Validate with measurements made by other instrumentation and with models.

4.2 Pre-flight Calibration Plans

The EVE calibration plan includes unit level and system level calibrations. At the unit level, the individual optical elements and detectors are tested to verify they meet expectations and to select the best elements, usually based on sensitivity and uniformity. At the system level, each EVE subsystem (MEGS and ESP) is calibrated at the National Institute of Standards and Technology (NIST) Synchrotron Ultraviolet Radiation Facility (SURF) in Gaithersburg, MD as the principle pre-flight calibration. The synchrotron source provided by NIST SURF is a primary radiometric source and provides the most accurate calibration for any UV instrument. The SURF Beam Line 2 (BL-2) is dedicated for NASA instrument calibrations and includes a very large vacuum tank with a gimbal system. Furthermore, the calibration of all SDO solar UV instruments at NIST will establish a common pre-flight reference. The SURF calibrations provide sensitivities referenced to the radiometrically accurate synchrotron standard, polarization sensitivity, FOV mapping using the BL-2 gimbal table, non-linearity correction factors by adjusting the SURF beam current, and higher order corrections by using multiple SURF beam energies. By using SURF, only small calibration systems are needed elsewhere to perform unit level tests. The uncertainty of the SURF synchrotron source is less than 1%, which permits uncertainty of the instrument sensitivity of 2-7%, depending on the measurement precision and the correction factors applied in deriving the sensitivity [Eparvier et al., 2001; Woods et al., 1999].

4.2.1 MEGS Pre-flight Calibrations

At the unit level, the individual optical elements of all the MEGS channels will be characterized and verified. The slit areas will be measured with a translation microscope and with diffraction techniques. The filters will be checked for visible light leaks at LASP. The filter transmissions will be modelled by the manufacturers and verified at NIST SURF. The gratings will be characterized for reflectivity, efficiency, scattered light, and FOV variations using LASP facilities. The CCD detectors will also be characterized at LASP for flatfield response, dark noise, readout noise, integration timing, and readout timing.

At the system level, the MEGS subsystem as a whole will be exposed to XUV and EUV line sources for wavelength range verification and to the NIST-SURF beam for primary sensitivity calibration of all channels. On the SURF BL-2 vacuum and gimbal facility the MEGS channels will be individually calibrated for absolute radiometric sensitivity over their entire wavelength ranges and for FOV variability of sensitivity. Filters both internal to the MEGS-A and MEGS-B and in the beamline external to the MEGS will be used to provide information about second and third grating order contributions. In addition, multiple SURF beamline energies will also be used to determine the relative contributions to the signal from first, second, and third orders. Dark signals and detector flatfields (using internal flatfielding LEDs) will also be performed repeatedly at the system level for MEGS.

4.2.2 ESP Pre-flight Calibrations

At the unit level, the individual optical elements of the ESP will be characterized and verified. The electrometers will be tested for transfer function and linearity at USC. The filters will be checked for light leaks and the filter transmissions will be measured at NIST SURF. The grating transmissions and FOV response will also be calibrated at NIST SURF, as will the quantum yield of the ESP photodiodes.

At the system level, the ESP subsystem as a whole will be calibrated at NIST SURF for quantum throughput as a function of wavelength and FOV, similar to the MEGS subsystem.

4.3 In-flight Tracking of Short-Term Changes

During such a long mission and in the harsh environment of geosynchronous orbit, many factors can cause the response of the EVE instruments to change in-flight. These include contamination, radiation damage, exposure-related degradation, temperature effects, and so on. All EVE channels will undergo regular dark measurements. The SDO spacecraft will perform regular off-nominal pointing maneuvers to use the Sun to make maps of the EVE instrument fields of view. This will allow for corrections based on exposure “burn-in”. Both MEGS have LED lamps to perform regular flatfielding of the CCDs to track degradation of individual pixels. Two different visible wavelengths are used (separately) for flatfielding. The penetration depths of the visible wavelengths in the silicon of the CCDs are similar to those of the EUV wavelengths that MEGS is detecting.

The MEGS detectors are cooled, so can serve as traps for contaminants. The CCDs have heaters that will allow for periodic “burning off” of the detectors if necessary. Unfortunately heating can change the responsivity of the detectors; therefore, a means of tracking this sort of short term change is necessary. This is the purpose of the ESP and MEGS-P. The ESP broadband channels overlap with MEGS wavelengths and can provide a source of continuity of calibration over weeks and months. The MEGS-P at 121.5 nm does not overlap with MEGS wavelengths, but since the solar Lyman- α emission varies similarly to the hydrogen continuum (which peaks near 90 nm) and Lyman- β (at 102.6 nm), it can be used as a proxy to track changes in wavelengths that are measured by MEGS. The silicon photodiodes used in ESP and MEGS-P are considered standard radiometric detectors by NIST and so are expected to be fairly stable. In addition, overlapping wavelengths between the two slits in MEGS-A and between MEGS-A and B, and the higher order filters on MEGS also provide some level of redundancy for tracking changes.

4.4 Long-term Absolute Calibration Tracking (Re-Calibration)

Even with careful pre-flight calibration and fastidious contamination control, it is difficult to guarantee that the absolute calibration of the instrument won’t change once the spacecraft has been launched and the instrument begins operations. On-board redundant or overlapping channels can only track short-term, relative changes because there is no guarantee that those channels have not undergone absolute calibration changes similar to the primary channels (such as by contamination). Some sort of periodic re-calibration to absolute standards is necessary, particularly right at the start of the mission and at regular intervals throughout. As part of the EVE project, sounding rocket versions of all the EVE channels are being built. The sounding rocket will fly soon after SDO normal operations begin and at regular intervals thereafter. The first two flights will be about 6 months apart, but later flights may have longer intervals based on

the measured changes in the spacecraft instruments. The rocket instruments will be calibrated at NIST SURF-III both before and after each rocket flight. The rocket instruments and the spacecraft instruments will make simultaneous measurements of the Sun during the rocket underflights. This allows for a transfer of absolute calibration from NIST to EVE via the rocket instruments.

4.5 Validation

The best way to validate a measurement is to make a measurement at the same time with a different instrument, preferably one that is fundamentally different in design. Unfortunately, there are not very many on-going measurements of the solar EUV. The EVE measurements will be compared to the SEE and SEM measurements, if TIMED and/or SOHO are still in operation when SDO launches. EVE will also be compared to the EUV spectrometer (EUVS) on the NOAA GOES-N satellite, if it is in operation at the time. This is a broadband instrument similar to the ESP. One can also consider the measurements of MEGS and ESP capable of validating each other, since they are fundamentally different instruments. Validation by comparisons to solar EUV models is also planned. Empirical models based on measurements from missions not necessarily overlapping with SDO can span temporal gaps, though more often comparisons between measurements and models are used to validate the model rather than the measurements.

5 EVE Measurement Algorithm Descriptions

5.1 Theoretical Basis

The purpose of the EVE instrumentation is to disperse and measure solar light. All of the EVE channels convert solar photons into electronic signals in a manner that can be quantified and calibrated. In the MEGS and ESP this conversion is accomplished by having the light fall on silicon detectors (CCDs and photodiodes). In the MEGS-A, MEGS-B, and ESP channels the solar light is limited in wavelength range by filters and dispersed spatially on the detector systems using reflection gratings (MEGS) and transmission grating (ESP). In the MEGS-P the wavelength limitation is provided by filters for the zeroth order trap photometers and by spectral dispersion from the first grating MEGS-B. In MEGS-SAM the energy (wavelength) of incident photons is determined by the method of detection itself.

To correctly determine irradiance from the measured signals sent down in EVE science telemetry, one must model the entire chain of events from incidence of solar photons on the entrance aperture of each channel all the way through to the creation of Data Numbers (DN) in the EVE electronics. Then this instrument model must be inverted to derive an algorithm which goes from signal (DN) back to irradiance in a series of steps. Each step has quantities which are known from calibration measurements or modelling, and each step has uncertainties associated with it. This section will describe the algorithms for calculating irradiance from each of the EVE channel signals.

5.2 Conversion of Instrument Signals to Irradiance Units

5.2.1 MEGS-A and MEGS-B Measurement Equations

The algorithm described in Equations 4.1 shows the derivation of solar spectral irradiance from raw signal for the MEGS-A and MEGS-B channels.

$$C_1(x,y) = \frac{S(x,y)}{\Delta t} \cdot G(T) \cdot f_{FF}(x,y,t) \cdot f_{Lin}(S) \quad (1a)$$

$$C_2(x,y) = C_1(x,y) - C_{Dark}(x,y) - C_{SL}(x,y) \quad (1b)$$

$$C_3(\lambda) = \frac{\sum_{Good(x,y)} f_{Image}(x,y) \cdot C_2(x,y)}{\sum_{Good(x,y)} f_{Image}(x,y)} \quad (1c)$$

$$E(\lambda) = \frac{C_3(\lambda)}{A \cdot \Delta\lambda \cdot R_{Center}(\lambda,t) \cdot f_{Degrad}(\lambda,t) \cdot f_{FOV}(\lambda,\theta,\phi) \cdot f_{IAU}(t)} \cdot \frac{hc}{\lambda} - E_{os}(\lambda) \quad (1d)$$

The first step (1a) takes the raw signal, S (in DN) at a given detector location (x,y) , and converts it to the physical units of electrons (e-) with the gain factor, G (in e-/DN) which is a function of the temperature, T . This is then divided by the integration time to give e-/sec. Then a correction factor, f_{FF} , for flat-field effects is applied, as is a linearity correction, f_{Lin} . The second step (1b) is to apply subtractive corrections for dark count rate, C_{Dark} , and scattered light, C_{SL} .

Next (1c), since the slit image on the detector falls on hundreds of pixels, a weighted average is taken over all the pixels in the non-dispersive direction which have the same wavelength incident. At this time any pixels that are deemed to be bad by reason of damage or spurious signal due to high-energy particles are excluded from the average (hence the “ $Good(x,y)$ ” for the range of the summations). The weighting, f_{Image} , is based on the relative contribution of each pixel to the slit image on the detector.

Finally (1d), this corrected count rate for wavelength λ is converted to irradiance ($\text{W m}^{-2} \text{ nm}^{-1}$) by dividing by the area of the slit, A (in m^2), the dispersion, $\Delta\lambda$ (in nm), the detector responsivity at the center of the field of view, R_{Center} , a degradation factor, f_{Degrad} , and a field-of-view correction factor, f_{FOV} , a normalization factor to 1 AU, f_{IAU} , and then multiplied by a factor of hc/λ to convert from photon units to energy units. At this point an order-sorting correction, E_{os} , is applied to remove second and higher order contributions from the spectrum.

The degradation of the MEGS is actually tracked through three functions: daily flatfield images (f_{FF}), weekly degradation (f_{Degrad}) from comparisons to redundant channel measurements (ESP and MEGS-P), and regular sounding rocket calibrations (adjusted R_{Center}). The flat-field correction is derived from the flat-field images taken most recently in flight that are normalized using the pre-flight flat-field image. The flat-field function, therefore, includes the local degradation on the CCD that should primarily occur at the brighter emissions. The weekly degradation function is derived using trends in the ratios of the MEGS irradiances to the ESP and MEGS-P irradiances. For transfer of the rocket results to MEGS, the responsivity is adjusted for the MEGS so that its irradiances on the rocket flight dates match the rocket irradiances. A model based on multiple rocket comparisons (when they become available) is used to interpolate between rocket dates.

5.2.2 MEGS-SAM Measurement Equation

Equation 2 describes the derivation of the solar irradiance for the MEGS-SAM in spectral mode. Similar to the final step of the MEGS algorithm, the SAM algorithm is a straightforward calculation converting detector signal to irradiance, but with fewer correction factors because of its simpler optical design and because the detector registers each photon event individually. The wavelength, λ , is determined from the number of electrons of each photon event.

$$E(\lambda) = \frac{S(\lambda) \cdot G \cdot f_{FF}(x, y, t) \cdot f_{Lin}(S)}{\Delta t \cdot A \cdot \Delta\lambda \cdot R(\lambda) \cdot f_{Degrad}(\lambda, t) \cdot f_{IAU}(t)} \cdot \frac{hc}{\lambda} \quad (2)$$

Here S is the sum of all the signals from all the pixels in the SAM region of the detector which are associated with a bandpass of $\lambda - \Delta\lambda/2$ to $\lambda + \Delta\lambda/2$, G is the gain, f_{FF} is the flatfield correction, f_{Lin} is the linearity correction, Δt is the integration time, A is the pinhole area, R is the responsivity, f_{Degrad} is a degradation function, and f_{IAU} is a scaling to a constant distance from the Sun. The responsivity includes the quantum efficiency of the CCD and the transmission of the X-ray filter. A SAM irradiance spectrum is essentially built up as a histogram of photon events with the same energies (wavelengths).

5.2.3 ESP and MEGS-P Measurement Equation

The irradiance algorithm is essentially the same for both the ESP and the MEGS-P and is given by Equation 3.

$$E(\lambda) = \frac{S(t) - S_{Dark}}{A \cdot \sum [R(\lambda) \cdot f_{Weight}(\lambda) \cdot f_{Degrad}(\lambda, t) \cdot \Delta\lambda] \cdot f_{IAU}} \cdot \frac{hc}{\lambda} \quad (3)$$

Here S is the count rate from the diodes, S_{Dark} is the dark count rate, A is the aperture area, R is the responsivity of the diode, f_{Weight} is the weighting of the spectral flux within the bandpass ($\Delta\lambda$) of the diode, f_{Degrad} is a correction for degradation, and f_{IAU} is the normalization to 1 AU distance. The summation is over the bandpass of the diode. The weighting functions are determined with Equation 4.

$$f_{Weight}(\lambda) = \frac{\int F(\lambda)}{\int F(\lambda) \cdot d\lambda}, \quad (4)$$

where $F(\lambda)$ is either an assumed spectral distribution or one measured by MEGS-A or B over the bandpass of the ESP or MEGS-P photometer. In the cases where a filter is in front of the diode, the spectral distribution, $F(\lambda)$, is multiplied by the transmission function, $\tau(\lambda)$, of the filter.

5.3 Signal Estimates and Error Analyses for Subsystems

5.3.1 MEGS Signal Estimates and Error Analysis

Computer models of the anticipated response to solar incident light for each of the MEGS spectral channels have been made. These models include slit functions, filter transmissions, grating reflectivities, grating efficiencies, grating dispersion properties, optical imaging properties, and detector sensitivities as they were known in the design phase of the project. The models were given representative solar incident spectra for solar minimum, solar maximum, and

solar flare conditions, as provided by the NRLEUV solar spectral model. In addition, noise estimates were made for each of the MEGS channels including anticipated CCD read-out noise, dark current, fano noise (important for the shorter wavelengths), analog-to-digital conversions, and counting statistical noise. Figures 9, 10, and 11 show the estimated signals in each of the MEGS spectral channels for solar minimum, solar maximum, and solar flare conditions. The signals shown are in electrons per 10-sec integration in a single pixel. The End of Life signal requirement is at around 20 and is the estimated minimum brightness needed for one of the required 18 lines to meet the 25% uncertainty requirement by the end of the mission, given estimated degradation. There are many more than 18 lines which meet this requirement.

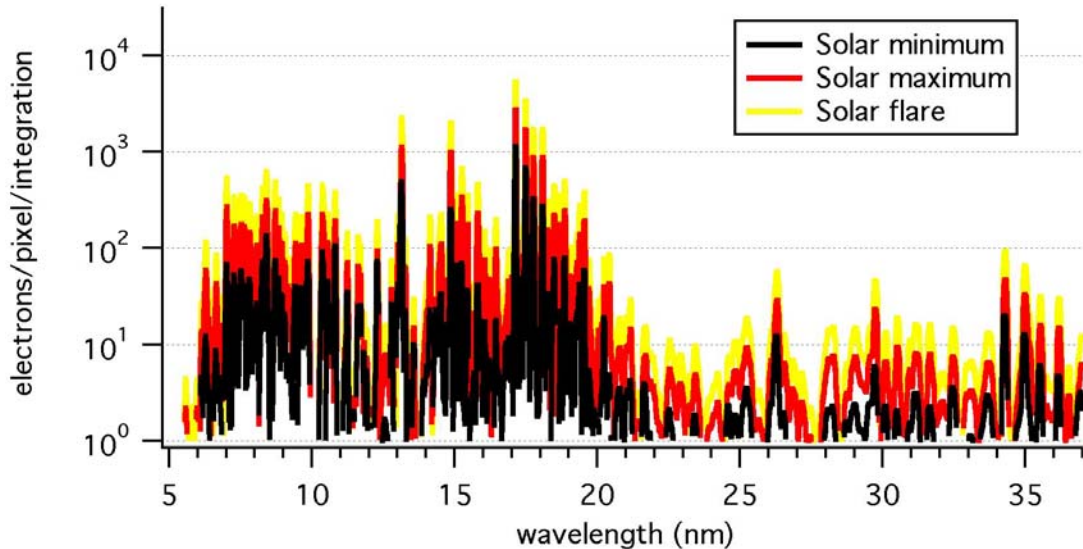


Figure 9: MEGS-A Slit 1 signal estimates for solar minimum, maximum, and flare conditions.

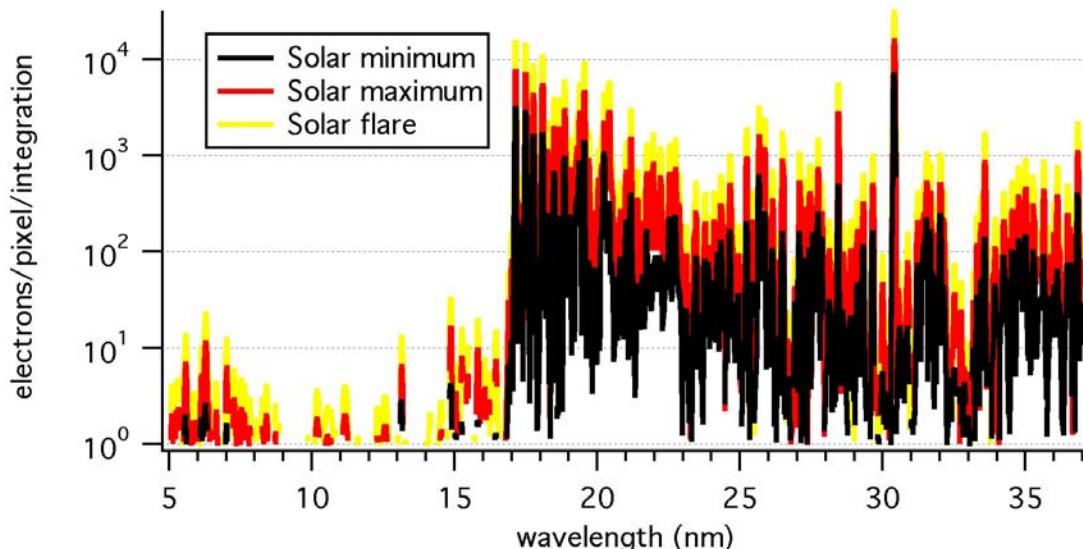


Figure 10: MEGS-A Slit 2 signal estimates for solar minimum, maximum, and flare conditions.

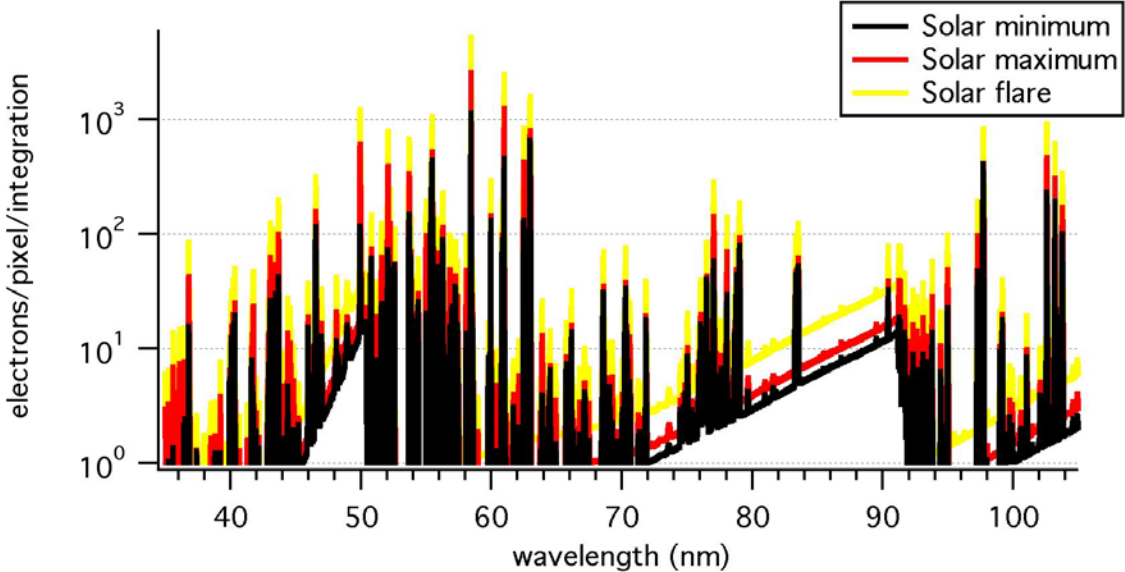


Figure 11: MEGS-B signal estimates for solar minimum, maximum, and flare conditions.

The propagation of uncertainties through the irradiance algorithms (Equations 4.1) for MEGS-A and MEGS-B is given in Equations 5, where σ_{var} represents the uncertainty of a variable *var*, in the units of *var*.

$$\sigma_{C_1}^2 = C_1^2 \cdot \left[\frac{\sigma_S^2}{S^2} + \frac{\sigma_{\Delta t}^2}{\Delta t^2} + \frac{\sigma_G^2}{G^2} + \frac{\sigma_{f_{FF}}^2}{f_{FF}^2} + \frac{\sigma_{f_{Lin}}^2}{f_{Lin}^2} \right] \quad (5a)$$

$$\sigma_{C_2}^2 = \sigma_{C_1}^2 + \sigma_{C_{Dark}}^2 + \sigma_{C_{SL}}^2 \quad (5b)$$

$$\sigma_{C_3}^2 = \sum_{Good(x,y)} \left\{ \left(\frac{f_{Image}(x,y) \cdot C_3}{\sum_{Good(x,y)} f_{Image}(x,y)} \right)^2 \cdot \left[\frac{\sigma_{f_{Image}(x,y)}^2}{(f_{Image}(x,y))^2} \cdot \left(1 - \frac{f_{Image}(x,y)}{\sum_{Good(x,y)} f_{Image}(x,y)} \right)^2 + \frac{\sigma_{C_2(x,y)}^2}{(C_2(x,y))^2} \right] \right\} \quad (5c)$$

$$\sigma_E^2 = E^2 \cdot \left[\frac{\sigma_{C_3}^2}{C_3^2} + \frac{\sigma_A^2}{A^2} + \frac{\sigma_{\Delta \lambda}^2}{\Delta \lambda^2} + \frac{\sigma_{R_{Center}}^2}{R_{Center}^2} + \frac{\sigma_{f_{Degrad}}^2}{f_{Degrad}^2} + \frac{\sigma_{f_{FOV}}^2}{f_{FOV}^2} + \frac{\sigma_{f_{IAU}}^2}{f_{IAU}^2} + \frac{\sigma_{\lambda}^2}{\lambda^2} \right] + \sigma_{E_{os}}^2 \quad (5d)$$

The measurement precision, being the uncertainty for a single measurement, is represented by equation 5c. The absolute accuracy, being the uncertainty for the absolute value of the irradiance from a single measurement, is given by equation 5d.

Table 3s shows an error propagation for an “acceptable” spectral line, which is defined as the dimmest spectral line (with a margin of a factor of two) that we deem to be still usable to meet our science objectives as one of the 18 solar lines to measure through the life of the mission. The estimated uncertainty for such a line is about 13%. The final column of the table is an estimated breakdown of the error budget allowable for each parameter in the measurement equation to meet the 25% requirement for the mission.

Table 3: MEGS-A and MEGS-B Uncertainty Estimate and Error Budget

Parameter	Value for “Acceptable” spectral line	Uncertainty Estimate (“Acceptable” spectral line)	Error Budget (allowable error)
$S(x,y)$	12 DN/pix	2 DN/pix (17%)	34%
Δt	10 s	0.001 s (0.01%)	0.02%
$G(T)$	2.0 e-/DN	0.5%	1%
$f_{FF}(x,y,t)$	1.0	1%	2%
$f_{Lin}(S)$	1.0	0.1%	0.2%
$C_I(x,y)$	2.4 e-/s/pix	0.4 e-/s/pix (17%)	34%
$C_{Dark}(x,y)$	0.2 e-/s/pix	0.02 e-/s/pix (10%)	20%
$C_{SL}(x,y)$	0.2 e-/s/pix	0.02 e-/s/pix (10%)	20%
$C_2(x,y)$	2.0 e-/s/pix	0.16 e-/sec/pix (8%)	16%
$f_{Image}(x,y)$	1	1%	2%
$Good(x,y)$	100 pix	-	-
$C_3(\lambda)$	200 e-/s	1.6 e-/s (0.8%)	1.6%
A	$4 \times 10^{-8} \text{ m}^2$	$1.6 \times 10^{-9} \text{ m}^2$ (4%)	8%
$\Delta\lambda$	0.1 nm	0.003 nm (3%)	6%
$R_{Center}(\lambda,t)$	1 e-/ph	0.06 e-/ph (6%)	12%
$f_{FOV}(\lambda, \theta, \phi)$	1.0	5%	10%
$f_{Degrad}(\lambda,t)$	0.95	9%	18%
$f_{IAU}(t)$	1	0.01%	0.02%
λ	20 nm	0.02 nm (0.1%)	0.2%
$E_{os}(\lambda)$	$10^{-4} \text{ W/m}^2/\text{nm}$	1%	2%
$E(\lambda)$	$5 \times 10^{-8} \text{ W/m}^2/\text{nm}$	$0.65 \times 10^{-8} \text{ W/m}^2/\text{nm}$ (13%)	25%

5.3.2 MEGS-SAM Signal Estimates and Error Analysis

Figure 12 shows the estimated signal for the MEGS-SAM in irradiance mode, using a solar spectral input for solar minimum conditions, and binning the signal into 1 nm intervals.

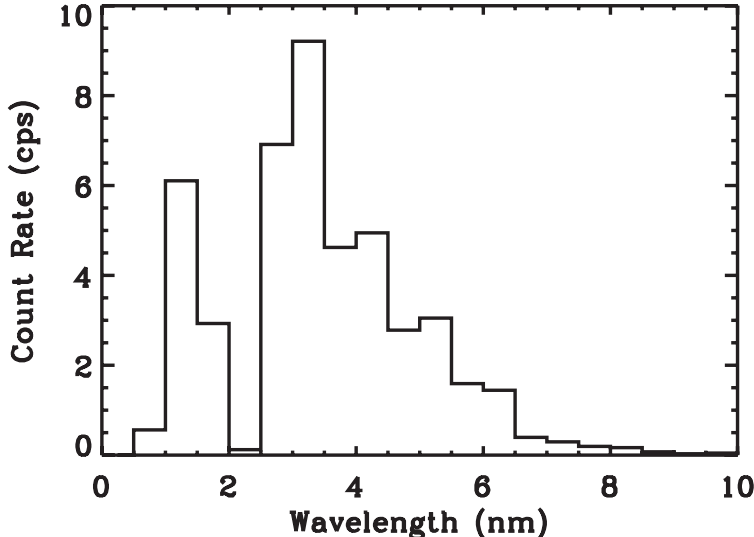


Figure 12: MEGS-SAM irradiance signal estimates for solar minimum conditions.

The spectral resolution of the SAM X-ray spectrum is limited by the CCD pixel noise and Fano noise (deviation from the nominal electron per 3.65 eV of photon energy). The energy (spectral) resolution, Δe in eV, is given by:

$$\Delta e = \cdot (2.355) \cdot \sqrt{(3.65 \text{ eV/e}^- \cdot G \cdot \sqrt{S_{Dark}})^2 + \frac{hc}{\lambda} \cdot F_a} \quad (6)$$

where the first term under the square root is the dark noise (about 2 e⁻), and the second term is the Fano noise, with F_a as the Fano factor of about 0.1 for silicon [Janesick, 2001]. For the SAM the ideal energy resolution varies from 41 eV (0.008 nm) at 0.5 nm and 20 eV (0.7 nm) at 6.5 nm. Because individual photon events are recorded in the CCD image, the binning of the X-ray spectrum is done in the data processing on the ground and thus is not on any specific wavelength grid. It is currently planned to bin the SAM X-ray spectrum into 1 nm intervals (0-7 nm) in order to achieve < 10% measurement precision within each 10-sec integration period of the MEGS-A CCD. The estimated SAM count rate in these 1-nm intervals is shown in Figure 12. The size of the pinhole diameter is determined from the requirement to keep the probability of two photon events in a single CCD pixel below 10% per CCD image. The resulting pinhole diameter is 25 μm, and the SAM count rate is expected to vary between 100 and 300 counts per second (cps) for solar minimum and maximum conditions, respectively.

The measurement precision, being the uncertainty for a single measurement, is the standard photon counting uncertainty of \sqrt{S} . The typical measurement precision is expected to be less than 10% for a single 10-sec integration but can be improved by merging counts from additional integration periods.

The absolute accuracy, being the uncertainty for the absolute value of the irradiance from a single measurement, is given by equation 7. The largest source of uncertainty for the MEGS irradiance accuracy is the uncertainty of the pre-flight sensitivity, which should be less than 15%. The error budget (uncertainty) for each parameter is listed in Table 4.

$$\sigma_E^2 = E^2 \cdot \left[\frac{\sigma_S^2}{S^2} + \frac{\sigma_G^2}{G^2} + \frac{\sigma_{At}^2}{At^2} + \frac{\sigma_A^2}{A^2} + \frac{\sigma_{\Delta\lambda}^2}{\Delta\lambda^2} + \frac{\sigma_R^2}{R^2} + \frac{\sigma_{f_{Degrad}}^2}{f_{Degrad}^2} + \frac{\sigma_\lambda^2}{\lambda^2} \right] \quad (7)$$

The degradation of SAM is primarily tracked through ESP 0.1-7 nm irradiance measurements, as well as, longer-term degradation is tracked using the bi-annual rocket calibrations (adjusted R).

Table 4: MEGS-SAM Uncertainty Estimate and Error Budget

Parameter	Range	Uncertainty
S	30-300 DN	5-17 DN
G	1.95-2.05 e-/DN	0.1%
At	10 sec	0.001 sec
A	0.002 mm ²	0.0001 mm ²
$\Delta\lambda$	1 nm	0.01 nm
R	0.005-0.05	15-20%
f_{Degrad}	0.5-1.0	5%
λ	0-7 nm	0.01-0.7 nm
E	2-36 μW/m ² /nm	17-30%

5.3.3 ESP Signal Estimates and Error Analysis

The estimated uncertainties and their sources for ESP measurements are given in Table 5. For moderate solar activity the zero order detector will register ~ 180 pA, and the signal for each 1st order detectors is ~ 15 pA, based on SOHO experience. The Si photodiodes are unbiased; therefore, only Johnson noise is expected. At a temperature of 20° C and with a shunt resistance of 100 MΩ, the thermal noise will only amount to $13 \text{ f A/Hz}^{1/2}$. The noise in an ESP-like instrument due to ambient particles has been analyzed by Ogawa and Judge [1995a and 1995b] for the GOES missions. This study has been updated to encompass the ESP, an is included with this CSR. The study considered silver, as an example, and trade studies on the optimum shielding strategy are underway. The results of these studies have been adapted to the ESP. Local detector shielding, and spot shielding with Al/Ta/Al on the case and internal baffles will reduce the radiation induced signal to less than 0.5pA giving a SNR of about 30 for all the wavelength bands of interest.

Table 5: ESP Uncertainty Estimate and Error Budget

Source		Notes
Calibration	5%	NIST
Spectral Distribution	5%	MEGS
Aperture Area	0.05%	JPL
Weak Line Statistics	15%	
Strong Line Statistics	1%	
Irradiance Uncertainty (Weak Line)	16.6%	
Irradiance Uncertainty (Strong Line)	7.1%	

5.4 Preflight Calibration Algorithms

Calibrating an instrument at NIST-SURF is fairly straightforward. The EVE subsystems are placed in the beamline 2 and aligned to be centered in horizontal, vertical, and FOV angles. The measurement equations for each of the EVE subsystems (Equations 1, 2, and 3) are solved for the responsivity at the center, R_C , and knowing the irradiance, E , of the beamline incident on the instrument aperture, which is provided by NIST-SURF staff. Using a gimbal, the FOV can be mapped out and the f_{FOV} can be obtained by ratioing with the responsivity at the center of the FOV. Note that since the same slits are used during calibration and in flight, the area of the slits, A , actually is not relevant to the calibration or measurement except that it be large enough to give good signals and of the appropriate width for the resolution of the instrument.

APPENDIX A: List of EVE Variable Definitions

General Rules: Indicate dependence of one variable on another by parentheses (eg. $R(x)$ means that R depends on x). Use subscripts to further clarify or identify a variable (eg. R may be a responsivity, but R_{Center} is the responsivity at the center of the FOV).

A = area of aperture (slit, pinhole, ...) (m^2)

C_{Name} = quantities with dimensions of count rate (counts/sec = cps = e-/sec)

$C_{Analyzer}$ = analyzer count rate (cps)

C_{Corr} = corrected count rate (cps)

C_{Dark} = dark signal correction (cps)

C_{Part} = particle noise correction (cps)

C_{SL} = scattered light correction (cps)

C_{OS} = higher grating order correction (cps) (unless done at irradiance level)

χ = cross section (m^2)

e = energy (eV or Joules)

e_I = ionization energy

e_{KE} = kinetic energy

e_p = photon energy ($= hc/\lambda$)

E = spectral irradiance in energy units (W/m^2 or $\text{W}/\text{m}^2/\text{nm}$)

F = spectral irradiance in photon units (flux) (photons/ m^2/sec or photons/ $\text{m}^2/\text{sec}/\text{nm}$)

f_{Name} = dimensionless correction factors

f_{IAU} = 1 AU correction

f_{Degrad} = degradation correction

f_{Weight} = flux-weighted contribution function of wavelength to bandpass (was β)

f_{Image} = weighted contribution function of pixel to slit image for MEGS

f_{FF} = flatfield correction

f_{FOV} = Responsivity variation over FOV

f_{Lin} = linearity correction (function of signal)

G = gain (function of temperature, T) in e-/DN

hc/λ = conversion from photon to energy units

I = current (amperes)

λ = wavelength (nm)

$\Delta\lambda$ = bandpass or wavelength interval or dispersion (nm)

n = number density of a gas (m^{-3})

R = Responsivity, sensitivity, or quantum yield (cnt/ph or DN/ph or e-/ph)

S = raw signal (DN)

σ_{var} = error or uncertainty of var in the units of var

Ψ_{var} = error or uncertainty of var as a fraction of 1 ($\Psi_{var} = \sigma_{var}/var$)

t = time (sec)

Δt = integration time (sec)

τ = transmission (dimensionless)

T = temperature ($^{\circ}\text{C}$ or Kelvin)

θ, ϕ = angular pointing within FOV (degrees)

x, y = pixel location on a 2-D detector with x in dispersion direction

Appendix C: End of Mission Plan

The SDO End of Mission Plan (EOMP) was last updated in July 2018. It was accepted as compliant to the requirements in NASA-STD-8719.14A on January 10, 2020.

The current evaluation memo by the Office of Safety and Mission Assurance (OSMA) is attached following this summary.

During the Third Extended Mission the SDO Team will again update the EOMP and submit it to OSMA for re-evaluation. During the Second Extended Mission the SDO Team evaluated scenarios for placing SDO in its disposal orbit. The results of this analysis will be used to improve the reliability of the disposal plan in the SDO EOMP.

TO: 300/Director, Safety & Mission Assurance Directorate
FROM: 370/Quality & Reliability Division/Viens
SUBJECT: Code 300 Evaluation of End of The Solar Dynamics Observatory
REF: a) NASA-STD-8719.14B, Process for Limiting Orbital Debris
b) Call for Proposals, Rev 2b — Senior Review 2020 of the Mission Operations and Data Analysis Program for the Heliophysics operating missions, Revision 2b: February 7, 2020. NASA HQ / N. Fox / Director, Heliophysics Division, NASA HQ / J. Leisner / Senior Review, Program Scientist, NASA HQ / Heather Futrell (W. Stabnow retired effective May 2020) / Senior Review, Program Executive
c) Solar Dynamics Observatory End of Mission Plan, SSMO-SDO-EOMP-0010, Revision A
d) Evaluation of Solar Dynamics Observatory End of Mission Plan, Mr. Colon to Mr. Stabnow; dtd 01/10/20

The Solar Dynamics Observatory (SDO) mission has demonstrated full compliance with NASA-STD-8719.14B in an End of Mission Plan (EOMP), dated July 2018. The EOMP was developed using a baseline end of mission date of May 2028, though the mission will continue to be in compliance if continued beyond that date. The SDO spacecraft is in Geosynchronous Earth Orbit (GEO), with 28° inclination. At the end of the mission the spacecraft will be raised to at least 314 km above GEO, the orbit circularized, and the spacecraft will be fully passivated. Propellants and pressurant will be vented as much as is safely practical, the spacecraft subsystems powered down, and the batteries disconnected from the charging circuit. SDO was intentionally designed to be able to meet the passivation requirements at the end of the mission.

As there are no planned changes in orbital configuration, no additional EOMP analysis is required. Further details are documented in the EOMP, available from the SSMO Configuration Management Office. Please feel free to contact me (301-286-2505), if you have any questions or concerns.

Michael Viens

Michael Viens

Cc: 370/Nowak, Sticka, JIRA,
380/Maggio
300/Leitner
592/Hull
HQ-SMD/H. Futrell
SSMO/R. Burns

Appendix D: Acronyms & Abbreviations

ADS	Astrophysics Data System
AIA	Atmospheric Imaging Assembly
AIMI	Atmospheric-Ionospheric-Magnetospheric Interactions
AIM	Aeronomy of Ice in the Mesosphere
ANS	Alert Notification Service
AO	Announcement of Opportunity
API	Application Program Interface
ApID	Application Identification
AR	Active Region
AVC	AIA Visualization Center
AWSOM	Alfven-Wave driven SOlar wind Model
CARA	Conjunction Assessment Risk Analysis
CCB	Change Control Board
CCD	Charge Coupled Device
CCSDS	Consultative Committee for Space Data Standards
C&DH	Command and Data Handling
CI	Collaborative Investigator
CINDI	Coupled Ion-Neutral Dynamics Investigations
CMAD	Calibration and Measurement Algorithms Document
CME	Coronal Mass Ejection
Co-I	Co-investigator
CtL	Center to Limb
CU	University of Colorado
DDS	Data Distribution System
DEM	Differential Emission Measure
DRMS	Data Record Management System
EDS	Event Detection System
EGSE	Electrical Ground Support Equipment
EIS	EUV imaging Spectrometer
EIT	Extreme ultraviolet Imaging Telescope
EM-1	First Extended Mission
EM-2	Second Extended Mission
EM-3	Third Extended Mission
EOMP	End of Mission Plan
ESP	EUV SpectroPhotometer
EUV	Extreme Ultraviolet
EUVI	Extreme Ultraviolet Imager
EUVS	Extreme Ultraviolet Sensor
EVE	Extreme ultraviolet Variability Experiment
FDF	Flight Dynamics Facility
FITS	Flexible Image Transport System
FOT	Flight Operations Team
FOV	Field of View
FTE	Full-time equivalent
FTP	File Transfer Protocol
GB	Gigabyte (10^9 bytes)
GOES	Geostationary Operational Environmental Satellite
GOLD	Global-scale Observations of the Limb and Disk

GSFC	Goddard Space Flight Center
HCR	Heliophysics Events Knowledgebase Coverage Registry
HDF5	Hierarchical Data Format, version 5
HDS	Heliophysics Decadal Survey
HEK	Heliophysics Events Knowledgebase
HER	Heliophysics Events Registry
HMI	Helioseismic and Magnetic Imager
HPA	High-Power Amplifier
HSO	Heliospheric System Observatory
I&T	Integration and Test
ICD	Interface Control Document
ICON	Ionospheric Connection Explorer
IDL	Interactive Data Language
IOC	Instrument Operations Center
IRIS	Interface Region Imaging Spectrograph
IRU	Inertial Reference Unit
ISON	International Scientific Optical Network
ISR	Incoherent Scatter Radar
ISS	Image Stabilization System
JMD	JSOC Mirroring Daemon
JSD	JSOC Series Definition
JSOC	Joint Science Operations Center
LASP	Laboratory for Atmospheric and Space Research
LMSAL	Lockheed Martin Solar and Astrophysics Laboratory
LWS	Living With a Star
LYRA	Large Yield RAdiometer
MA	Mission Archive
MAVEN	Mars Atmosphere and Volatile EvolutioN mission
MB	Megabyte (10^6 bytes)
Mbps	Megabits per second
MDI	Michelson Doppler Imager
MEGS	Multiple EUV Grating Spectrograph
MHD	Magnetohydrodynamics
MIL-STD	Military Standard
MinXSS	Miniature X-ray Solar Spectrometer
MK	Million Kelvin
MOC	Mission Operations Center
netCDF	network Common Data Form
NIST	National Institute of Standards and Technology
NLFFF	Non-Linear Force Free model
NOAA	National Oceanic and Atmospheric Administration
NRT	Near-realtime
NSF	National Science Foundation
OSMA	Office of Safety and Mission Assurance
PB	Petabyte (10^{15} bytes)
PDMP	Project Data Management Plan
PFSS	Potential Field Source Surface model
PI	Principal Investigator
PSF	Point Spread Function
PSG	Prioritized Science Goal

PSP	Parker Solar Probe
PZT	Piezoelectric Transducer
RA	Resident Archive
RAISE	Response of the Atmosphere to Impulsive Solar Events
RFA	Research Focus Area
RHESSI	Reuven Ramaty High Energy Solar Spectroscopic Imager
ROSES	Research Opportunities in Space and Earth Sciences
RWA	Reaction Wheel Assembly
SAM	Solar Aspect Monitor
SAO	Smithsonian Astrophysical Observatory
SCP	Secure Copy
SDAC	Solar Data Archive Center
SDO	Solar Dynamics Observatory
SDOGS	SDO Ground System
SDP	Science Data Processing
SEE	Solar Eruptive Event
SEE	Solar EUV Experiment
SEM	Solar EUV Monitor
SEP	Solar Energetic Particles
SIT	Science Investigation Team
SMD	Science Mission Directorate
SO	Solar Orbiter
SOC	Science Operations Center
SOHO	Solar and Heliospheric Observatory
SORCE	SOlar Radiation and Climate Experiment
SPP	Solar Probe Plus mission
SQL	Structured Query Language
SSH	Secure Shell

STEREO	Solar TERrestrial RElations Observatory
SU	Storage Unit
SUMS	Storage Unit Management System
SURF	Synchrotron Ultraviolet Radiation Facility
SUVI	Solar Ultraviolet Imager
SVM	Support Vector Machine
SWAP	Sun Watcher using Active Pixel system detector and image Processing
SWG	Science Working Group
SWPC	Space Weather Prediction Center
SXR	Soft X-Ray
T&C	Telemetry & Control
TB	Terabyte (10^{12} bytes)
TBD	To Be Determined
TIMED	Thermosphere, Ionosphere, Mesosphere Energetics and Dynamics mission
TLM	Telemetry
UC	University of California
USC	University of Southern California
UV	Ultraviolet
VC	Virtual Channel
VCDU	Virtual Channel Data Unit
VM	Virtual Memory
VSO	Virtual Solar Observatory
WSMR	White Sands Missile Range
WYE	Work Year Equivalent
XML	eXtensible Markup Language
XPS	XUV Photometer System
XRS	X-Ray Sensor

see also <http://sdo.gsfc.nasa.gov/resources/acronyms.php>

Appendix E: Budget Spreadsheets

E.1: In-guide Budget Spreadsheets

E.2: Over-guide Budget Spreadsheets